Draft Final Report

Demonstration of Sensor Technologies for On-Road and Off-Road Heavy-Duty Vehicles

Contract No. 21RD007

Prepared for:

Georges Saliba
California Air Resources Board
Research Division
1001 I street
Sacramento ▪ CA ▪ 95812
Georges.Saliba@arb.ca.gov

December 2025

Submitted by:

Author: Dr. Kent Johnson
Contributing Authors: Dr. Thomas D. Durbin, Dr. Georgios Karavalakis, Dr. Zisimos Toumasato, Dr. George Scora, Ms. Grace Johnson
College of Engineering-Center for Environmental Research and Technology
University of California, Riverside, CA 92521

Disclaimer

The statements and conclusions in this Report are those of the contractor and not necessarily those of the California Air Resources Board. The mention of commercial products, their source, or their use in connection with material reported herein is not to be construed as actual or implied endorsement of such products.

Acknowledgments

The authors thank the following organizations and individuals for their valuable contributions to this project.

We acknowledge the funding from CARB under contract 21RD007.

We acknowledge the fleets that participated in this project. They will remain anonymous, but we could not have completed this work without their support and help.

We acknowledge Mr. Mark Villela, Mr. Daniel Gomez, Mr. Marcos Alvarez, Mr. Luke Johnson, Mr. Zachary Johnson, Mr. Jacob Johnson, Mr. Jose Rocha-Rocha, and Mr. Casey Collier of the University of California at Riverside, for their contribution in setting up and executing this field project, the data collection and quality control.

Table of Contents

List of Tables

List of Figures

Acronyms and Abbreviations

ARB .....Air Resources Board
bs .....brake specific
eBC .....equivalent black carbon. Equivalent to elemental black carbon from the soot measurement system.
CARB.....California Air Resources Board
CE-CERT .....College of Engineering-Center for Environmental Research and Technology (University of California, Riverside)
CFO.....critical flow orifice
CFR .....Code of Federal Regulations
CO .....carbon monoxide
COV .....coefficient of variation
CO_2.....carbon dioxide
CVS.....constant volume sampling
CPC .....condensation particle counter
DGM .....Diesel Goods Movement
DMM.....Dekati Mass Monitor
DOC .....diesel oxidation catalyst
DOR .....Diesel Off Road
Dp.....particle diameter
DPF .....diesel particulate filter
DR .....dilution ratio
DTT.....Diesel Transfer Truck
EAD .....electrical aerosol detector
EC .....elemental carbon
ECM.....engine control module
efuel.....ECM fuel consumption rate
EMA.....Engine Manufacturers Association
EPA .....United States Environmental Protection Agency
FID .....flame ionization detector
FTP.....Federal Test Procedure
GFM.....gravimetric filter module
g/hp-h .....grams per brake horsepower hour
HDIUT .....heavy-duty in-use testing
lpm .....liters per minute
MA .....Measurement Allowance
MASC .....Measurement Allowance Steering Committee
MDL.....minimum detection limit
MEL .....CE-CERT's Mobile Emissions Laboratory
MFC .....mass flow controller
nm .....nanometers
NMHC.....non-methane hydrocarbons
NTE.....Not-to-exceed
NO_x .....nitrogen oxides
OC .....organic carbon

OSAR.....UCRs name for its PAMS + measurement system which includes NOx, PM, and ECM data only
OEM.....original equipment manufacturer
PAMS.....portable activity measurement system. Collection of ECM data
PAMS + ...portable activity measurement system plus NOx and PM emissions plus ECM data
PEMS .....portable emissions measurement systems
PM.....particulate matter
QCM .....quartz crystal microbalance
RPM .....revolutions per minute
SCAB .....South Coast Air Basin
scfm.....standard cubic feet per minute
SEE .....standard error estimate
fSMPS.....fast scanning mobility particle sizer
Soot .....black carbon emissions equivalent measured by the photo acoustic principle of the PM PEMS system
SOC.....State of charge
SOF .....soluble organic fraction
SwRI .....Southwest Research Institute
THC.....total hydrocarbons
UCR .....University of California at Riverside
ULSD .....ultra-low sulfur diesel

Executive Summary

Reducing emissions from mobile sources remains one of the most important environmental challenges in the near term, and extending out over the next few decades. The California Air Resources Board (CARB) has been a leader in developing and implementing regulations to deal with both air pollutants, such as nitrogen oxides (NOx), and carbon dioxide (CO_2) emissions, as the primary greenhouse gas (GHG) of concern. This is being carried out through a range of different regulatory programs that include both increasing tighter emissions standards, as well as the monitoring of heavy-duty diesel vehicle (HDDV) performance and emissions using sensors and the vehicle's on-board diagnostic (OBD) system.

The objective of this research is to evaluate the potential of state-of-the-art and innovative sensor technologies in meeting the monitoring needs for recently implemented and future regulatory programs. The research included the monitoring of NOx, particulate matter (PM), and CO_2 emissions from on-road HDDVs and large off-road diesel engines (ORDEs) using sensors.

A total of 100 on-road and 20 off-road HDDVs are expected to be installed with a continuous monitoring Onboard, Sensing, Analyzing, and Reporting (OSAR) systems or Hydraulics + Electrical + Mechanical (HEM) loggers for a period of one month per vehicle. A total of 65 vehicles have been monitored to date from a total of 8 fleets. Preparations are being made for OSAR installs with three additional fleets, which will complete the 100 on-road vehicles. These fleets consist of six goods movement fleets, one transfer truck fleet, and one off-road fleet. The goods movement fleets have been named Diesel Goods Movement (DGM), the transfer truck fleet has been named Diesel Transfer Truck (DTT), and the off-road fleet has been named Diesel Off Road (DOR).

The sensor calibration intercepts ranged from 0.9 to 10.0 for the initial calibrations and -0.8 to 17.3 for the final calibrations. The R^2 ranged from 0.751 to 1.000 for the initial and final calibrations. Percent differences ranged from 0.6% to 25% for the R^2, 1% to -5027% for the slope, and -1693% to 1318% for the intercept.

On a g/bhp-hr basis, average NOx emissions across the fleets ranged from less than 0.02 to about 0.82 g/bhp-hr, as seen in Figure ES-1. The results for individual vehicles did show some variability, indicating a wider range in emission rates for the individual vehicles. Several fleets showed outliers that were greater than 1.0 g/bhp-hr, even though the average emissions were around 0.2 g/bhp-hr. The DGM 3 fleet had the lowest emissions, which can be attributed to the highway speeds, and the higher aftertreatment temperatures. In contrast, DGM 1, which had the highest emissions, showed lower aftertreatment temperatures, closer to 200 ºC. DGM 1 also included much older model year vehicles, ranging from 2013 to 2019, compared to DGM 3, which only utilized 2023 model year vehicles with low odometer readings.

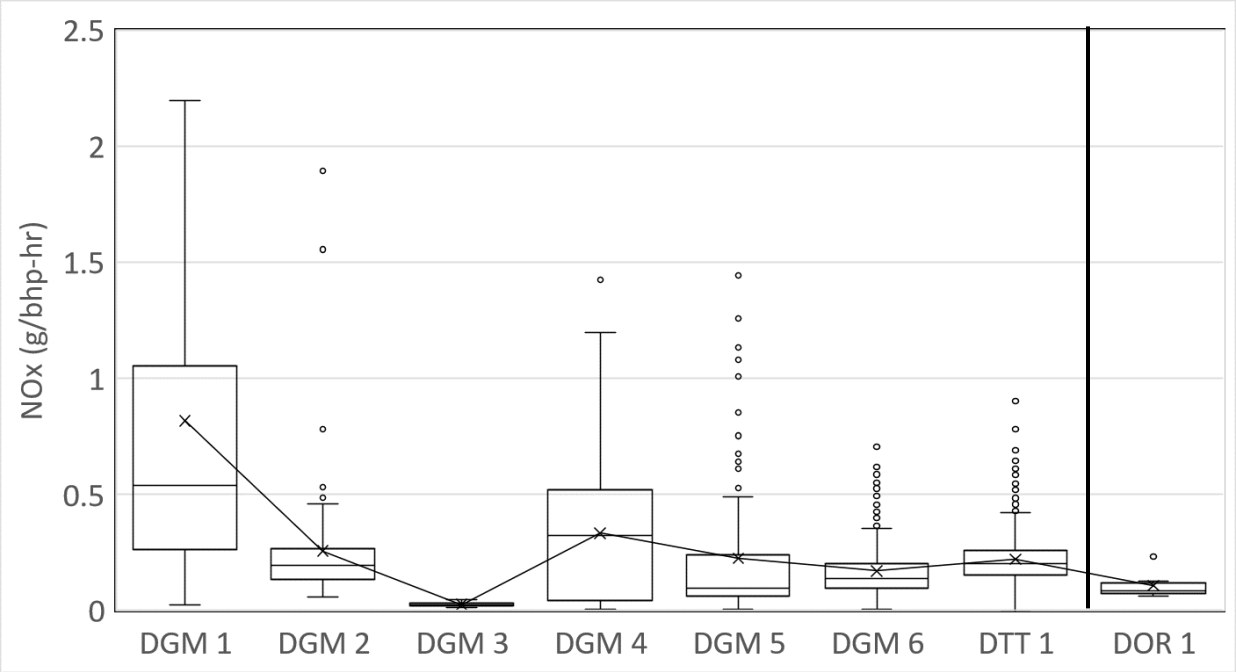

Figure ES-1: OSAR NOx Emission Rates in g/bhp-hr units

The results from the histogram show that the majority of the vehicles (36 of 56) showed emissions below 0.2 g/bhp-hr, with another 15 of 56 vehicles showing emissions below 0.4 g/bhp-hr. A total of 5 vehicles showed emissions >0.6 g/bhp-hr, with 2 of those having emissions >1.0 g/bhp-hr, as seen in Figure ES-2. The higher emitting vehicles ranged in model year from 2013 to 2022, and included three vehicles from the same fleet. The two highest emitters included on older 2013 vehicle, and 2019 vehicle, and were both from the same fleet. The other two vehicles, with emission rates of 0.66 and 0.67 g/bhp-hr, included on older 2015 vehicle and one newer 2022 vehicle.

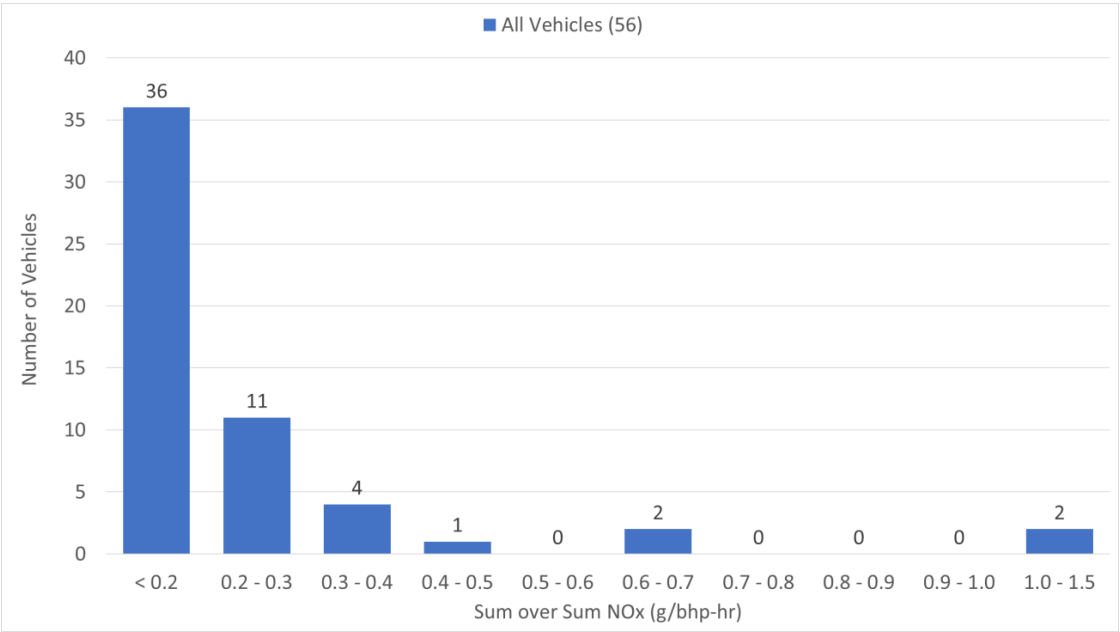

Figure ES-2: OSAR NOx Sum over Sum Emissions Factor Histogram

For EPA Bin 1, the two tables show that the idling NOx emissions were on average less than 20 g/hr for all but the DTT 1 and DGM 1 fleets. For EPA Bin 2 all but DGM 3 and 4 were on average above the 0.035 g/hp-hr in-use off-cycle requirement. The REAL binning analysis shows that most of the NOx emissions were generated when the fleet vehicles are under low load (i.e., < 25%), low speed, and idle conditions. The emission rates under idle conditions ranged from 0.552 to 17.34 g/bhp-hr and under low load conditions ranged 0.081 to 1.487 g/bhp-hr of NOx across the different fleets. Once higher speeds and loads are reached, NOx emissions greatly decrease, with the average emission rates for most bins with loads above 25% being comparable to or below 0.2 g/bhp-hr.

The daily results show a broader distribution of emission rates with a number of days showing emissions above 1 g/bhp-hr DGM 6 and DTT 1 showed a bulk of the days of operation with emissions from 0.2 to 0.4 g/bhp-hr, which is still within twice the standard. The DGM 3 fleet showed the lowest emissions, with all of the daily emissions well below 0.2 g/bhp-hr.

Figure ES-3, below, shows the average daily emission rates plotted with aftertreatment temperature, with a work gradient applied. Note that the individual days in these graphs only include days of operation where the vehicle was operated for at least 20 minutes and had worked at least 23 bhp-hr. Overall, these plots show a relationship between higher emissions and lower aftertreatment temperatures, but that other factors are also contributing to the emissions differences between different days as well. The DGM 3 fleet showed the lowest emissions, with all of the daily emissions well below 0.2 g/bhp-hr, with can be attributed to the aftertreatment temperature being above 250 °C for the all of the days of operation. The DGM 2, DGM 6, and DTT 1 fleets had the majority of days below 0.4 g/bhp-hr, with DGM 6 also showing a patch of days from 0.4 to 0.7 g/bhp-hr.

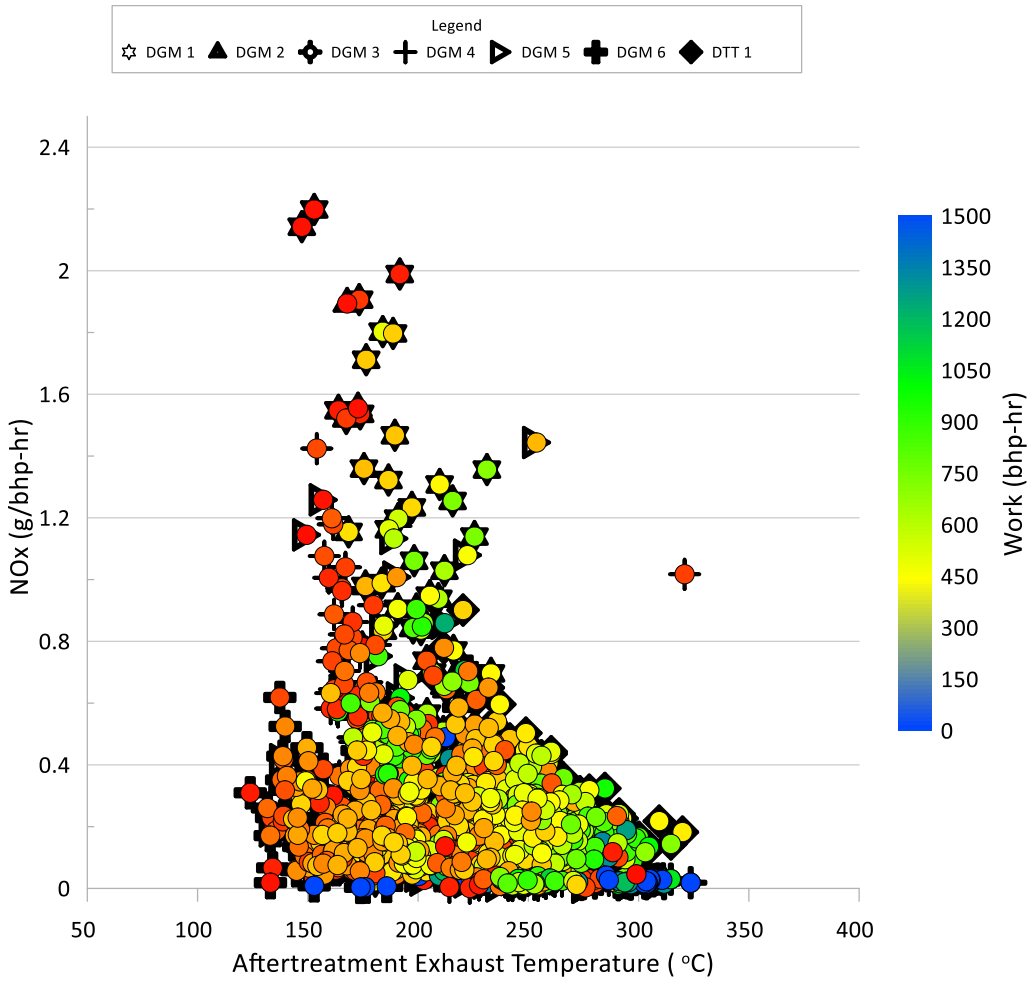

Figure ES-3: Average Daily Emission Rates for all Fleets

Average PM emissions across the fleets ranged from 0.5 to 46 mg/bhp-hr. DGM 4 showed the highest PM rate at 46 mg/bhp-hr. While DGM 2 and DTT 1 showed the lowest emission rates, of 8.1 and 6.5 mg/bhp-hr, respectively. The daily average CO_2 emissions for each fleet type ranged from 441 to 516 g/bhp-hr. On average, the fleets emitted 473 g/bhp-hr, with DOR 1 and DTT 1 showing slightly higher CO_2 values. The average CO_2 emissions on a g/mi basis was 1645 g/mi for the on-road fleets, with a range from 1271 to 2066 g/mi.

1 Background

Reducing emissions from mobile sources remains one of the most important environmental challenges in the near term, and extending out over the next few decades. The California Air Resources Board (CARB) has been a leader in developing and implementing regulations to deal with both air pollutants, such as nitrogen oxides (NOx), and carbon dioxide (CO_2) emissions, as the primary greenhouse gas (GHG) of concern. This is being carried out through a range of different regulatory programs that include both increasing tighter emissions standards, as well as the monitoring of heavy-duty diesel vehicle (HDDV) performance and emissions using sensors and the vehicle's on-board diagnostic (OBD) system. From an enforcement standpoint, the monitoring of emissions from HDDVs using sensors, such as under CARB's Real Emissions Assessment Logging (REAL) program, plays a key role in ensuring the regulatory benchmarks being put into place to be met over the lifetime of the vehicles, such that the anticipated emissions benefits are achieved under in-use conditions. Given the key role that sensors will play in CARB's regulatory programs, it is important that these sensors have the accuracy, stability, and durability to meet the requirements of upcoming regulations. As engine certification limits drop to levels of 0.05 g/bhp-hr and below for NOx, it is known that improvements in NOx sensor technology are needed to meet the challenges of monitoring NOx in-use at such low levels, or over the full range of vehicle operations. There is also going to be a need to monitor real fuel consumption as part of CARB's updated Heavy Duty (HD) OBD regulations to characterize in-use CO_2 emissions.

The objective of this research is to evaluate the potential of state-of-the-art and innovative sensor technologies in meeting the monitoring needs for recently implemented and future regulatory programs. The research included the monitoring of NOx, particulate matter (PM), and CO_2 emissions from on-road HDDVs and large off-road diesel engines (ORDEs) using sensors. The NOx sensors included state-of-the-art sensors as well as emerging technology sensors, such as laser-based systems, that are targeted to measure NOx at the much lower levels that are expected with future regulations. The potential of sensors to monitor other pollutants, such as ammonia (NH_3), was also investigated. This research included both a laboratory and a field-testing component. The laboratory testing included bench scale testing to evaluate sensor accuracy, precision, linearity, detection limit, measurement range, cross-species interference, and other metrics, as well as testing at CARB laboratories to evaluate the sensor-based monitoring systems as a whole, as well as the specific component sensors. The field testing included deployment of the sensor-based monitoring systems on 100 HDDVs and 20 ORDEs to characterize the accuracy, stability, durability, and operation limitations of different types of on-board sensors, with a primary focus on NOx sensors, while measuring real-time real-world diesel vehicle emissions. The real-time datasets collected from both HDDVs and ORDEs during the field testing was used to characterize emissions and activity patterns that can be used for regulatory programs and emission inventories, and identify advantages and limitations of using on-board sensors for regulatory programs.

This study built on the University of California at Riverside's (UCR's) Bourns College of Engineering – Center for Environmental Research and Technology (CE-CERT) extensive experience in the area of sensors and data logging, and our OSAR (on-board sensing and reporting) programs, making us uniquely qualified to successfully carrying out this program.

2 Literature Review

This section describes the setup and testing approach for the baseline equipment tested as part of this research..

2.1 Objective

The CE-CERT team conducted a comprehensive review of the sensor technology related literature, as well as information that CE-CERT has acquired through industry and other sources that may not specifically be available in the published literature. The results of this literature were summarized in a report that has been provided to CARB and the project advisory committee (PAC), as well as a list of potential sensors for use in the remaining tasks. This builds on a preliminary information gathering effort that is being done as part of CE-CERT's OSAR study with the SCAQMD. The literature review includes information on both on current state-of-the-art sensors as well as emerging technology sensors, as well as sensors designed to measure a variety of parameters, including real-time NOx, CO_2, PM, NH_3, nitrous oxide (N_2O), nitrous acid (HONO), and vehicle weight measurements. Each of the identified sensors were characterized in terms of detection limits, accuracy, precision, durability, operation range, and cost of the sensors. As NOx sensors are the most critical sensors of need, for NOx sensors, the evolution of their advancement were reviewed over the last few decades, current efforts on-going in NOx sensor development were reviewed, and the potential capabilities of more advanced sensors going out into the future were evaluated. For PM sensors, this included an evaluation and characterization of sensors that are designed to characterize PM emissions based on different properties, such as particle mass, black carbon, particle number, and opacity.

An important element of this study is to determine how effective state-of-the-art and emerging technology sensor was in achieving the monitoring goals of existing and future regulations. To this end, the CE-CERT team reviewed federal and California regulations that include the application of on-board sensors, such as HD OBD requirements, or regulations that sensors and/or mini-PEMS could be used to provide information comparable to laboratory-grade instruments, such as HD I/M programs. This included the identification of different emission characterization metrics (e.g., g/bhp-hr, g/mile, g/hr, g/CO_2, etc.) that are incorporated into the regulations. Part of this included a meta-analysis of existing data from previous programs (many of which were originally conducted by CE-CERT) to evaluate the performance of on-board sensors compared to laboratory-grade 1065-compliant PEMS or mini-PEMS, and to evaluate how effective these sensors might be in characterizing these different emissions metrics. For the meta-analysis, the data from these different studies was analyzed together to look for different statistical relationships. The potential of state-of-the-art and emerging NOx, PM, and CO_2 sensors to meet regulatory requirements was based on metrics that are identified in the regulations, such as the measurement accuracy needed to determine compliance with a particular low-level standard, and to the extent that gaps are found in the capabilities of sensors, the possibility of more advanced technology sensor to bridge these gaps was evaluated.

2.2 Review of Sensor Technology

This section provides a review of the status of current technology sensors, including their operating principles, what sensors are commercially available, and the available literature on performance testing of sensors.

2.2.1 Commercial NOx Sensors

This subsection provides an overview of the status of available NOx sensors, including different types of NOx sensors, different commercially available NOx sensors, and NOx sensor performance tests.

2.2.1.1 NOx Sensor Types

2.2.1.1.1 Operating principle and technology

NOx sensors have been the subject of a number of studies to date (Zhang et al. 2020; Cheng et al. 2019; Tan et al. 2019; Aliramezani et al. 2018; Guardiola et al. 2017; Kotz et al. 2016; L. Yang et al. 2016; Viricelle et al. 2016; Wang et al. 2016; Qiu et al. 2015; Tang et al. 2015; Chou et al. 2014; Ioannou et al. 2013; Querel et al. 2013; Galindo et al. 2011; Hofmann et al. 2004; Schenk et al. 2001). These studies have predominantly used commercial NOx sensors. Generally, these sensors are known to use yttria-stabilized zirconia (YSZ) as the sensing material. YSZ ceramics are known for their high conductivity for O_2 ions at high temperatures, making them a good choice for NOx sensors. These sensors are electrochemical sensors, specifically of the amperometric type. Amperometric systems read the current that is generated as a result of the oxidation or reduction of ions at the surface of the electrodes. An example of these types of sensors can be seen in Figure 2-1, this figure shows a NOx sensor's operation.

As seen in the figure, NOx sensors have two cells. One for oxygen reduction, the other for NO sensing. The first cell reduces oxygen (O_2) out of the sample so it does not cause any interference with the NOx sensing in the second cell. This removal of O_2 from the exhaust gas allows for the detection of O_2 in the exhaust. This cell should also handle the reduction of hydrocarbons and carbon monoxide to avoid any cross-sensitivity issues. Nitrogen dioxide, a component of NOx, is reduced in this cell as well.

After the O_2 removal cell, the remaining exhaust gas diffuses into the second cell where the NOx gas is reduced into nitrogen (N_2) and O_2. Once again, the resulting O_2 is reduced again and this time the oxygen ions are electrochemically read as NOx. By having reduced the NO_2 in the first cell, the sensitivity between NO and NO_2 readings in the second cell is effectively the same, the only time there would be any issues with this method is under a high flow or low temperature exhaust conditions. In these cases, the sensitivity to NO_2 could be slightly lower than the sensitivity to NO.

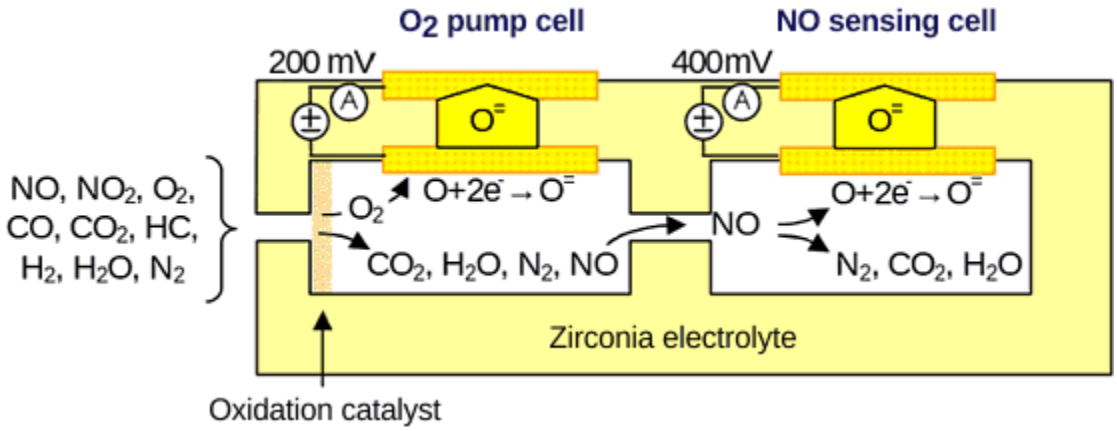

Figure 2-1. Operation of NOx amperometric sensor (Rheaume, 2010)

2.2.1.1.2 Aftermarket NOx Sensors and the main drawbacks of existing sensors

The majority of the aftermarket NOx sensors are fabricated by using the amperometric measurement principle of YSZ electrochemical sensors (8 wt.% Y_2O_3-doped, NTK). NiO-powder (Miura et al., 2006) paste can be applied on the outer surface of the YSZ and sintered at 1400°C to form a sensing electrode. A Pt lead wire can then be wound around the oxide layer to make a good electrical contact. Sensor elements can be fabricated using yttria (Ono et al., 2001; Pohle et al., 2017) and Sr (Sekhar et al., 2010) doped YSZ substrates and screen-printed Pt (Pohle et al., 2017; Sekhar et al., 2010) and Pt-Rh alloy (Ono et al., 2001) electrodes. These designs result in improved sensitivity, selectivity, and response time over conventional mixed potential sensors incorporating a stable three-phase interface using a porous electrolyte coated over a dense electrode.

The main drawbacks of the existing amperometric technology NOx sensors are summarized in the following points:

- Cold start speed: Specific warm-up sensor temperature and exhaust gas moisture levels are required for the NOx sensor to operate efficiently. Light-off temperature for these sensors is in the order of 60 seconds (s). Hence, high NOx emission events during cold-start operation are not monitored effectively, so aftertreatment control systems must rely on imprecise lookup table-based feedforward controllers during the cold-start. The current dew point for most of the NOx sensors is on the order of 150 °C, but sensor manufacturers are looking to develop dew-point free sensors going into the future, which operate from the time the engine turns on without any problems.
- Dynamic response speed: 10% - 90% response time for NOx is 3s while this number can be increased in aged sensor to 4s (Sasaki et al., 2010). High dynamic response during transient engine operation is essential for low NOx engine/aftertreatment technologies. In addition, current technology NOx sensors require a timeframe of 200-300s from when the engine turns on in order to have a good response and accuracy.
- Resistance to cross-sensitivity: Amperometric sensor technology is sensitive to competing species generated either from the combustion (engine-out products) or from the catalyst (for example three-way catalysts (TWCs) or selective catalytic reduction (SCR) catalysts). The most notable case is the presence of NH_3 in the exhaust that has a

1:1 cross-sensitivity (Sur et al., 2022). The cross-sensitivity to NH_3 is caused by the oxidation of NH_3 to NO/ NO_2 in the first chamber (oxygen pump cell) of the sensor. The cross-sensitivity is particularly strong at low concentrations. Since these sensors cannot effectively distinguish NH_3 and NOx emissions, the measured signals cannot be used directly for applications such as post-SCR feedback control systems.

- Low NOx emission detection limits: Detection limits of current NOx technology sensors are in the order of 10 ppm to 5000 ppm in most cases. The accuracy at the lower detection limits is on the order of ±10 ppm NOx. This sensitivity is insufficient for the future stringent ultra-low NOx regulation limits.
- Thermal shock or contamination: Contamination from soot or lube oil may deteriorate NOx sensor output. For example, lube oil additive such as magnesium can poison and lead to permanent sensor damage

2.2.1.1.3 Failure modes

Some of the previously described drawbacks can potentially lead to fault signal (fault modes) generation in the NOx sensors. In general NOx sensor failure modes can be due to electrode heating, ageing of heaters, clogging, damage in diffusion barriers, or combinations of any of these reasons. A summary of the different types of NOx sensor fault modes is given in Figure 2-2, and includes the following:

- Drift fault: A positive or negative change in the linear reaction results in a gain fault.
- Spike fault: The presence of spikes in the sensor output signal can be termed as a spike fault.
- Stuck fault: When the sensor output gets stuck at a fixed value, it can be termed as a stuck fault.
- Offset fault: Changing the zero level of the sensor permanently either to positive or negative levels.
- Slow response: NOx sensors have a response time in order of seconds. If the response time is more than that, it is called a slow response of the sensor.
- Unstable values: When the sensor output changes or oscillates between a high and a low value in slow or occasional intervals, this gives unstable values.

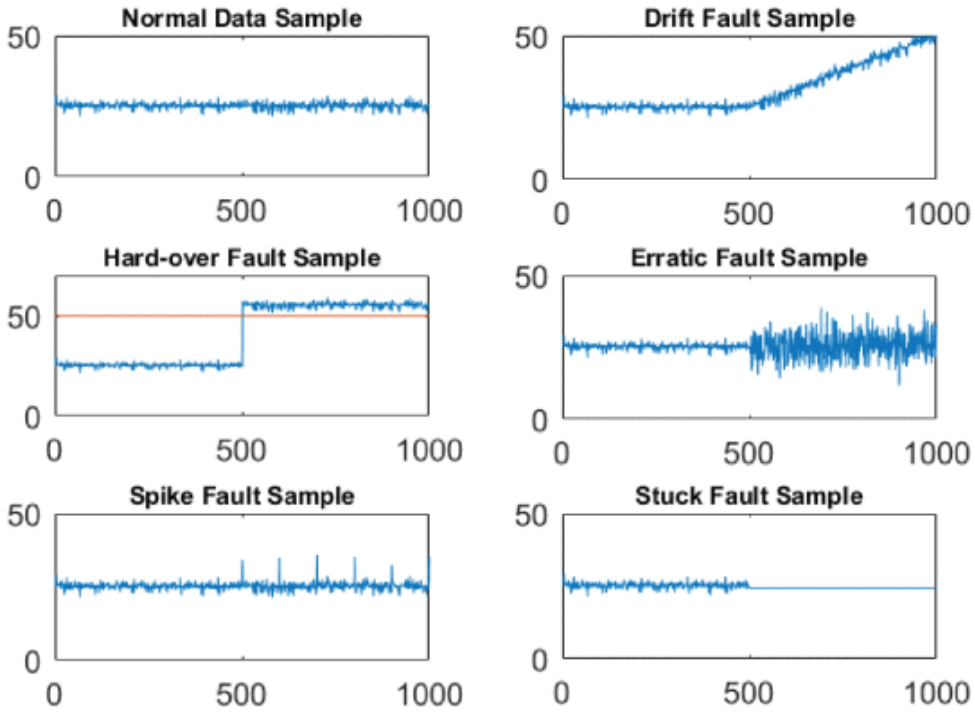

Figure 2-2 Examples of a normal and faulty signals

2.2.1.2 Advanced Emerging Future Sensor Technology NOx Sensors

Working to improve the efficacy of NOx sensors has become more important in recent years with the proposed low NOx engine requirements being implemented and enacted by CARB and the United States (U.S.) Environmental Protection Agency (EPA). Commercial NOx sensors are effective at measuring emissions above 10 ppm. These sensors have a difficult time consistently measuring below this threshold, however (Khalek et al., 2021). So, an importantn need is to develop sensors with lower detection limits. Additionally, research into sensor heat capacity and connectivity innovation will be also beneficial due to the high temperatures within the exhaust plume and ease of use in the field.

Metal oxide NOx sensors are the next step in the development of higher accuracy NOx sensors. Metal oxide NOx sensors, also called Cermet sensors, eliminate ammonia cross-sensitivity issues (Bleicker & Noack, 2016), and have lower limit concentration thresholds that are below 10 ppm NOx (Sasaki et al., 2010). The fundamental operating principle of CerMet consists of two electrodes which relate to each other via a solid-state electrolyte. By applying a constant voltage to the electrodes, an ion flow results, which flows through the solid-state electrolyte. A heater mounted on the rear side of the sensor element brings the electrolyte into the sensitive temperature range. At a constant temperature and with a constant electrode voltage, the resulting sensor current shows a linear relationship to the NOx concentration surrounding the sensor (Bleicker & Noack, 2016). However, the vital feature of this sensor is the selection of a suitable electrolyte material that could provide acceptable sensitivity, selectivity, and stability. For NOx detection, CerMet sensors are mostly based on WO3 (Gouma & Kalyanasundaram, 2008), SnO_2, TiO_2 (Ménil et al., 2000), or In_2O_3 (Kannan et al., 2010). Test results with barium nitrate-based ($Ba(NO_3)_2$) sensors

show excellent NOx sensor sensitivity in the concentration range of 0-60 ppm. However, the optimum performance is achieved when operated atapproximately 360°C (Meyer et al., 2013).

Pulsed-polarization sensor mechanism in YSZ-based NOx sensors is an alternative to complex and higher in manufacturing cost amperometric pumping cells (Pohle et al. 2017). Planar YSZ-based structures can be used for NOx detection based on pulsed-polarization technique. A voltage change is applied to the electrodes for a certain amount of time (t1), followed by a circuit discharge phase (t2). To avoid unilateral charge effects, the voltage charge was repeated with an electrode polarization of opposite sign under the same voltage amplitude, charging (t1), and discharging (t2) durations. The different NOx concentration levels can shift discharge curves to lower voltage values, discharge phase shows a logarithmic dependency on NOx concentration levels. The advantage of planar Pt electrodes on YSZ is that they offer the potential of NOx detection in lower concentration levels (below 10 ppm). However, sensor sensitivity drops significantly in temperatures greater than 400°C due to decreasing resistance and accelerated discharging (Fischer et al. 2014).

One more recent breakthrough in NOx sensing technology has been made by Indrio Technologies by using laser spectroscopy to measure concentrations. This method is capable of greatly lowering the concentration values at which the sensors are able to identify pollutants (Sur et al., 2017). The use of laser-absorption spectroscopy (LAS) was enabled by key advances in the development of optical probes technology, that is suitable for the high-temperature, engine-out exhaust gas environment. LAS prototype sensors have been utilized in both synthetic gas bench (SGB) and chassis dynamometer emission testing. Emission performance with LAS sensor suggests that: (1) the sensor has no cross-interference with key exhaust species (especially NH_3), (2) it can be operated across a wide range of expected vehicle operating conditions, including cold-start/low-load, and (3) it demonstrated detection limits of less than 1 ppm NOx and accuracy that matched the results from Fourier Transform Infrared (FTIR) and chemiluminescence (CLD) reference instruments (Sur et al., 2022).

Field effect transistors (FET) have also been developed for exhaust gas applications. Research at Linköping University has led to FET NOx and NH_3 sensing technologies (Spetz & Bjorklund, 2012). The gas molecules being detected react at the catalytic gate to charge the transistor to produce an electric field and a change in the current flowing through the transistor. The voltage required to maintain a constant current through the transistor is the sensor signal and varies according to the concentration of gas in contact with the gate. The sensor's selectivity to different gases can be controlled by the choice of the catalytic metal and its structure along with the working temperature and operation mode of the transistor (Spetz & Bjorklund, 2012). A good response of NOx was reported with $SrTiO_3$ at exhaust gas temperature conditions around 600ºC (Andersson et al., 2020).

Researchers at the University of New Mexico have been working on mixed potential sensors. These mixed potential sensors combined dense electrodes with a porous electrolyte overcoat to achieve improved sensor sensitivity and improved long term stability. Tsui et al. (2019) evaluated advanced manufacturing techniques in the production and prototyping of mixed potential electrochemical sensors. They have reported on additive manufacturing by ceramic extrusion and metal direct ink writing of two- and four-electrode mixed potential devices for hydrocarbon, NOx,

and NH_3 sensing (Tsui et al., 2019). Increased sensitivity with larger gas reaction impedances, higher platinum (Pt) electrode surface areas, and slower diffusion affects the sensitivity of the sensor to the above-mentioned gaseous species.

Researchers at the Ohio State University have been conducting research in sensor development for several decades. This has included the development and application of NOx, CO, and CO_2 sensors. An important development with respect to NOx sensors has been the use of a temperature-controlled catalytic filter (Figueroa et al., 2005). Pre-conditioning of the analyte gas temperature is thought to be beneficial for any gas-sensing application because it better decouples the local sensor temperature from the exhaust temperature. Since both the sensor and the pre-filter are in thermal contact, the temperature control must be tuned for various environments. This controller tuning in a commercially viable concept can be done with model-based algorithms or artificial intelligence methods.

Apart from the sensing technology itself, signal and network processing between sensors is under development. In 2019, a study of applications of wireless connectivity sources for commercial sensors was conducted. Current sensors rely on CAN connections to the vehicle's ECU via OBD ports, whereas this study investigated the feasibility of wireless, Bluetooth, Arduino storage, and application-based sensing systems (Soufian et al., 2019).

Instead of developing a physical or chemical methodology for sensing, artificial neural network (ANN) techniques learn and get trained using input data of analyte concentrations in order to obtain the relation between the latter and the signal output of a set of sensors. ANN methodology has already been used in amperometric sensor arrays to compare binary mixtures of sulfur dioxide (SO_2) and NOx (Dmitrzak et al. 2020) and NOx and NH_3 (Tsui et al. 2018). Examples of 3-layer fully connected ANNs can identify single and binary mixtures of propane (C_3H_8), CO, and NOx with good accuracy by operating 3-electrode mixed potential sensors in open circuit and current bias modes (Tsui et al. 2016).

2.2.1.3 Commercialized NOx Sensors

2.2.1.3.1 Bosch

Bosch is one of the leading manufacturers of sensors for various purposes. Bosch has been making mechanical pressure sensors for fuel-injection systems since the late 1960s and making lambda sensors since the 1970s. Bosch began the development of electronic sensors in the late 1980s, as the automotive industry began to incorporate more electronics into their vehicles. The microelectromechanical system (MEMS) sensor was the first electronic sensor that Bosch began mass producing in 1995. This mass production was made possible by a plasma-etching process, which became known as the Bosch process. These first 4th generation electronic sensors were primarily used in automotive safety and comfort systems, but they also played a role in running engine management software and complying with tightening pollution regulations. MEMS sensors were deployed in a number of applications, including anti-lock braking systems, electronic stability control, and airbag deployment. The demand for electronic sensors has grown considerably since the 1990s as sensors have become smaller and more powerful, and spread to other applications. Bosch currently manufacturers about 4.5 million sensors a day for a variety of different applications.

The amperometric NOx sensor from Bosch is called EGS-NX 2ndGen and is presented in Figure 2-3. The sensor utilizes a YSZ ceramics electrolyte and operates according to the amperometric double chamber principle, but it has been simplified to some degree. Some of the basic features of this sensor are:

- It has only 6 connection cables instead of 8 in the first version in the Lupo.
- The NOx measurement range is 0-3000 ppm.
- The accuracy is ±10 ppm at 90 ppm.
- The response time is 1800 ms.
- It is specified for 6000 h/186,500 miles (300,000 km).
- It has as working principle the Nernst Principle in combination with ionization.
- It has an additional pin for position detection and sensor is classified in QM system (ASIL).
- It has digital output -CAN bus capable- which enables it for:
    - Standardized protocol (e.g., SAE J1939) or customer-specific CAN.
    - NOx and O_2 signal recorded.
    - NH_3 as an additional contribution to the NOx signal.
    - 125°C environmental temperatures SCU, engine mounting of SCU possible.

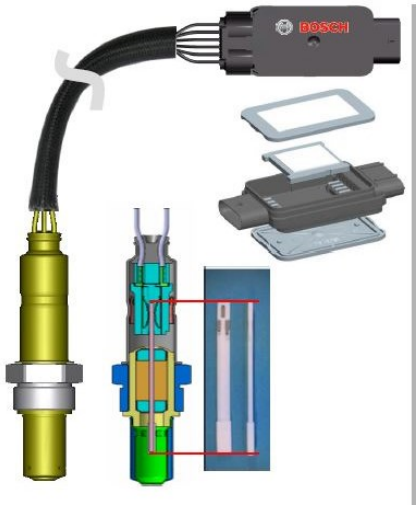

Figure 2-3 EGS-NX 2nd generation NOx sensor

2.2.1.3.2 EmiSense

Emisense Technologies, LLC was formed in 2009 to combine signal processing expertise with technical ceramics fabrication capabilities. This included technologies for both electrochemical gas sensors and electrostatic soot sensors. PMTrac® and NOxTrac® technologies are two main products that EmiSense developed in the 2010-2014 timeframe. The PMTrac® development is discussed in greater detail in section 3.2. Emisense ceased all development on NOx sensors in ~2017. While Emisense has some expertise in using electrochemical NOx (and other) sensors, they are not directly developing or producing an alternative next-generation sensor of our own.

2.2.1.3.3 NGK-spark plugs

NGK Spark Plugs (USA), Inc. was founded in 1966 as a subsidiary of NGK Spark Plug Co, Ltd., Japan. NGK Spark Plugs supplies ignition and sensor products to the automotive, motorcycle, marine and power tool markets. Ignition products include spark plugs, glow plugs, ignition coils and ignition leads that are supplied under the NGK Ignition Parts brand. Its vehicle electronics products, including oxygen sensors, exhaust gas temperature sensors (EGTS), manifold air pressure (MAP)/mass air flow (MAF) sensors and, since 2018, engine speed & position sensors, are all supplied under the NTK Vehicle Electronics brand. Additionally, the company's Technical Ceramics business unit produces fine ceramics, cutting tools and products for the medical industry, under the NTK Technical Ceramics name. Many of these products are supplied via the aftermarket market, through parts wholesalers and distributors. In December 2017, the company announced that it is shifting its focus more towards solid-state batteries, leveraging on its expertise in ceramics. This move was precipitated on the anticipation that EVs will grow to become the dominant mode for transportation, and will gradually displace internal combustion engines where the NTK spark plug and oxygen sensor products are currently used.

An example of a prototype advanced low temperature capable NO_x sensor from NTK is shown below in Figure 2-4. This NOx sensor is designed based on an original equipment manufacturer (OEM) product used for engine control and meeting OBD requirements for SCR systems. The NOx sensor, as shown in Figure 2-5, utilizes an amperometric method similar to that described in section 3.1.1.

Figure 2-4. Picture of NOx Sensor with Ford NOx controller

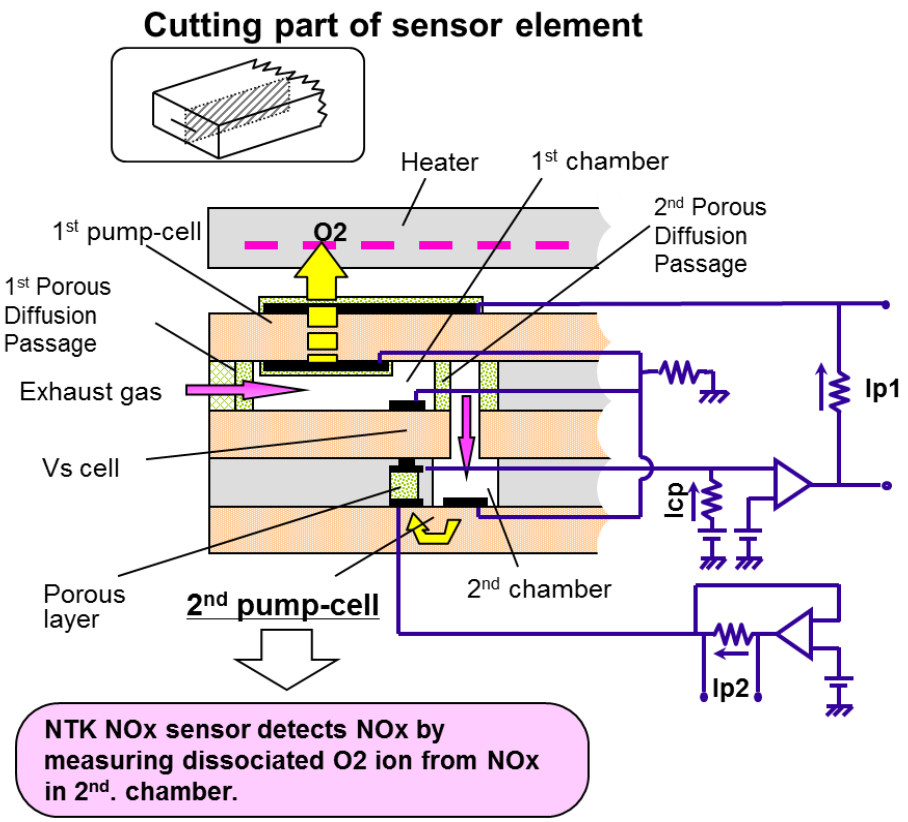

Figure 2-5. NCEM NOx Measurement Design Schematic

2.2.1.3.4 CPK

In 2019, CPK Automotive released an update on state-of-the-art NOx sensors that the company had been working on creating. The sensors were capable of acting as a dosimeter at temperatures of 350 ºC in the ppb range and as a gas sensor at temperatures of 650 ºC in the ppm range. Testing was not done to explore the concentration range of such a device, but the high temperature range performance was promising (Bleicker et al., 2020). CPK subsequently drew down their NOx sensor development efforts, however, in anticipation of a market shift to electric vehicles.

2.2.1.3.5 Denso

Denso is a major supplier of Lambda/oxygen sensors for both OEM vehicle manufacturers and as aftermarket products. Denso supplies sensors to Toyota, Jaguar, Ford, Kia, Daewoo, Lexus, Suzuki, Subaru, VW, Seat and Volvo and many others for OEM applications. Denso also provides a range of aftermarket sensor components under the DOX-* product line that are based on the corresponding OEM products. This includes direct fit models that are fitted with connectors and cables of the appropriate length to directly work in a given application and Universal models that can modified or adapted to an original connector. Denso relies on YSZ electrochemical sensor technology. Denso has also developed strategies to mitigate deterioration of their NOx sensors over the time. This latter was feasible by subduing different mechanisms of deterioration with the use of three methods: (1) controlling the oxygen concentration during the manufacturing process,

(2) increasing the ratio of Rh in the sensor electrode, and (3) the controlled addition of pore-forming materials in the sensor electrode (Kawamoto et al., 2019). More recently, Denso has pivoted its strategic planning away from further NOx sensor development and no further research and development in the field is expected due to the expected expansion of the electric vehicle market. Some of the basic technical specifications for the latest commercially available Denso NOx sensor are shown below:

- It has direct gas flow to the sensor cell and a one chamber structure.
- The residual oxygen is cancelled by a "monitor" cell.
- The measuring range is 0-2000 ppm.
- The NOx sensors measurement accuracy is ±10 ppm at ≤ 100 ppm.
- The response time is 1800 ms.
- The light-off time is ≤ 60 sec

2.2.1.3.6 Vitesco/Continental

The Continental sensor segment, which was spun off to Vitesco Technologies in 2021, was in the sensor development and production market for several decades. Continental began developing NOx sensing systems with integrated electronic controllers in the late 1990s. These sensors were developed in partnership with Japanese company NGK Insulators, which remained the main sensor supplier for Continental and now Vitesco Technologies. This sensor system went into limited production in 2002, with production expanded in 2007 to levels of approximately 250,000 units. This NOx sensor was the first volume-produced emissions sensor capable of directly measuring low-ppm level pollutant concentrations. Previously, emissions sensors had only been capable of measuring excess or deficient oxygen for a given air-fuel ratio. This NOx sensing system is currently incorporated in more than 50 car and commercial vehicle manufacturers models in Europe, the U.S. and Asia. Since its inception, Continental produced over 35 million sensors, and production through its spin off company Vitesco Technologies is expected to expand going into the future to meet needs in applications for direct-injection gasoline engines and SCRs for diesel engines.

The "Smart NOx Sensor" (Figure 2-6) has been developed and manufactured in cooperation between Continental, who supplies the electronic control unit and NGK Ceramics (NGK Insulators), who manufactures the ceramic sensing element. The basic dimensions and design parameters of the sensor are given in Table 2-1. Since 2005, almost all diesel engines with SCR and NOx adsorber aftertreatment systems have been equipped with these sensors. The Smart NOx sensor is available in diverse designs. The most common version for vehicle applications is a 12V sensor with a NOx measurement range of 0-5000 ppm and a 500 kb/s CAN bus. Continental replaced the complex, analog control circuits used in the first NOx sensor by NTK with a fully digital evaluation unit. The solid-state electrolyte element is shown in the Figure 2-6 with both cavities arranged on one level such that far fewer ceramic layers are necessary, which greatly reduces the probability of errors during production. The oxygen reference is not pumped but rather produced via a separate air duct. The heating element is based on a Al_2O_3 substrate with zirconia layers (Khalek, 2019).

Selected parameters for the Continental/NGK NOx sensor are listed in the Table 2-1:

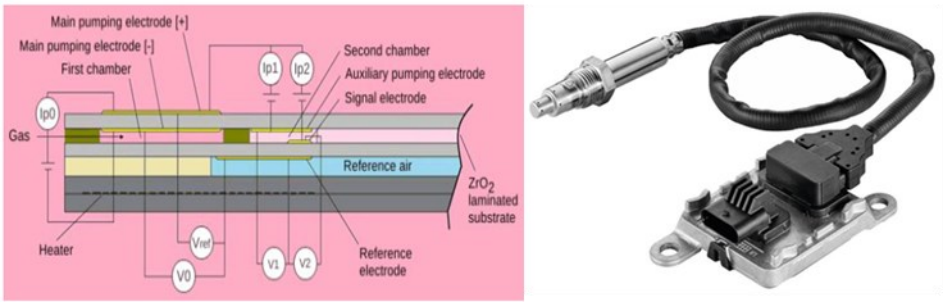

Figure 2-6. The solid-state electrolyte element (left) and continental Smart NOx / UniNOx sensor 5WK9 6614J (right)

Table 2-1 Specifications of Continetal/NGK Ceramics NOx sensor

Measurement principle	Multilayer ceramic sensor made of the yttrium-stabilized zirconia (YSZ) with integrated heater and 3 oxygen pumps	
Supply voltage	11-28V	
Operating temperature	100-800 ºC	
Measurement range	NOx	0-5000 ppm
	λ	0.4 to 0.25
	AFR*	6 to 364
	O_2	0-25 %
Accuracy	NOx	±15 ppm (@0 to 1000 ppm) otherwise ± 1.5 %
	λ	± 0.008 (@ λ = 1) ± 0.016 (@ λ = 0.8 to 1.2) otherwise ± 0.018
	AFR*	± 0.15 (@ AFR* = 14.6) ± 0.4 (@ AFR* = 12 to 18) otherwise ± 1
	O_2	± 0.4 (@ O_2 = 0 TO 2) otherwise ± 0.8

*AFR – Air Fuel Ratio

Vitesco is also working on a NOx sensor for On-board Monitoring (OBM) and emissions control for Euro 7 vehicles. These sensors were evaluated over an RDE route and did not show any underreporting or was able to identify higher emissions events under stop and go driving. The device function as a simultaneous NOx and NH_3 sensor along with a lambda sensor based on the rich/lean conditions of the combustion. The NOx and NH_3 signals are separated based on the lambda signal, with NOx more prevalent under lean conditions and NH_3 more prevalent under rich conditions. The sensor was tested with 3 vehicles with catalyst aged to different mileages, and showed good correlation with an FTIR and an AVL AMA bench. The separation algorithm has also been verified over a full range of applications.

2.2.1.3.7 SenSic

The SenSiC's gas sensor technology has been developed over 20 years of research at Linköping University (LiU) in Sweden and is based on the use of Silicon Carbide (SiC) materials for the

semiconductors and long-term experience with combustion processes. This technology has just recently become viable for commercial production of high-volume, price-competitive products. Unlike existing in sensors on the market, the SenSiC sensors offer full functionality at very high temperatures and harsh environments and can also withstand thermal shocks. Because the sensor semiconductor chip is placed directly in the exhaust gases (in situ), there is no extra cooling delay as with other sensors, and therefore, the response is quick. A single sensor unit can also detect multiple gases as well as pressure. The external control unit is fully software controlled and offers industrial interfaces for programmable logic controllers, as well as low-cost integration within existing control electronics for domestic biofuel heaters. SenSiC also provides sensor control software for customer-produced control electronics. With regards to the NOx/NH_3 exhaust gas detection sensors SenSic has developed a field effect transistor (FET) structure that has a thin catalytic metal film as the gate (G) as depicted in Figure 2-7.

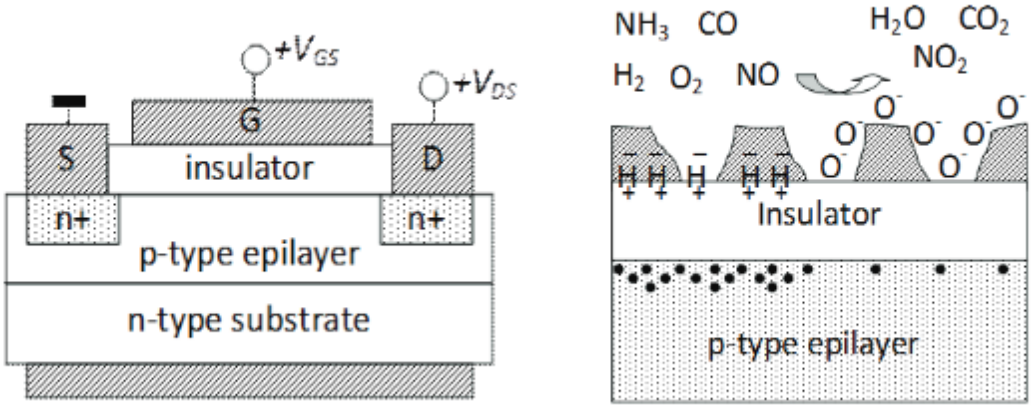

Figure 2-7 Field effect transistor based gas sensor and the mechanism behind its gas-sensitivity (Andersson et al., 2020)

2.2.1.3.8 ECM

ECM has 34 years of experience on ceramic sensor development for exhaust emission measurements. ECM control modules can act as CAN-based components of a mini-PEMS unit. In particular, ECM can provide three different types of NOx sensors:

1. NOx type F sensor: The NOx sensor tip accommodates an NH_3 filter to reduce potential cross-sensitivity with ammonia
2. NOx type T sensor: Type T NOx sensors are recommended for general-purpose NOx measurement for combustion processes that can be rich, lean, and stoichiometric (i.e., spark ignition engines).
3. NOx type G sensor: Type G NOx sensors are recommended for NOx measurement of combustion processes that are only lean of stoichiometric (i.e., diesel engines).

Some general characteristics of the ECM NOx sensor can be found in the following table.

Table 2 Specifications of ECM Ceramics NOx sensor

Measurement principle	Ceramic sensor-based NOx and O_2 analyzer for the development of engines and their aftertreatment systems.	
Supply voltage	11-28V	
Operating temperature	100-800 ^oC	
Measurement range	NOx	0-5000 ppm
	λ	0.4 to 0.25
	AFR	6 to 364
	O_2	0-25 %
	FAR (fuel air ratio)	27 to 1667
	Exhaust pressure measurement range	0 to 517 kPa

2.2.1.4 NOx Sensor Effectiveness

Previous studies have evaluated the performance of Onboard Sensing (OBS) monitoring systems for NOx emissions by conducting simultaneous comparison tests between portable emissions measurement systems (PEMS) and OBS systems (Zhang et al. 2020; Cheng et al. 2019; Kotz et al. 2016; L. Yang et al. 2016; Hofmann et al. 2004). A strong correlation (Pearson's R2) has been seen between OBS NOx concentrations and PEMS NOx concentrations with the original 1-s time resolution. Several studies have suggested correlations between PEMS and OBS system in the 94% to 98% range, including studies by Yang et al. (L. Yang et al. 2016) and (Tan et al. 2019). Other results have shown relatively lower correlations between PEMS and OBS that have ranged from 82% to 90% (Zhang et al. 2020; Cheng et al. 2019; Kotz et al. 2016).

Other researchers have conducted comparisons of NOx emissions measured by NOx sensors and laboratory gas analyzers (Horiba, and CLD 700) under engine dynamometer test conditions (Pohle et al. 2017; Qiu et al. 2015; Ioannou et al. 2013; Galindo et al. 2011; Schenk et al. 2001). Most of the NOx emissions measured with NOx sensors were well correlated with Horiba gas analyzers. For example, several studies reported that the accuracy of NOx emissions from NOx sensors was close to 5% compared to Horiba instruments (MEXA7100D, SGD-710C, and CLA-720MA) (Qiu et al. 2015; Galindo et al. 2011; Gautam et al. 2002; Schenk et al. 2001). Ioannou et al. (Ioannou et al. 2013) found that the accuracy of NOx emissions measured by a NOx sensor was ± 3% compared with measurements with a CLD 700 NOx analyzer. Pohl et al. (Pohle et al. 2017) found a larger deviation between a NOx sensor and Horiba (MEXA 7000) analyzer of approximately 25%.

In other research, Montes (2018) compared these same OBD sensors with the laboratory instruments and found that the sensors on average were within 15% (with a range from -5% to +50%) of the laboratory measurement (Montes 2018). The laboratory NOx emissions ranged from 2.5 to 0.046 g/bhp-hr and the OBD NOx sensor emissions ranged from 2.6 to 0.061 g/bhp-hr. So, the variability between the sensor and the laboratory measurements was considerably less than the day-to-day differences in the vehicle emissions that can be attributed to different driving/operating patterns. Yang et al. (2018) evaluated a prototype NOx sensor from NGK-sparkplugs that was developed to operate at lower temperature conditions than typical commercial OBD sensors and also have improved accuracy (Yang et al. 2018). The ability to operate at lower temperatures is

particularly important, as OBD NOx sensors are typically disabled below 200 °C to prevent humidity damage to the ceramic sensing element. It is important to characterize low temperature operation, however, because this is where some of the highest NOx emissions are generated for SCR-equipped diesel engines (Gieshoff et al. 2000). Yang et al. (2018) evaluated this prototype sensor and found NOx measurements were within approximately ±10% of those of the full 1065 compliance PEMS system over a range of driving conditions and with emissions sources with emission rates ranging from 15 g/bhp-hr to 0.2 g/bhp-hr, including cold start conditions. Tan et al. (2018) also demonstrated the potential viability of utilizing typical on-board diagnostic (OBD) sensors to characterize in-use NOx emission rates. For this study, they evaluated NOx sensor data from 72 HDDVs and found that high NOx emissions were still a common problem in in-use heavy-duty diesel fleets, primarily due to low SCR conversion efficiencies during low temperature operation as well as potentially from malfunctioning SCRs.

The aging of NOx sensors is one more variable that affects sensor effectiveness. Aging refers to the phenomenon where NOx sensors lose their sensitivity over time under high thermal stresses (Siegberg and Killinc 2014). The main reasons for aging can be found below:

- Reduced conductivity due to the tendency of YSZ electrolytes to phase separate.
- Accumulation of Yttrium on/at surfaces, changes in resistance within the NOx sensor, exposed surface areas, and micro-pores resulting from the diffusion of heater metal and electrodes.
- Clogging and poisoning can be also considered as forms of aging (Siegberg and Killinc 2014).

In addition, the placement of the NOx sensor in the aftertreatment layout can affect NOx sensor aging performance. One such study investigated how NOx sensors perform when using different aftertreatment setups (Orban et al. 2005). This study addresses the durability of sensors by assessing the NOx sensor's detection levels over time. The sensors were subjected to engine operation of 6000 hours and they were placed at three different locations. The measured locations were immediately after the engine, in engine-out conditions (location 1), between the DPF and SCR system (location 2), and immediately after the clean-up catalyst (location 3), as seen in Figure 2-8. The sensors located at location 1 degraded less when compared to the sensors located at location 2. After 6,000 hours, sensors at locations 1 and 2 were degraded by 5% to 6% and 7% to 11%, respectively. One possible reason for the difference in sensor degradation is that sensors at location 2 are exposed to lube oil ash, which causes relatively more degradation than the sensors at location 1.

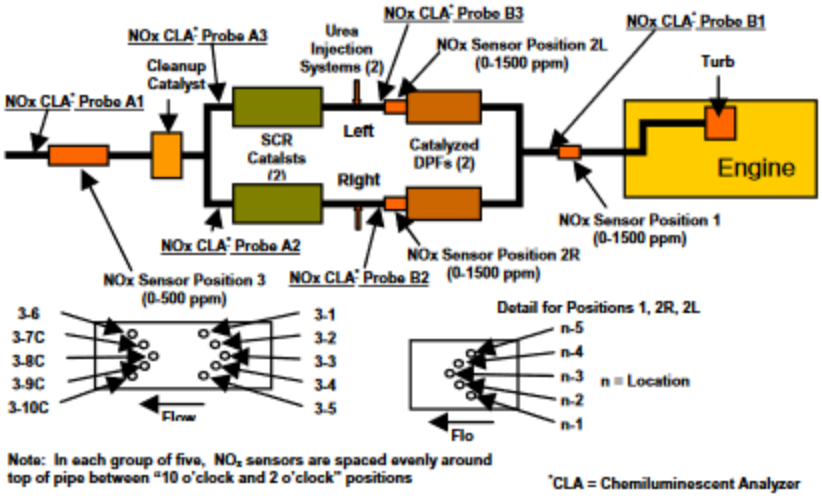

Figure 2-8 Exhaust NO x Instrumentation Layout (Orban et al., 2005)

2.2.1.5 NOx Sensor Monitoring Applications

Various studies have been conducted using NOx sensors to investigate and evaluate whether vehicles meet the latest NOx emission certification standards or real-driving emissions (RDE) standards (Jeong et al. 2022; Söderena et al. 2020; Zhang et al. 2020; Cheng et al. 2019; Tan et al. 2019a).

Cheng et al. (2019) investigated the performance of OBS monitoring of NOx emissions on a diesel freight truck by conducting PEMS and NOx sensor tests at the same time. This study was conducted in conjunction with an OBS pilot program in Beijing beginning in 2018. The experiments used four different test conditions according to the weight load (empty load, half load) and the usage of urea solution (i.e., Diesel Exhaust Fluid (DEF) added, no DEF added). It showed a strong correlation (Pearson's R ~ 0.8) between the NOx sensor concentrations and PEMS NOx concentrations on an instantaneous and moving-average basis. Furthermore, during a simulation of improper SCR operation (no DEF added), where the average vehicle emissions increased from 22 g/kg-fuel to 48 g/kg-fuel, the PEMS and NOx sensor still showed consistent trends. These results suggest that NOx sensors can effectively and accurately identify high-emitting situations for in-use diesel vehicles.

Jeong et al. (2022) compared NOx emissions during lab and on-road conditions between a sensor-based (SEMS) and a PEMS. The comparative study was based on different diesel aftertreatment technologies that included a lean NOx trap (LNT), SCR, and LNT with SCR. The performance of an amperometic NOx sensor, indicated that SEMS technology could be applied for RDE testing. The RDE results suggest a good correlation between PEMS and SEMS data with R2>0.93. However, higher discrepancies between PEMS and SEMS data were found for the SCR and LNT with SCR aftertreatment technology configurations. The reasons for the higher discrepancies for these configurations can be the potential cross-sensitivity with NH_3 due to ammonia slip and the generally lower NOx concentration levels with the SCR/LNT configuration, that can be at the same levels as the SEMS detection limits.

Zhang et al. (2020) conducted technical and policy assessments for state-of-the-art OBM programs that use NOx sensors in China. They collected OBM data from a fleet of OBM-instrumented vehicles and compared it with PEMS data to examine the reliability of sensor-based NOx concentrations. The results showed high data integrity and quality for the OBM systems, and also a good agreement between OBM and PEMS results (an average relative error of ~10%). These results suggested that the OBM approach has the potential to play a central role in in-use emission inspections for HDDVs in China.

Söderena et al. (2020) investigated the NOx emissions of four Euro 6 diesel passenger cars (Euro 6b, Euro 6d-TEMP) in different ambient conditions and over different driving routes with a PEMS and NOx sensors for one year. The Euro 6b car had NOx emissions of 350 mg/km over a non RDE compliant route under urban driving conditions, whereas the Euro 6d-TEMP car had NOx emissions of 81 mg/km and 70 mg/km under the same route during summer and winter, respectively. It also showed that the road infrastructure (crossroads and speed limitations) and cold ambient temperatures could significantly affect to NOx emissions. The study demonstrated that the NOx sensors offer a tool for investigating the day-to-day emissions of diesel passenger cars.

Tan et al. (2019) estimated real-world NOx emissions using NOx sensors to explore the potential for a better regulatory framework to meet emission reduction goals. They collected data from 72 heavy-duty diesel vehicles (HDDVs with an SCR system) operating in various vocations in California. During hot-running and idling operations, they found in-use NOx emissions of 12 heavy-duty diesel vehicles were more than three times the standard. Insufficient SCR NOx conversion was the main reason for the high in use NOx emissions found in the study. The study showed that NOx sensors could be more efficient than laboratory or PEMS testing in characterizing large numbers of vehicles to ensure that the benefits of the emission standards are achieved in-use throughout the entire life of the vehicle by monitoring SCR performance and identifying conditions where high NOx emissions occur.

NOx sensors were also used in studies to evaluate and develop control strategies for an optimized aftertreatment system that could maintain low NOx emissions despite changes in the environmental and real-driving route conditions (Bonfils et al., 2014; Ko et al., 2019; Lee et al., 2021; Wang et al., 2015).

Bonfils et al. (2014) proposed a control strategy for an SCR system using a NOx sensor in a feedback loop. With this strategy, the NH_3 coverage ratio was estimated using of a NOx sensor located downstream of the catalyst. Tests conducted with an engine dynamometer over the New European Driving Cycle (NEDC) test conditions, showed the control strategy led to 68% ~ 81% NOx reduction efficiencies with minimal NH_3 slip

Ko et al. (2019) evaluated the effects of ambient temperature, DPF regeneration, traffic congestion, NOx conversion efficiency, and uphill/downhill sections on on-road NOx emissions for a lean NOx Trap (LNT)-equipped diesel vehicle with NOx sensors installed upstream and downstream of the LNT. The study showed that NOx emissions were higher in the urban section, in congested traffic conditions because of accelerations and decelerations, on uphill sections, at lower exhaust temperatures, and during DPF regeneration conditions.

Lee et al. (2021) investigated NOx emission characteristics of diesel vehicles based on RDE route phase and season with NOx sensors. They conducted RDE tests with NOx sensors on two Euro 6b diesel vehicles - with LNT or SCR - to analyze the effects of seasonal factors and different phases of RDE routes on NOx emissions and the NOx conversion efficiency of the catalyst. Two NOx sensors were placed upstream and downstream of the LNT or SCR. In the study, both vehicles emitted excessive NOx in the winter. Moreover, the NOx emissions were higher by 1.3 to 28.4 times in the urban phase than in the rural or motorway phases in spring/autumn and summer. The NOx conversion efficiency of the SCR was affected by the combined factors of season and phases.

Wang et al. (2015) investigated NOx sensor reading corrections in diesel engine SCR system applications. It was observed that the NOx sensor had a cross-sensitivity to ammonia concentration, and that the cross-sensitivity factor was related to the temperature. These researchers developed an algorithm to correct the NOx sensor reading for ammonia cross-sensitivity. They employed an adaptive-network-based fuzzy inference system (ANFIS) and obtained a reliable relationship between the cross-sensitivity factor and the exhaust temperature.

Other researchers have also used NOx sensors to identify NOx emissions hot spots in communities and find solutions to reduce their impacts (Sato et al. 2020; Kotz et al. 2016). Kotz et al. (2016) showed how spatial emissions mapping techniques using data recorded from NOx sensors could identify systematic and physical causes for in-use emissions from buses over routes with gradients and at different ambient temperatures. They used two 2013 model year transit buses in Minnesota. They demonstrated that NOx hotspots occurred at bus stops, during cold starts, on inclines, and during accelerations. The buses also emitted 2.3 times the route averaged NOx emissions factor at the beginning of each route. The study suggested that spatial analysis with sensor technology could assist with emission-based analysis or regulations such as taxing for certain areas through a practice known as Geo-Fencing, whereby different rules are set based on geographic location.

Sato et al. (2020) focused on analyzing of real-world emissions using NOx/PM sensors and examined analysis methods based on exhaust gas flowrate, CO_2 concentration, and local emissions. They tested a diesel passenger vehicle on a chassis dynamometer to verify the sensor operation. After that, on-road driving tests were conducted. It showed that local emissions of NOx and CO_2 could be analyzed by combining calculated emissions per unit distance and GPS data. With this method, they demonstrated, where and how much NOx and CO_2 was emitted, including hot spots.

Also, Qiu et al. (2015) used a NOx sensor to calculate the fuel injection quantity in a heavy-duty diesel engine (Qiu et al. 2015). A mathematical model was derived from calculating the fuel injection quantity based on the oxygen concentration from the NOx sensor in the exhaust gas. The results showed that the absolute error between the oxygen concentration measured by the NOx sensor and that measured by a gas analyzer at high engine loads was less than 2%. The study demonstrated that the on-board calculation of the fuel injection quantity based on oxygen concentration signals from the NOx sensor could be used at high engine loads.

Table 2-3 Technical specifications of commercially available NOx sensors

NOx sensor suppliers	ECM	Bosch	Vitesco	Siemens VDO / NGK	Cubic Sensor and Instrument Co	Denso	Continental
Operation principle	ceramic sensor	a ceramic sensor with amperometric double chamber principle	ZrO_2-based multilayer sensor with integrated heater	ZrO_2-based multilayer sensor	ceramic sensor	Direct gas flow to sensor cell – 1 chamber structure Residual oxygen cancelled by "monitor" cel	ZrO_2-based multilayer sensor 3 cavity system with 3 pumping electrodes
Measurement range (ppm)	0 to 5,000 ppm 0.4 to 25 (λ) 0 to 25% (O_2)	0–3,000 ppm	N/A	0 to 500 ppm	0 to 1,500 ppm	0 to 2,000ppm	0 to 1,500 ppm
Accuracy (ppm)	from 0 to 200 ppm: ± 5 ppm from 200 to 1,000 ppm: ± 20 ppm ± 2% elsewhere at stoichiometric: ± 0.8%, ± 1.8% average elsewhere (λ) ± 0.2% absolute (O_2)	±7 ppm	for NO < 100 ppm: ± 10 ppm above 100 ppm: ± 10%	from 0 ppm to 100 ppm: ± 10ppm from 100 ppm to 500 ppm: ±10%	from 0 ppm to 100 ppm: ± 10ppm from 100 ppm to 1500 ppm: ±10%	± 10 ppm below 100 ppm	± 10 ppm At low concentrations
Cross sensitivities	1:1 cross-sensitivity to NH_3	N/A	N/A	N/A	N/A	N/A	N/A
Response Time	Less than 1 s (NOx) Less than 150 ms (λ, O_2)	1,800 ms (NOx)	N/A	750 ms (NOx)	1,300 ms (NOx)	1,800ms ≤60s light off time	N/A

2.2.2 PM Sensors

This subsection provides an overview of the status of available PM sensors, including their operating principles, the types of commercially available PM sensors, and PM sensor performance tests. Table 2-4 provides a summary of the current technology of soot sensors based on application and technology.

Table 2-4 List of the current PM sensor technologies

Soot sensor technology	Application			Manufacturers
	DPF soot mass estimate	OBD		
		DPF failure monitoring	PN monitoring	
Delta-P (differential pressure)	✓			Bosch, Delphi, Continental, Sensata, EngineSens
Radio frequency (RF)	✓			GE, Amphenol Corporation, CTS
Accumulating electrode		✓		Bosch, Stoneridge, Continental, Delphi, Electricfil, Denso, NGK, Heraeus
Electric charge		✓	✓	Pegasor, NGK-NTK, Emisense, Continental, Honywell

2.2.2.1 PM Sensor Principles

PM sensors can be generally categorized into 4 types based on the different measurement principals.

Electric Resistance Cumulative Sensors typically operate using several measurement stages and are vertically fitted into the exhaust line. In the first stage, soot is collected on the surface within the sensor via an electric field. In the following stages, the soot builds up on the surface of a ceramic-like plate from aluminum oxide Al_2O_3 or zirconium dioxide ZrO_2 (Kontses 2019), so the change of electrostatic current (Kondo et al. 2011) can be detected and correlated to the exhaust soot concentration. Two or more platinum electrodes are mounted on a ceramic plate with a specific distance between them. When the sensor is clean from soot, the electrical resistance between these two electrodes is infinite. The sensor has a series of different mode stages during operation that are listed below:

- Percolation phase or “deadband” during which the resistance is either infinite or too high (above a specific limit) such that it is too unstable to be accurately measured. During this period the signal is set to zero by the ECM, although smaller amounts of soot are accumulated on the sensor.

- Main loading phase. The resistance between the two electrodes is reduced rapidly due to complete soot dendrites building up between the electrodes
- Regeneration period: When the resistance of the sensor is now below a specified limit set by the ECM, and a sensor regeneration is triggered. Thus, the accumulated soot is oxidized, and the sensor is ready for the next accumulation period.

To protect the sensor element from damage and to eliminate measurement discrepancies due to water condensation in the exhaust, the sensor is activated after the temperature in the exhaust reaches a predefined dew point. Before the activation point, the sensor is in preheating mode. During this period, the sensor is heated (e.g., at 100°C) to avoid particle accumulation due to thermophoresis. Also, during DPF regeneration the sensor is not operated (neither preheating nor sensing), and this is called standby mode.

An upgraded version of resistive sensors are accumulating electrode sensors based on capacitance measurement. Capacitance-based collecting sensors can use an electrode configuration similar to that used in resistive sensors (Kondo et al. 2011). The sensor accumulates soot in DPF-like structure and the operation principle is based on three stages. During the first measurement stage, soot is forcibly collected under an electric field, and a thin soot layer is formed on the surface of the comb-type detecting electrode. In the second stage, soot is naturally accumulated and detected by measuring electrostatic capacitance changes in the comb-type detecting electrode. In the third stage, a heater is utilized to regenerate the sensor. The advantages of capacitive soot sensors are a lower soot detection ability and a lower temperature dependency compared to the regular soot sensors (Hagen et al. 2015).

Charging and Electric Current Sensors directly measure the current from charged particles ions generated by a corona discharge, which is generated around a sharp tip at high voltage. As charged particles leave the sensor, they produce an electrical current through a Faraday cup. Measurement of this current is proportional to the particle concentration (Ntziachristos et al. 2011). These sensors are designed as a flow through the device, and therefore do not have collection systems or contact with particles in the exhaust stream, which is especially advantageous for long-term stability and operation without frequent maintenance. This makes this type of sensor well suited for in-use applications (Besch et al. 2011). Diffusion charging technology is also utilized in particle detection systems, such as PEMS. Even though PEMS diffusion charging technology is PMP compliant for PN testing, the DC method is less accurate than CPC measurements at lower concentration levels (Schwelberger et al. 2019).

Natural Charge Deposition & Release Sensors are based on the natural charge state of exhaust particles and the deposition of these particles on the surface of electrodes having a potential difference between them (Premnath et al. 2020). The fragments produced due to the deposition and aggregation of the charged particles break away and the resulting electrical current can be correlated with the exhaust particle concentration.

Radio Frequency (RF) sensing is another method to detect DPF loading, based on different dielectric properties for different DPF trapped materials (soot and ash), which can be related to differences in ceramic filter structures and/or the air/exhaust medium. Soot and ash accumulation in the DPF affects the frequencies, amplitude, and width of the resonant modes. Comparison between pressure drop measurements and RF sensing measurements suggest that the RF technique is unaffected by exhaust flow variations and exhibits a high degree of sensitivity to DPF PM

loading compared to a pressure drop method, and good dynamic response over transient operating conditions (Sappok et al. 2010). Further research in this area suggests that RF technology could also measure ash concentrations in the DPF with a different sensor calibration (Sappok and Bromberg 2014).

Monitoring Soot via differential pressure sensors are the most widely used method for PM soot estimation and buildup in the DPF. Although not a direct PM measurement, these sensors are currently one of the key elements for PM control on diesel engines. The operating principle is based on the pressure measurements between pre and post-DPF positions. Then the ΔP difference is correlated with soot mass. There is an extensive amount of work regarding the correlation of soot mass accumulation in a DPF with the resulting pressure drop (Schwelberger et al. 2019; Konstandopoulos et al. 2002; Masoudi 2002).

2.2.2.2 PM Sensor Effectiveness

PM sensors are located in harsh and demanding environments in engine-out and post DPF exhaust gas conditions. Impingement of water, post-DPF ash release, and high exhaust gas temperatures, that can reach up to 700 °C (under DPF active regeneration), are some of the more challenging conditions. In addition, ammonia release in the exhaust flow may deteriorate PM sensor performance. Table 2-5 summarizes the exhaust gaseous elements that can potentially deteriorate PM sensor effectiveness.

Table 2-5 List of exhaust gas components that affect PM sensor performance.

Cross sensitivities (elements)	Levels	Direct effect on RT	Remaining effect on RT after short exposure	Effect on RT for sensor lifetime
AdBlue (Urea)	0, 50, 100, 150, 200 ml (on sensing element)	-	(Slightly) increased	-
Ammonia (NH_3)	0-700 ppm (exhaust gas)	(Slightly) decreased	(Temporary) increased	Unaffected
Ash	0-33 g (exhaust gas)	Increased	Increased	Increased

A small fraction of the solid PM engine-out emissions is composed of ash (Kittelson 1998). Ash mainly originates from the lubricant oil and more specifically from the inorganic additives in modern lubricants, which are primarily consumed in the engine cylinder (Johansson 2008). Lubricant-derived constituents include Ca, Mg, Zn, S, Cl, Na and P. Additional, but less significant, sources of ash are the engine wear byproducts, corrosion of engine parts or exhaust lines, metals in the fuel and fuel-borne additives that are used to enhance DPF regeneration (Sappok and Wong 2007). The main constituents of this fraction of ash are Fe, Pb, Al Cr, Cu, Ni, Sr, Ti and Si, which can enter the exhaust stream through a variety of pathways. Impurities in the urea mixture used on modern SCR-equipped vehicles can also contribute to ash build-up.

DPFs in modern diesel vehicles significantly reduce the ash emissions (Vouitsis et al. 2011) and PM emissions (Toumasatos et al. 2022; Samaras et al. 2020). However, ash content is not

combustible and accumulates in the DPF (mostly in the rear channel walls) (Toorisaka et al. 2004). The accumulation of ash over time results to higher backpressures and thus more frequent DPF active regeneration events (Tan et al. 2017). The high ash filtration efficiency in the DPF is beneficial for the durability and contamination resistance of the PM sensor. Nevertheless, ash-slipping events from or through the DPF can be significant during the following situations (Liati et al. 2013a; Baier et al. 2012) that may heavily affect soot sensor operation:

- Cold start operation: During cold engine start, the exhaust gas, line and components temperatures are below the dew point of exhaust gas water. The condensed water inside the DPF can act as carrier of ash particles to penetrate the filter wall and slip downstream of the DPF.
- Clean DPF: A recently cleaned filter with active or passive regeneration, has low filtration efficiency due to the high permeability of filter walls compared to the soot layer permeability (Suresh et al. 2000). Also, during DPF regeneration, particles can escape through the clean walls of the DPF assisted by the high exhaust flow.
- Frequent engine stop and start events: Measurement data proves that a blow-off event is possible, especially for clean DPFs.
- Cracked, damaged or removed DPF: The low filtration can be caused by cracks on the DPF substrate medium or melting of the substrate due to extreme temperature build-up during active regeneration events. Intentional removal of DPF plugs or a DPF brick for tampering reasons can be also a reason for low filtration efficiency. Evidence in cracked DPF cases suggests the release of Ca, Fe, S, Na, K and Zn ash species that are not observed for properly working DPFs (K. Yang et al. 2016). Although it is within the scope of the implementation of the resistive sensor to promptly diagnose DPF damage, partial damage below the OTL can lead to the release of significant amounts of ash, that can have a detrimental effect to the sensor.
- Escape of large agglomerates through DPF walls: Sintered ash can accumulates either in the filter substrate or as individual entities that bind to soot during normal operation (Liati et al. 2013a). The accumulation of ash can grow into larger particles that can block the pores of the substrate and they can escape due to the increased pressure caused by the pore blockage.

2.2.2.3 Commercialized PM Sensors

2.2.2.3.1 Bosch

The Bosch particle sensor technology analyzes the amount of soot particle contained in diesel exhaust emissions by means of a resistance measurement. Based on the values thus obtained, the control unit analyzes the functionality of the DPF. Prior to each measurement, the sensor element is regenerated by heating it up in order to keep the sensor in the same condition for all measurements. Bosch PM sensors are mostly utilized for DPF filtration efficiency monitoring by comparing the actual sensor response with estimates of predicted soot emissions based on a model. Bosch has been developing resistive technology PM (EGS-PM) sensors since 2010 (Ochs et al., 2010). The measurement principle is based on soot particle accumulation, as described in PM sensor principles section. The interval time between the PM sensor regeneration events is 15 – 20 min while the temperature in the sensor during regeneration can reach almost 800 °C. A picture of the latest generation Bosch EGS-PM sensor is provided in Figure 2-9.

Figure 2-9 Bosch EGS-PM latest technology sensor

2.2.2.3.2 EmiSense

Emisense Technologies, LLC developed the PMTrac® in the early 2010s based on a PM sensing technology developed at the University of Texas at Austin (Steppan et al., 2011). In 2014, EmiSense licensed the PMTrac® sensor to Continental Automotive which was acquired by CoorsTek, a leading company in technical ceramics. Under the CoorsTek umbrella, EmiSense continued to work on the development of sensors, sensor components, and complete sensor systems, with applications that include those for gasoline direct injection (GDI) vehicles, China-6b, Euro-7, and other pending regulations. In 2022, a management buyout of Emisense was executed, with CoorsTek retaining an interest in the independent company.

The PMTrac® utilizes electrostatic sensing of particulates to provide a robust and cost-effective in-situ measurement of PM. With a proven resolution to less than 0.5 mg per cubic meter, ePM (tradename PMTrac®) can be used in a wide range of applications where quantification of near-zero PM or PN is required. In combining a low detection threshold with good accuracy and response time, the PMTrac® ePM technology can meet requirements for the new CARB OBD regulations, GDI, Euro-7, and China-7. In contrast, it is doubtful that current generation resistive accumulator sensors, which are used for existing OBD applications, would be able to perform well in these next-generation applications.

The PMTrac® is pictured in Figure 2-10. The basic sensor is a high voltage (~1kV) concentric electrostatic trap. A field directed assembly of soot dendrites result in an equilibrium in which highly charged soot agglomerates exit the sensor, and the charge loss is proportional to the PM mass concentration or PN. The PMTrac® sensor utilizes two electrodes that are put into the exhaust flow stream. These electrodes are protected with a perforated metal shroud. One of the electrodes is put at a voltage of 1000 volts DC. This is known as the field electrode. The other electrode is the sensor electrode, which measures the flux of charged particles created in the electric field. The PMTrac® also has a built in wire-wound heater to periodically burn off soot that has accumulated on the electrodes. Aerosol Scientists from Ford Motor Company have published a paper on the measurement principle for the PMTrac® (Bilby et al., 2016), and have further studied its application for monitoring DPFs (Maricq and Bilby, 2016).

Both independent labs and OEMs have done extensive testing of the ePM technology, establishing solid correlations to reference instruments. Premnath et al., (2020) compared the PM measurements for a PMTrac® with state-of-the-art laboratory particle instruments capable of measuring real-time soot mass and solid particle number and size for a 2011 heavy-duty, on-highway diesel engine. The correlation between the sensors and the reference soot mass concentration was $R^2 = 0.72$ when integrated over 100 second windows and $R^2 = 0.98$ when integrated over the full cycle length. The performance of the PMTrac® was characterized by tests at the University of California at Riverside during chassis dynamometer and on-road tests over a range of steady-state and transient conditions and in comparisons with several PM monitoring instruments (AVL MSS-483, Dekati DMM-230, and TSI DustTrak) (Steppan et al., 2011). For the steady-state measurements, the PMTrac showed a good correlation with gravimetric filter PM measurements (slope = 1.01, $R^2 = 0.93$) with results temperature corrected to the different sampling conditions. The average percentage difference between the 12 PMTrac® sensors and AVL MSS

483 ranges from −8% to −14% for 2 different UDDS driving cycles with standard deviations of 8% and 9%, respectively.

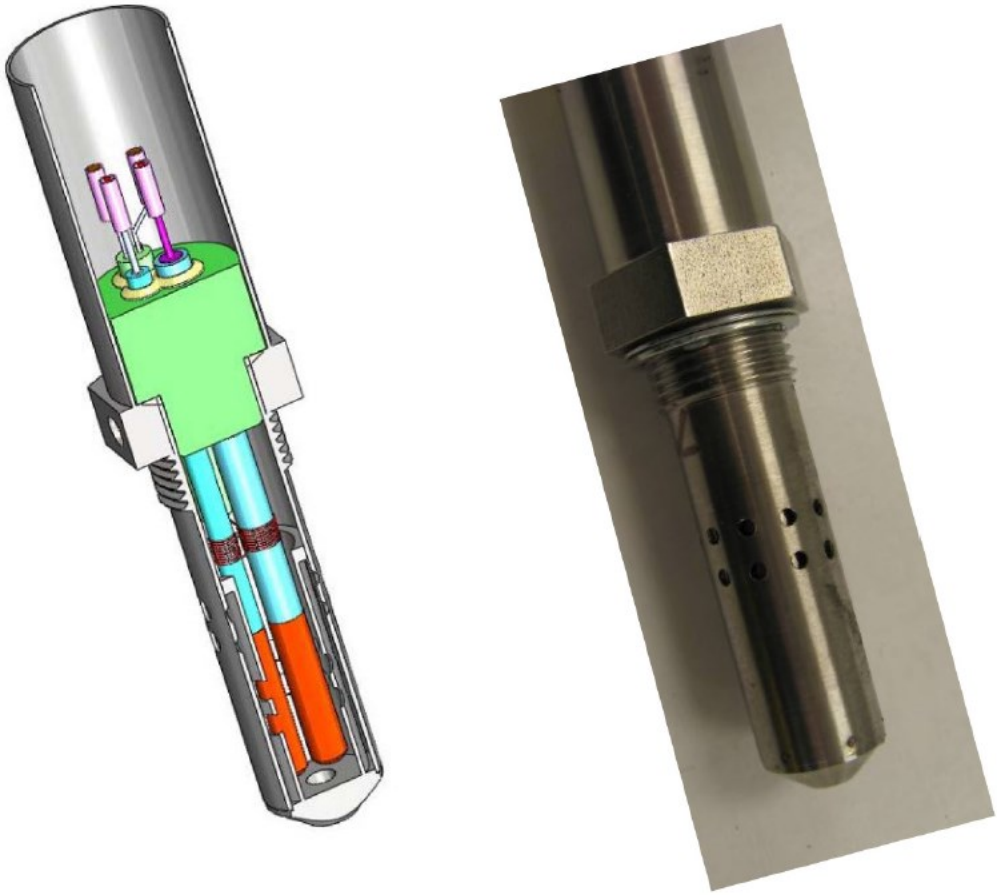

Figure 2-10 Picture of EmiSense electronic soot sensor

2.2.2.3.3 NGK-spark plugs

NGK Spark Plugs (USA), Inc. was founded in 1966 as a subsidiary of NGK Spark Plug Co, Ltd., of Japan. NGK Spark Plugs supplies ignition and sensor products to the automotive, motorcycle, marine and power tool markets. Recently NGK/NTK developed a miniature PPS which is highly portable, cost-effective and integrated into the NGK/NTK compact emissions meter (NCEM) along with NOx and lambda sensors (Rostedt et al., 2017). The PM sensor is based on diffusion charging technology that can support PM and PN measurements simultaneously and in real time. Details of the operation of the PPS and the first results on a diesel engine were presented in recent study with chassis and engine dynamometer dedicated tests (Johnson et al., 2018). These results suggested PM values were within 70% with PM 2.5 for engine dyno tests.

2.2.2.3.4 Denso

Denso introduced a patent on a resistive PM sensor in 2012 (Maeda & Kimata, 2012). The sensor element has a concaved chamber on a PM detection surface of an insulating substrate body, and a detection electrode formed on a bottom surface of the chamber. An insulating protecting layer covers an upper opening of the concaved chamber. The insulating protecting layer has a plurality

of penetrating holes through which only the PM to be detected can pass. Although Denso has a patented technology for PM sensing, Denso is not planning any further evaluation and development of PM sensors in their strategic outlook, as discussed above.

2.2.2.3.5 Continental

Continental applied for PM soot patent in 2014 (Achhammer et al. 2014). The patented soot sensor technology is based on the resistive measurement principle. The measurement electrodes are divided into two regions, a first region in which no soot particles can be deposited and a second region where soot particles are deposited from the exhaust gas flow. The first region and the second region are exposed simultaneously to exhaust. In addition to these resistive soot sensors, Continental has Differential Pressure Sensor (DPS) that can be used to infer the exhaust gas flow through the DPF by measuring the differential pressure across the filter. Unlike the resistive soot measurement technology, which is mainly for PM/PN continuous monitoring, the DPS is only for soot mass estimate and filter failure motoring. The technology provides an analog or digital output voltage proportional to the differential pressure across the filter. At a predefined pressure delta, the engine control unit (ECU) initiates a active DPF regeneration to burn-off the PM accumulated on the filter, restoring good DPF functionality.

2.2.2.3.6 Stoneridge

Stoneridge, Inc. is a publicly traded company (NYSE: SRI) that offers highly engineered sensors and controls for applications in the global transportation industry. SRI has manufacturing operations in North America, Europe, South America, India and China. The Control Devices Division of SRI, with technical design centers located in Lexington, OH and Canton, MA in the U.S., and in Suzhou, China, has been designing and manufacturing sensors and controls for vehicle applications for over 40 years. The Stoneridge PM Sensor is designed for use in automotive exhaust systems to detect the presence of PM. The sensor communicates with the vehicle ECU via CAN, and outputs a linearized PM value based on the electrical resistance measurements. The on-board software automatically regenerates the sensor and performs self-diagnostics, including checks for circuit faults and tampering.

2.2.2.3.7 Borg-Warner

Borg-Warner Inc. is an American automotive supplier headquartered in Auburn Hills, Michigan. The company maintains production facilities and technical systems at 93 sites in 22 countries worldwide (as of June 6, 2022) and has around 49,000 employees. Borg-Warner is one of the 25 largest automotive suppliers in the world. The company has PM sensors for cumulative particulate mass sensing and measurements. The technology is based on electric resistance and can be coupled with OBD. An integrated heater optimizes sensor regeneration across a wide range of operating conditions. The portfolio of Borg-Warner was expanded in 2020 when the company acquired Delphi Technologies.

2.2.2.3.8 Delphi Technologies

Delphi Technologies is a technology company focused on providing electric vehicle and internal combustion engine propulsion solutions, in addition to solving emissions and fuel economy challenges for the world's leading automotive OEMs. Delphi Technologies also provides

aftermarket service solutions for the replacement market. In 2014, Delphi released the electric resistance cumulative type of PM sensors for self-diagnostic purposes in DPF equipped vehicles.

2.2.2.3.9 ECM

ECM developed a PM sensor based on the corona discharge principle. The PM sensor has three concentric metallic bodies: an outer shell, a high voltage electrode (1000 V), and a ground electrode. It operates by allowing exhaust (with PM) to flow through the sensor, where the PM particles become charged and are drawn to opposite polarity electrodes, generating a current. This current reflects the PM density in the exhaust.

The sensor needs its electrodes to be initially coated with soot to achieve functionality, creating dendrite-like structures. These dendrites grow toward each other until they reach a specific distance, called "seeding the sensor." At this point, additional PM striking the dendrites breaks off pieces, carrying charge across the electrodes. The current measured is correlated with PM concentration (mg/m3 and p/cm^3) and stored in a memory chip.

The dendrites can cause different flow-driven dynamics based on the flow that has to be taken into consideration during PM interpretation:

- Transitioning from low to high flowrate temporarily increases the gap between dendrites, causing a momentary PM signal drop. The duration depends on PM density, longer for lower PM levels.
- Transitioning from high to low flowrate decreases the gap, briefly increasing the PM signal as dendrites adjust.
- When the engine stops, dendrites point directly at each other, reducing the gap, and high voltage leads to slow "tree-trimming."

Reseeding the sensor depends on PM density and flowrate, occurring faster with higher PM density and greater flowrate. Deseeding can occur if the sensor is blown out with compressed air, left on in stationary exhaust or air, or exposed to liquid water. The reseeding time varies accordingly.

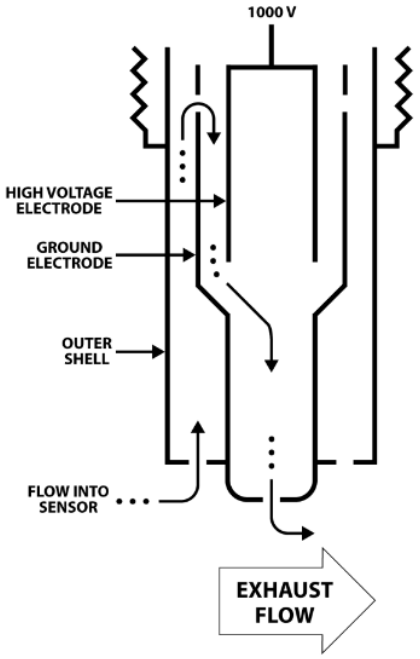

Figure 2-11 ECM PM sensor

Table 2-6 List of future PM /PN sensors for automotive applications

	NGK/NTK (NCEM)		**Miniaturized PPS**		**3DATX parSYNC**		**EmiSence-Continental**		**LII-JKU**		**Stoneridge**	
	PM	PN	PM	PN	PM	PN	PM	PN	PM	PN	PM	PN
Operation principle	Diffusion charge		Diffusion charge		Opacity, Scattering, Ionization		Electrostatic		Adsorption-Laser Induced Incandescence		Resistive	
Sample rate	0.2Hz		0.2Hz		<1Hz		0.1Hz		0.1Hz		0.1Hz	
Maximum range	50mg/m^3	1e+8p/cm^3	800mg/m^3	1e+8p/cm^3	n/a		600mg/m^3	1e+8 p/cm^3	n/a		25mg/m^3	n/a
Particle size range	10-2500nm		10-2500nm		10-10000nm		23-10000nm		n/a		10-10000nm	
Uncertainty	±10%		±8%	±17%	n/a		±10% above 5mg/m^3		n/a		n/a	n/a
Sampling	Sensor in exhaust		Sensor in exhaust		(Heated) sampling line		Sensor in exhaust		Sensor in exhaust		Sensor in exhaust	
Cross sensitivities	None		None		None		Relevant impact of ash		n/a		(see 4.6)	
Size and weight	Sensor: Miniature ECM: <12kg		Sensor: Miniature		3kg		Size of a spark plug		Miniature		Size of a spark plug	
Implication on the use	Continuous operation, needs compressed air		Continuous operation, needs compressed air		Continuous operation, needs replacement of consumables		Needs time to build-up initial dendrites, cross-sensitivity to flow		Not tested in-vehicle, requires cooling		Blind windows for regeneration	
Required time for setup	<1h		<1h		<0.5h		<10min		<0.5h		<10min	
Communication	CAN, ECM in the trunk		CAN, ECM near the sensor		Wireless		CAN, ECM near the sensor		n/a		CAN, ECM near the sensor	

2.2.3 NH_3 Sensors

Ammonia (NH_3) sensors are being developed to provide for direct control of urea injection levels in the SCR systems. Prior to the implementation of NH_3 sensors, NOx sensors were utilized for open-loop SCR control strategies. However, stringent NOx emission limits, the need for higher SCR conversion efficiencies, and the vulnerability of NOx sensors due to cross-sensitivity complicates the use of NOx sensors in closed-loop SCR systems (Willems et al. 2007). During the years of development, several types of solid-state NH_3 sensors have been proposed and examined for measurements in the range of 15-2000 ppm (Romanovskaya et al. 1999). Initial experiments with semiconductors with different concentrations of Au, WO_3, and MoO_3 elements achieved good NH_3 sensing performance in the range of 1-50 ppm (Xu et al. 2000). However, thin-film semiconductors were significantly impacted by other exhaust gas species, such as O_2, NO_2, and H_2O. In particular, changing the accompanying O_2 levels from 1% to 20% decreased the NH_3 response by approximately a factor of 20. In the same manner, a concentration of 100 ppm NO (10% O_2) decreased the NH_3 response by approximately a factor of three, while 1% water vapor decreased it by more than a factor of two (Prasad et al. 2003). Electrochemical, ZrO_2-based ammonia sensors have been under development by NGK Spark Plugs (NTK) (Nishiyama et al. 2003) and others (Elumalai et al. 2008). Results with a YSZ-based sensor attached to NiO/ Au-SE elements suggest NH_3 sensitivity was hardly affected by changes in water vapor concentrations (from 2-11%) in the sample gas (Elumalai et al. 2008). Researchers at Ohio State University evaluated the concept of using a p-type of NiO and n-type In_2O_3 placed side-by-side on a substrate for low level NH_3 detection. This sensor was developed for the possible application for breath analysis (Sun and Dutta, 2016). Researchers at the University of New Mexico have also evaluated mixed potential electrochemical sensors for measuring NH_3, in conjunction with other pollutants, as discussed further in section 3.5 (Tsui et al., 2016, 2019).

The first commercially available ammonia sensor was developed by Delphi (Wang et al. 2008), which is now under Borg-Warner, Inc. The Delphi ammonia sensor operates based on a non-equilibrium electrochemical sensing principle with sensing and reference electrodes exposed to the exhaust gas. The sensing element utilizes co-fired zirconia and alumina layers with NH_3 sensing, a Pt reference electrode, and an integrated heater circuit fabricated into the device to maintain the sensor temperature. Figure 2-12 shows a schematic of the Delphi NH_3 sensor.

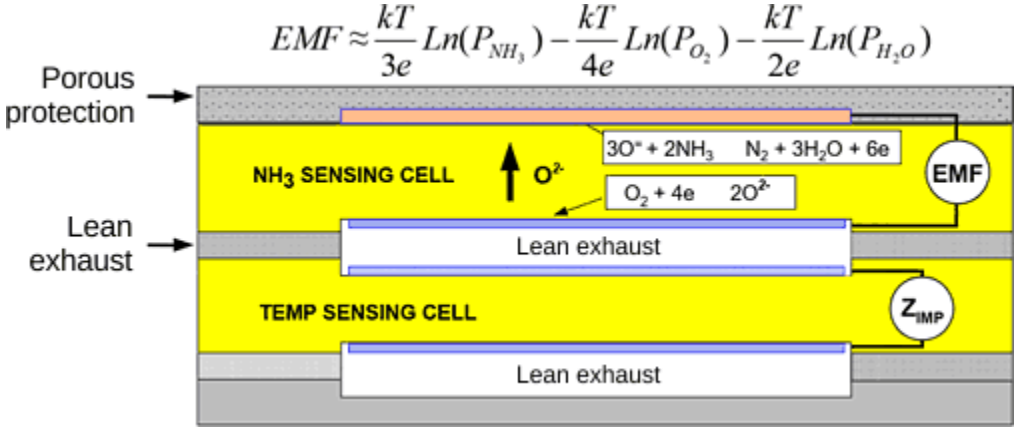

Figure 2-12 Schematic representation of Delphi ammonia sensor (D. Y. Wang et al., 2008).

As with NOx sensors, the NH_3 sensor relies on O_2 ion conductivity to operate. An NH_3 sensing electrode is selective to NH_3 so that only the amount of O_2 ions required to oxidize NH_3 will be conducted from the reference electrode through the YSZ solid electrolyte. The current is then proportional to the amount of NH_3 in the exhaust gas. Both electrodes are exposed to the same exhaust gas.

The Delphi NH_3 sensor is designed to detect ammonia in the range of 0 to 100 ppm. It was reported to be relatively insensitive to interferences from NOx, N_2O, CO and HC. It has, however, cross-sensitivity issues with H_2O and O_2 (Wang et al. 2008). The performance targets include an accuracy of ±5 ppm at 10 ppm NH_3, a T60 response time of 3 s and a T90 response time of 5 s, and a durability of 5,000 hrs / 250,000 km. As was mentioned in the NOx sensors section, FET-based sensors can also be designed for NH_3 sensing applications (Spetz and Bjorklund 2012). By selecting NiO as the gas sensing material, NH_3 can be detected in the temperature range of 425-500°C (Andersson et al. 2020). Preliminary specifications include a 0-200 ppm range, < 1 ppm detection limit, ±3 ppm or ±5% accuracy, and a T90 response time of 1-5 s (Andersson et al. 2020). The technical specifications of the commercially available NH_3 sensors are presented in Table 2-7.

Table 2-7 Specifications of commercially available NH_3 sensors

NH_3 sensor suppliers	**ECM**	**Delphi/Borg-Warner**
Operation principle	ceramic sensor-based	ceramic sensor-based
Measurement range (ppm)	0 to 2,000 ppm For $\lambda > 1$ only.	0–100 ppm
Accuracy (ppm)	± 5 ppm from 0 to 200 ppm	±5 ppm at 10 ppm NH_3
Operating Temperature (degC)	450°C (maximum gas temperature for specified accuracy), 700°C (maximum gas temperature without possibility of sensor damage)	200°C to 450°C. Nonfunctional safe temperature range is -40 °C to 750 °C. Durability
Response Time	Less than 1s	T60 < 3 second and T90 < 5 second. Interface

2.2.4 CO_2 Sensors

Sensors for the measurements of CO_2 are much more limited currently. CO_2 sensing technology is emerging, and CO_2 sensors can be found in the market. The Smart Emissions Measurement System (SEMS), which is basically a series of sensors suitable for automotive light duty applications, incorporates CO_2 sensors. CO_2 emissions concentration determination with SEMS technology, is based on the measured O_2 volume concentration and the fuel C:H ratio (Kadijk et al., 2017). In other words, CO_2 is calculated rather than measured with the SEMS technology. Some recent results on SEMS technology suggest a less than 3.7% difference compared with PEMS RDE reference technology (Heepen, 2019).

Another CO_2 measurement methodology is based on infrared radiation sources that are pulsable thermal emitters with a near black-body emittance (Chowdhury et al., 2016). These particular sensors are based on nondispersive infrared sensor (NDIR) gas analysis. Considering the high output power close to a blackbody emitter and radiation over a wide wavelength range of 2 µm to 20 µm, they are particularly suitable for simultaneous measurement of multiple gases. Researchers at Ohio State University have also evaluated an electrochemical gas sensor using Li_2CO_3 and Li_2TiO_3 + TiO_2 as sensing and reference electrodes, respectively, for CO_2 measurements (Lee et al., 2006).

Infasolid has patented a current measurement based technology CO_2 sensor under the brand name HISsmd (*Thermal Infrared Emitters | IST AG*, n.d.). Infrasolid's HISsmd uses a nichrome (NiCr) filament as a radiation source and thermal emitter. The sensor is manufactured in an surface-mount device technology (SMD) package, measuring only 3 mm by 3 mm. The filament of the HIS180smd fills the entire space of the small SMD package in the radiating area. Their low energy consumption, high efficiency, and miniaturized size make them useful for mobile, portable, and battery-powered applications, such as automotive sensing and testing.

Table 2-8 CO_2 specifications for commercially available ceramic sensors and PEMS

CO_2 sensor suppliers	**ECM**	**Horiba PEMS**
Operation principle	ceramic sensor-based	NDIR
Measurement range (%)	0-20%	0-20%
Accuracy (%)	± 0.15%	within ± 0.3% of Full Scale or within ± 2.0% of Readings (whichever is larger)
Response Time	200ms	Less than 2s (with 2m heated line)

2.2.5 Other Sensors

Sensors have also been developed for other pollutants for vehicle and other applications. CO sensors have been developed for automotive applications. Researchers at Ohio State University have developed CO measurements based on the resistance of thin-films of CuCl upon exposure to CO in reducing environments (Dutta et al., 2002). Adeyemo et al. 2011 developed a chemoresistive ambient CO sensor based on the interaction of CO with hydrous ruthenium oxide. The conductivity of thick films of RuOx(OH)y was found to decrease in the presence of CO in a background of air and this change was reversible. Infrared spectroscopy showed the formation of carbonates in the presence of CO, which disappeared upon replacement of CO with O_2, showing that the reaction was reversible.

Current sensor technology advancements for N2O and HONO exhaust emission formation is limited. Currently, N2O gas detectors are utilized for medical or industrial applications in the form of handheld detectors. The range of N2O gas detectors is 10 – 1000 ppm ("POLI Multi Gas Monitor | Portable Multi Gas Monitor" 2020). HONO is a fundamental atmospheric constituent that leads to the OH radical formation. Currently, there is no sensor development on HONO direct emission from vehicular exhaust emissions (Kramer et al., 2020). Direct spectroscopic measurement of HONO emissions can be made with larger applications of broadband cavity-enhanced absorption spectroscopy instruments (Langridge et al., 2009; Thalman et al., 2015).

Researchers at the University of New Mexico have been developing solid state mixed potential electrochemical sensors that can be used for the measurement of a full range of pollutants, including CH_4, C_2H_6, C_3H_8, H_2., and NOx and NH_3, as discussed above. Mixed potential sensors can be sensitive to gases of interest in 10-10000 ppm range (Tsui et al., 2019). Their mixed-potential sensor design incorporates dense electrodes and a porous electrolyte that helps to minimize heterogeneous catalysis to minimize the diffusion path through catalytically active electrodes, to avoid changes in morphology to control the interface and provide an electrolyte morphology that is stable and reproducible, to exploit differences in O_2 reduction kinetics for the electrode materials, and to have a sensor response that is dominated by electrochemical reactions. These characteristics allow sensor selectivity to be set by application of a bias current. They are working to develop additive manufacturing processes to prototype these devices and designs to achieve 10s of ppm resolution (Tsui et al., 2019). The sensors can be developed for more commercial production using ceramic manufacturing methods. They are also working to develop machine learning methods to optimize the accuracy of the readings. SensorComm Technologies, which is developing the UNM technology for commercial applications, has developed a CH_4 sensors for different applications, including pipeline and other leak detection. Such sensors could be further developed for vehicle applications.

3 Methodology

This section describes the vehicles tested and the OSAR system and its set up and integration, the bench scale laboratory tests to verify the sensor operation and accuracy, the fleet deployment and test vehicles, and the data analysis.

3.1 Test Vehicles

A total of 65 heavy-duty diesel vehicles were monitored as part of this study. These vehicles came from a total of 8 different fleets, with each fleet providing about 8 vehicles, with 100 vehicles being the end goal. The fleets included goods movement fleets, delivery fleets, and a transfer truck fleet. A description of the fleets and overall characteristics of the vehicles is provided in Table 3-1. Heavy-duty diesel vehicles ranged in model year from 2023 to 2013, with an average model year of 2021 and had odometer readings from 632,104 to 12 miles. More detailed information about the test vehicles is provided in Appendix B.

Table 3-1: Test Vehicles

UCR ID	DGM 1	DGM 2	DGM 3	DGM 4	DGM 5	DGM 6	DOR 1	DTT 1
Vocation	Goods Movement	Goods Movement	Goods Movement	Goods Movement	Goods Movement	Goods Movement	Off-Road	Transfer Truck
Model Years	2013 - 2019	2014 - 2022	2023	2015 – 2023	2017 - 2022	2023	NaN	2020 - 2023
Odometer Range	500,000 - 302,000	473,000 - 33,999	24 -12	632,000 - 73,000	584,000 - 10,000	23,182 - 2,603	NaN	175,000 - 57,500
Displacement (L)	12.8	12.8 - 6.7	14.8	12.8	12.8, 14.2	12.9	NaN	8.9
Engine Manufacturer	Detroit Diesel	Cummins, Volvo	Detroit Diesel	Detroit Diesel, Cummins	Detroit Diesel	PACCAR	Cummins	Cummins
Engine Model	DD13	ISB6.7260, D13J425, D13N-425	DD15	DD13, X15	DD13, DD15	MX-13	NaN	L9 370
Number of Vehicles	4	8	4	9	3	18	4	18

3.2 OSAR System

The combined OSAR system includes a NOx sensor, a PM sensor, a GPS, an ECM logger, and a cellular connection for real-time data reporting. The individual components of the OSAR system, as well as the system integration, are described in this section.

3.2.1 Sensors

The key elements of the OSAR system are NOx and PM sensors. The primary NOx sensors used for this study were Vitesco NOx sensors.The NOx sensors used for this system were provided by Vitesco. This is a prototype advanced low-temperature-capable NOx sensor based on an OEM that is designed to meet future regulatory requirements in Europe and the U.S. The NOx sensor detects NOx by measuring O_2 ions created by the dissociation of NOx into N_2 and O_2 in the detection chamber. The design used for this specific sensor dissociates NO_2 to NO and O_2 in a trap layer before the gases reach the detection portion of the sensor. As NO_2 is broken down directly to NO in a 1 to 1 ratio prior to the detection chamber, the sensitivity to NO and NO_2 is essentially the same. Only under conditions where there is a very high gas flow rate or very cold gas that the heater cannot overcome, would the ratio in sensitivities start to diverge from 1:1. In these cases, the sensitivity to NO_2 could be slightly lower than the sensitivity to NO.

Figure 3-1. Picture of Vitesco NOx Sensor

The PM sensors used for the OSAR system were provided by Emisense Technologies. These sensors utilize electrostatic technology to provide accurate, real-time PM measurements. This PM sensor is shown in Figure 3-2. The sensor works by allowing charged soot dendrites to form on the sensor element. A venture tip draws a small extract of the exhaust gas that passes through an electrical field between the electrodes, which is the measuring path. A field directed assembly of dendrites/filaments agglomerates particles with a high charge density at the filament tips. Overtime, these charged soot dendrites break off and the charge loss, as determined based on a measured current, is proportional to the particulate matter mass concentration as well as particulate number. The design has a response time ranging between 0.1 seconds and < 5 seconds, with the longer time frame used for calibration. The accuracy for these sensors averages at ± 10% for most applications.

Figure 3-2: Emisense Electrostatic Particulate Matter Sensor

The CO_2 sensors that were intended to be used for this project were used on natural gas vehicles initially and since the sensors were not calibrated to be used on the natural gas product, they had issues and were unable to be used for this project. The sensors were not calibrated as well.

3.2.2 Engine Control Module (ECM) Data Collection

The data acquisition system used for this set up was a "EmTrac-6 Onboard Telemetry System Rev. 1" data loggers, developed by Emisense Technologies specifically for this program. The data acquisition system includes printed circuit board components with an enclosure, interconnection, and cabling that were both electrically connected to the ECM logger. The data logger is an Advanced RISC [reduced instruction set computer] Machine (ARM)-based unit with two CAN buses, four analog inputs, an onboard K-type thermocouple amplifier, and a global navigation satellite system (GNSS) receiver for location information. Data is logged locally to an onboard MicroSD card and can be retrieved from the unit using either WiFi or by having data auto posted to a server via the onboard Internet of Things (IoT) (LTE Cat. M1 or Cat. NB1) radio. The data loggers communicate with the engine's ECM/OBD through industry standard communication protocols.

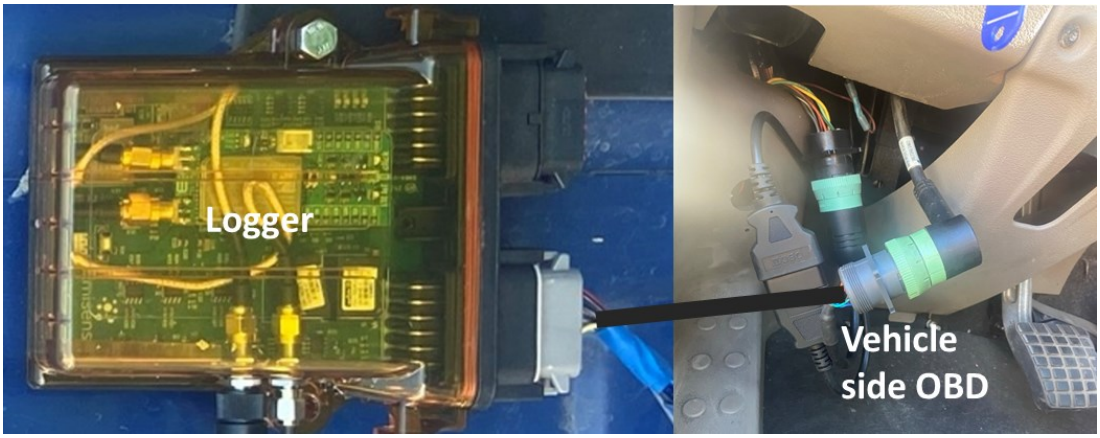

Figure 3-3 Data logger, connection cables, and installation for the ECM monitoring

A list of the data that was collected is provided in Table 3-2. The OSAR system was set up to collect ECM parameters at a frequency of 1 Hz. This speed was selected as previous studies have indicated that higher frequency collection rates can overload the CAN buses. UCR has found that a data rate of 1Hz for less than 200 parameters was a safe request rate and sufficient for the data desires of study. For this study, for the ECM data, a set of nearly 40 parameters was used with a 1 Hz data rate. The data loggers are also equipped to collect GPS data at a frequency of 1 Hz. The GPS can measure the vehicle's location (latitude and longitude) and altitude, from which speed and road grade can also be derived.

The data loggers were configured to be self-triggering to automatically start an hour before a vehicle's scheduled start time to capture cold start data. This configuration was based on talking to the fleet manager about the typical time when the vehicles began operation in the morning and adjusting the data logger programming accordingly. The data loggers were also configured such that there was a two-hour extension in the data loggers shutting off. This shut-off extension was used to ensure that the unit would be "on" for essentially the full day, even if there are multiple events where the engine is shut off, such that the start emissions for each engine-on event were captured.

Table 3-2. A Subset of Data That Was Collected from Each Heavy-Duty Vehicle[1]

Vehicle and Engine Information	ECM Data	GPS Data
Vehicle model year VIN number Vehicle weight and GVW Engine make Engine size Engine model Engine model year Fuel capacity (Appendix A)	Vehicle speed Engine horsepower, RPM Fuel rate Engine percent load Engine percent torque and ref Engine intake manifold temp Temps, SCR and DPF Engine coolant temperature Engine oil temperature ATS intake/outlet NOx	Speed Latitude Longitude Altitude Date & time Engine on/off

[1] This is a subset of data and actual data files may include more than 40 requested parameters, see Appendix A. Not all data was available on each vehicle model year, application, and equipment type.

3.2.3 System Integration and Setup

CE-CERT worked with Emisense for the integration of the OSAR system. The acquired sensors and ECM logger were interconnected into an operational telemetry-based sensor-based OSAR PEMS that was used for the field demonstration, as described below. The functionality of this system included a connection to the vehicles ECM/OBD and GPS, in addition to the emissions sensors, on-board data recording, a cellular option, and Wi-Fi connectivity. The NOx sensor and ECM data logger were electrically connected through a data acquisition system. A picture of the system components is shown together in Figure 3-4, with the data logger shown designed to acquire signals from the sensors, ECM, and other non-ECM related inputs.

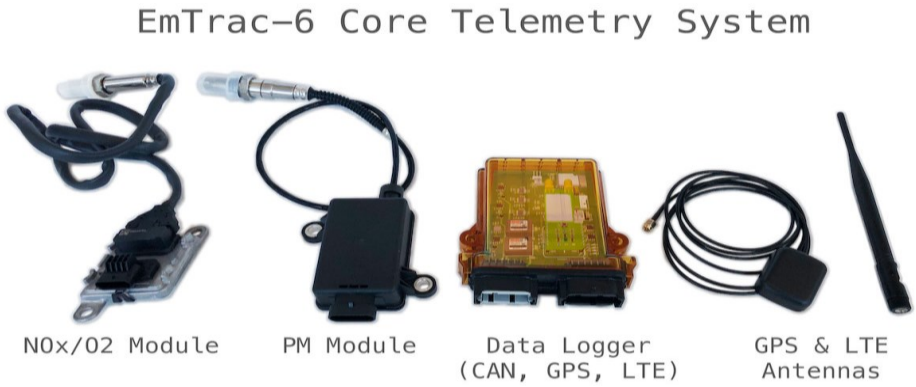

Figure 3-4. Picture of Sensor-based OSAR system[1]

3.3 OSAR and Sensor Validation

3.3.1 Sensor Calibration Methodology

For the system validation, a series of bench scale evaluations were conducted before and after an install was completed. The sensor calibration tests provided information on the accuracy, precision, linearity, detection limit, measurement range, cross-species interference, and other metrics for the individual pollutant sensors that were incorporated into the OSAR system. The bench scale tests were conducted initially with CE-CERT's sensor evaluation laboratory, which was developed previously for the evaluation of PM and NOx OBD sensors by Emisense according to typical industry standards (Cui, et al., 2018). Final calibrations were conducted with a more real-world set up that utilized an emission source and a reference instrument to evaluate the functionality of the NOx sensors as well as validate the startup, data logging, performance checks, and robustness of the OSAR units prior to reinstallation of the units into the field.

The initial calibrations used a NOx emission simulation system. This system was developed to evaluate commercialized and laboratory fabricated NOx sensor responses at typical NOx concentrations. This set up, called the High Flow Bench (HFB), included MKS mass flow controllers, a programmable furnace, inputs for several gas species, as shown in Figure 3-5. A gas

[1] **PMTrac® electrostatic PM/PN sensors and the NGK/Vitesco NOx/O_2 sensors**

manifold was developed to allow different concentrations of NO, NO_2 and O_2 to be utilized. A furnace is used to heat up the manifold to temperatures up to 200°C. This test stand is designed to provide various concentrations of NO, NO_2, O_2 and NH_3 at flow rates between 20L/min and 40L/min with water concentrations of 8%. There are a total of 4 test ports that can be used to simultaneously test up to 4 sensors. All the NOx and O_2 concentrations are controlled by MKS mass flow meters. This test stand is programed by a LabVIEW program that allows the gas concentrations to be automatically adjusted from a computer. Water vapor was added to the gas stream using a Bronkhorst Controlled Evaporator Mixer (CEM) and a Bronkhorst liquid flow controller (LFC). A Fourier transform infrared (FTIR) spectrometer was used to read the gaseous (NO, NO_2, NH_3, H_2O, and N_2O) values as a reference using a line that branches off from the test pipe to the FTIR. The gas stand and analysis methods have been used on several projects with a commercial sensor partner EmiSense, and it has been verified and demonstrated to be well controlled.

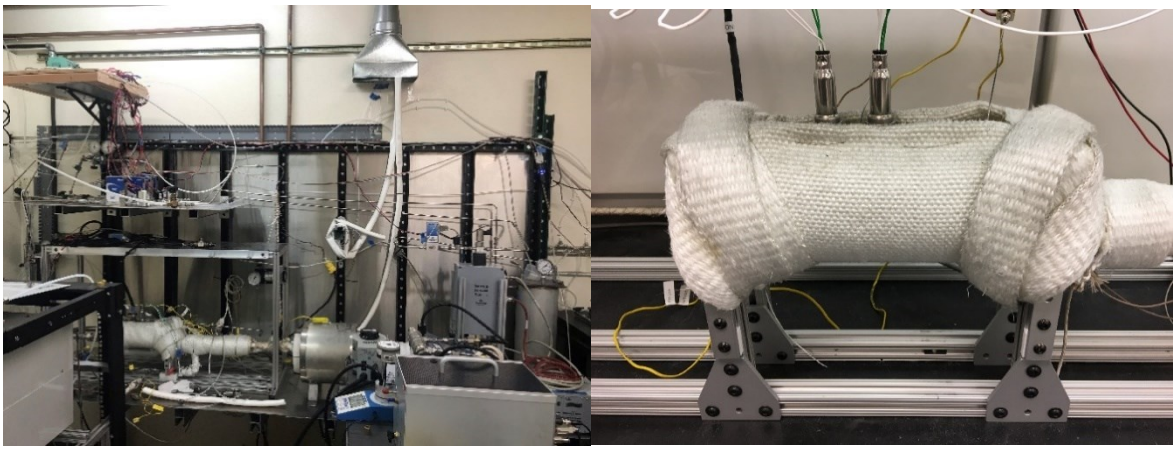

Figure 3-5. High Bench Flow

The second method of calibration was performed using an emissions source and a reference instrument. Figure 3-6 shows an example emission source and reference instrument with the sensors installed in a piece of exhaust pipe. This method allowed for up to 5 simultaneous calibrations of the NOx and PM sensors. The emission source was loaded in specific steps and the measurement of this source by the reference instrument, a PEMS unit or a PG350 unit, depending on availability, was compared to the NOx sensors. Unfortunately, due to the length of the exhaust piece, the PM sensors were unable to be appropriately compared to the reference instrument because they could not get hot enough. A heated wrap (shown in Figure 3-6 on the right) was attempted to be used but the appropriate temperature was unable to be reached. Originally, a vehicle was used as the emission source but due to maintenance issues, a diesel generator attached to CE-CERT's Mobile Emissions Lab (MEL) and a blower were used to generate the emissions steps required for calibration.

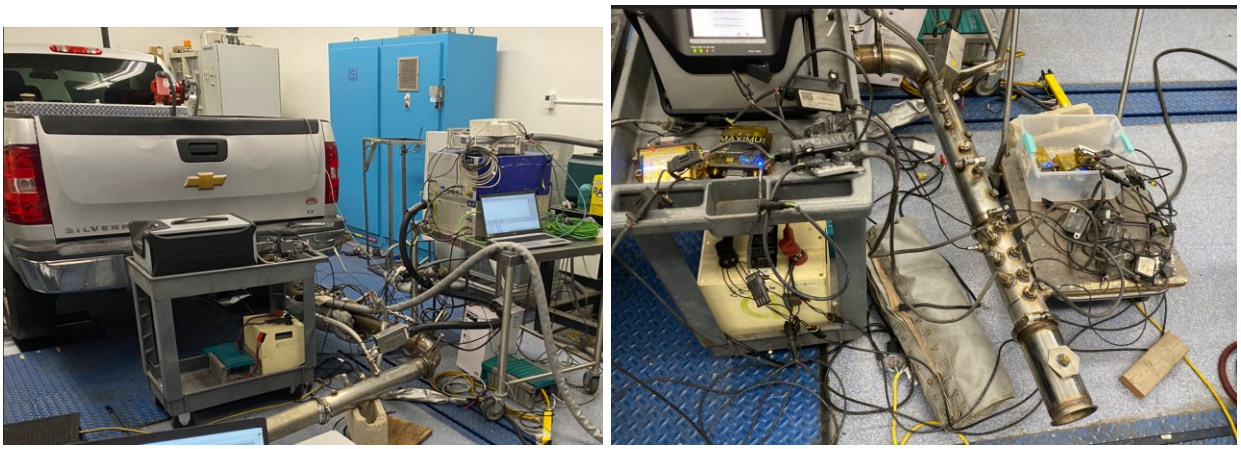

Figure 3-6. Emission Source and Reference Instrument with Sensors Installed

3.3.2 Sensor Calibration Test Matrix

The sensor calibration test matrix was designed to evaluate the accuracy of the sensors. The matrix performed on the sensors included tests for accuracy for both NO and NO_2, for cross sensitivity, and for repeatability. The sensors were initially calibrated utilizing the test matrix in

Table 3-3. The test matrix evaluated NOx sensors over varying concentrations of NO by ramping up from 0 to 100 ppm in eight steps and then ramping back down from 100 to 0 ppm in eight steps. The matrix also had a four-point linearity test for NO_2 from 0-50 ppm, a cross sensitivity test between NO and NO_2 at different blends, and then a final repeatability test where repeat measurements were made at concentrations of 0, 10, and 100 ppm for NO and of 0, 10 and 50 ppm for NO_2. This matrix was performed at two oxygen concentrations (8% and 10.5% O_2) and one water concentration (6%). A similar plan was used for the second method of sensor calibration, with the test matrix shown in Table 3-4. This method included 13 steps at varying levels of load on the emission source and the load was maintained for 120 seconds total to allow for any stabilization period and to allow for a good averaging period. The oxygen and water percentage were not explicitly controlled due to the emission source being more representative of the real-world operation these sensors would be operating under.

Accuracy, for this work, is defined by looking at the concentration differences between the reference instrument and the sensor measured values. A linear regression was performed between these values to provide a mathematical comparison of these differences. In addition, the slope, intercept, and correlation coefficient (R^2) of the linear regression were calculated for each sensor over the different steps. A 30 second average of the concentration values at each test point was used for the linearity regressions discussed below.

Table 3-3. Initial Calibration NOx Sensor Test Sequence for the Sensors on the HFB

Segment	Total Flow (LPM)	O_2 (%)	NO (ppm)	NO_2 (ppm)	NH_3 (ppm)	H_2O (%)	Duration (s)
1	40	8.0	0	0	0	6	120
2	40	8.0	5	0	0	6	60
3	40	8.0	10	0	0	6	60
4	40	8.0	17.5	0	0	6	60
5	40	8.0	25	0	0	6	60
6	40	8.0	50	0	0	6	60
7	40	8.0	75	0	0	6	60
8	40	8.0	100	0	0	6	60
9	40	8.0	0	0	0	6	60
10	40	8.0	0	10	0	6	60
11	40	8.0	0	25	0	6	60
12	40	8.0	0	50	0	6	60
13	40	8.0	0	0	0	6	120
14	40	8.0	10	25	0	6	60
15	40	8.0	25	10	0	6	60
16	40	8.0	10	10	0	6	60
17	40	8.0	25	25	0	6	60
18	40	8.0	0	0	0	6	120
19	40	8.0	10	0	0	6	60
20	40	8.0	100	0	0	6	60
21	40	8.0	0	0	0	6	60
22	40	8.0	100	0	0	6	60
23	40	8.0	10	0	0	6	60
24	40	8.0	0	0	0	6	60
25	40	8.0	0	10	0	6	60
26	40	8.0	0	50	0	6	60
27	40	8.0	0	0	0	6	60
28	40	8.0	0	50	0	6	60
29	40	8.0	0	10	0	6	60
30	40	8.0	0	0	0	6	60

Table 3-4. Second Calibration Test Matrix with Emission Source

Point	Step	Blower Setting	Loading Description	Duration (min)
1	Idle	100%	Generator on, no equipment on	10
2	Low	100%	Generator on, MEL on	3
3	Mid	100%	Generator on, MEL on, Oven on (x2)	3
4	High	0%	Generator on, MEL on, Oven on (x2), AC on (x2)	6
5	Mid	100%	Generator on, MEL on, Oven on (x2), AC off (x2)	3
6	Low	100%	Generator on, MEL on, Oven off (x2)	3
7	Idle	100%	Generator on, no equipment on	3
8	Low	100%	Generator on, MEL on	3
9	Mid	100%	Generator on, MEL on, Oven on (x2)	3
10	High	0%	Generator on, MEL on, Oven on (x2), AC on (x2)	6
11	Mid	100%	Generator on, MEL on, Oven on (x2), AC off (x2)	3
12	Low	100%	Generator on, MEL on, Oven off (x2)	3
13	Idle	100%	Generator on, no equipment on	3

3.3.3 Sensor Calibration Results

Figure 3-7 and Figure 3-8 show example regression plots for the initial and final NOx sensor calibration methods. The plots average 30 seconds of data at set concentrations to analyze how well the sensor data matches the reference data. Table 3-5 show results of the linear regression between the reference instrument and the sensor readings for a subset of the sensors that have completed a pre-install and post-install calibration. The intercept ranged from 0.9 to -6.4 for the initial calibrations and -0.8 to -7.5 for the final calibrations. The R^2 ranged from 0.917 to 1.000 for the initial and final calibrations.

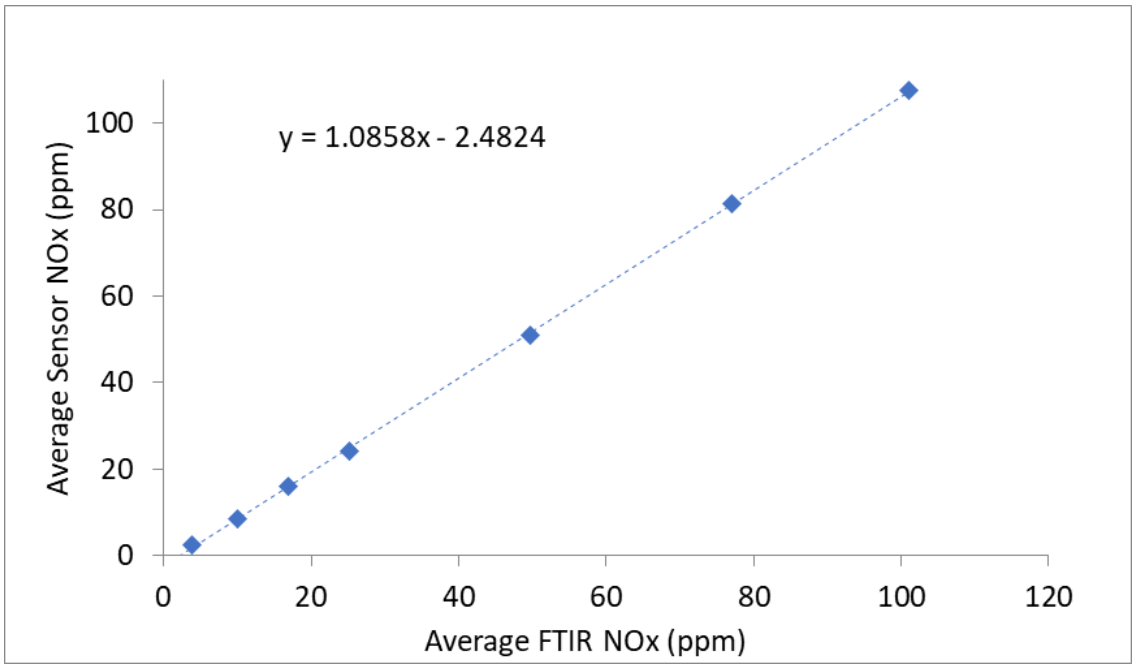

Figure 3-7. Average Initial Calibration Regression

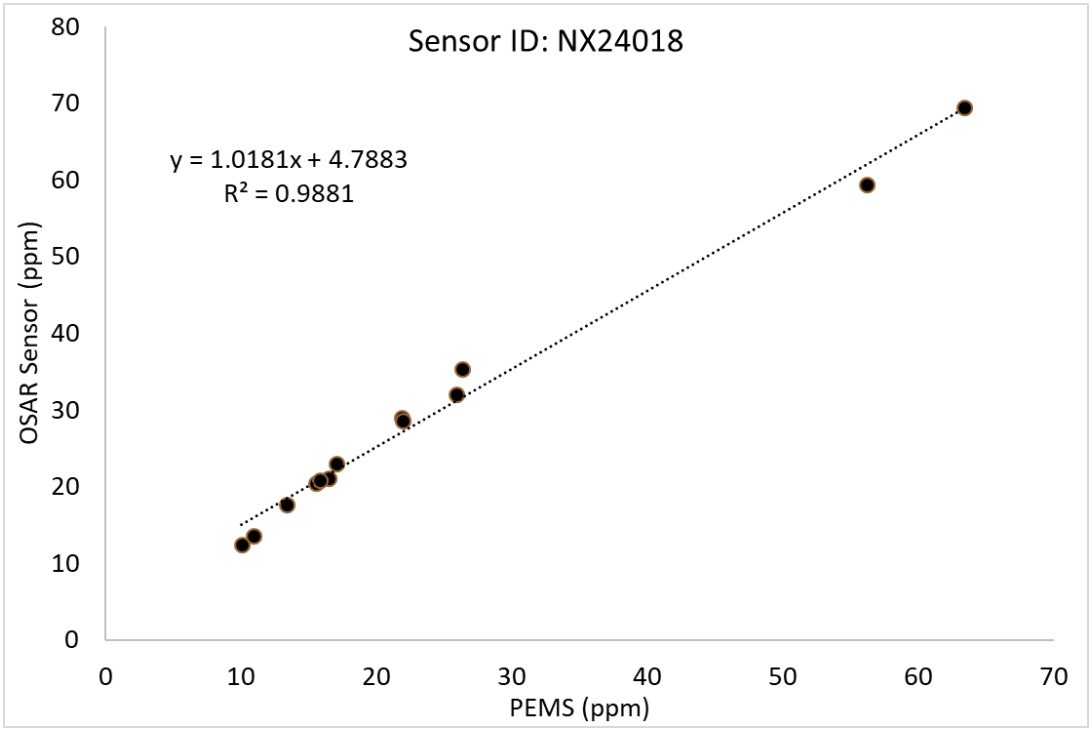

Figure 3-8. Average Final Calibration Regression

Table 3-5. Subset of Calibration Results for the NOx Sensors

Sensor ID	Date of Initial Calibration	Install Date	Date of Final Calibration	Initial			Final		
				Slope	Intercept	R^2	Slope	Intercept	R^2
NX23052	8/19/2024	8/21/2024	2/6/2025	1.05	-1.1	0.957	0.85	-0.8	0.967
NX23053	6/27/2024	7/31/2024	8/19/2024	1.05	-6.4	0.992	1.07	-4.0	0.982
NX23058	2/14/2023	6/2/2023	5/24/2024	0.84	1.0	0.999	0.86	3.7	0.917
NX23059	5/24/2024	6/14/2024	8/8/2024	0.82	1.7	0.947	1.06	-7.5	0.974
NX23060	2/13/2023	1/8/2024	8/8/2024	0.71	1.0	0.999	1.07	-4.6	0.937
NX23061	8/8/2024	8/16/2024	2/6/2025	1.10	-6.4	0.985	0.79	4.8	0.986
NX23066	2/14/2023	1/9/2024	8/8/2024	1.20	1.0	0.999	1.09	-6.1	0.959
NX23069	2/22/2023	12/20/2023	6/13/2024	0.85	1.0	1.000	0.98	0.5	0.960
NX23072	6/27/2024	7/28/2024	11/26/2024	1.05	-5.4	0.996	1.04	2.0	0.989
NX23074	2/14/2023	12/19/2023	6/27/2024	0.95	1.0	0.999	1.06	-1.6	0.997
NX23075	2/14/2023	1/14/2024	8/8/2024	0.76	1.0	0.999	1.11	-4.7	0.947
NX23077	2/14/2023	1/9/2024	6/27/2024	0.99	1.0	0.999	1.04	-2.0	0.998
NX23081	2/23/2023	10/4/2023	6/27/2024	1.15	0.9	0.999	1.01	-7.4	0.993
NX23087	5/24/2024	7/21/2024	2/6/2025	0.76	-1.9	0.956	1.04	0.7	0.995
NX23090	8/19/2024	8/20/2024	10/31/2024	1.03	-1.0	0.946	0.93	1.3	0.995

Real-time plots are provided in Figure 3-9 and Figure 3-10 for the initial and final calibration methods, respectively. These plots show the steps in the test matrix. The black line shows the NOx values determined by the FTIR, while the red line shows the NOx values determined by the sensors. While the data does show some noise in both the reference and NOx sensor measurements, on average, the concentration measurements show high accuracy between the reference and NOx sensor values. Additionally, the real-time data shows fast response times, as seen in the nearly vertical transition periods between concentrations.

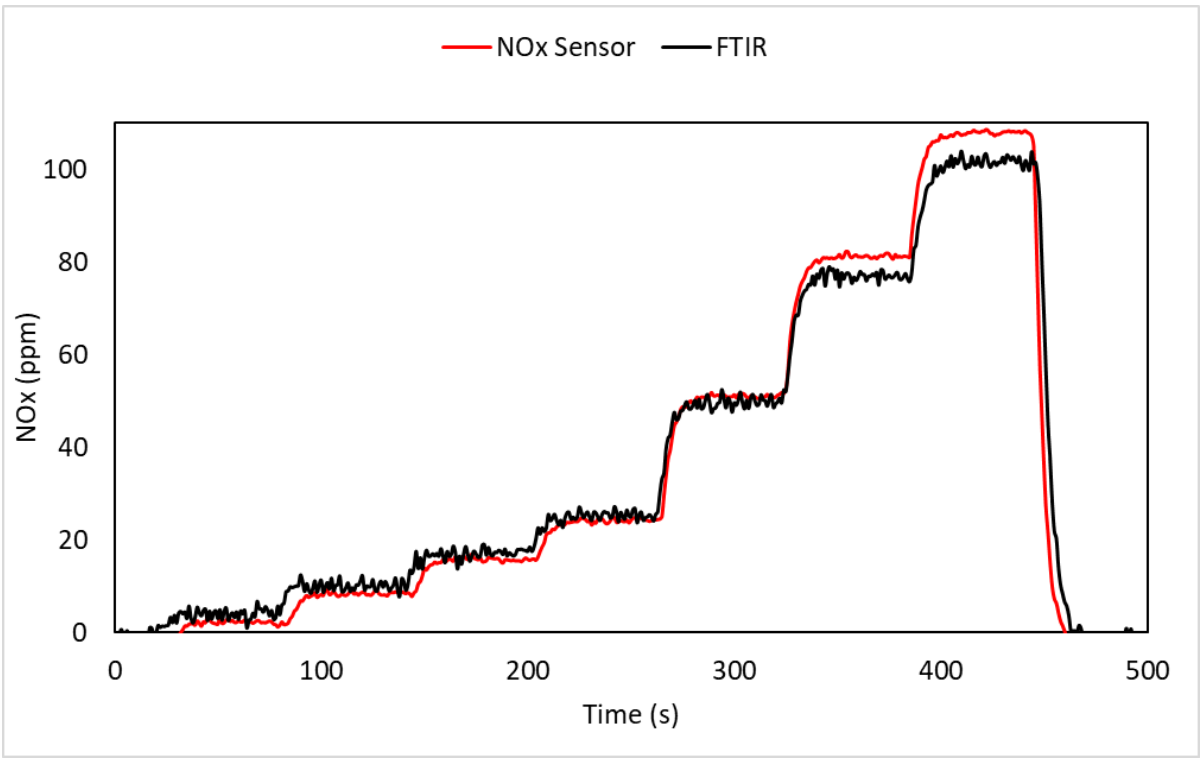

Figure 3-9. Average Real-Time Concentration Plot for the initial calibration method

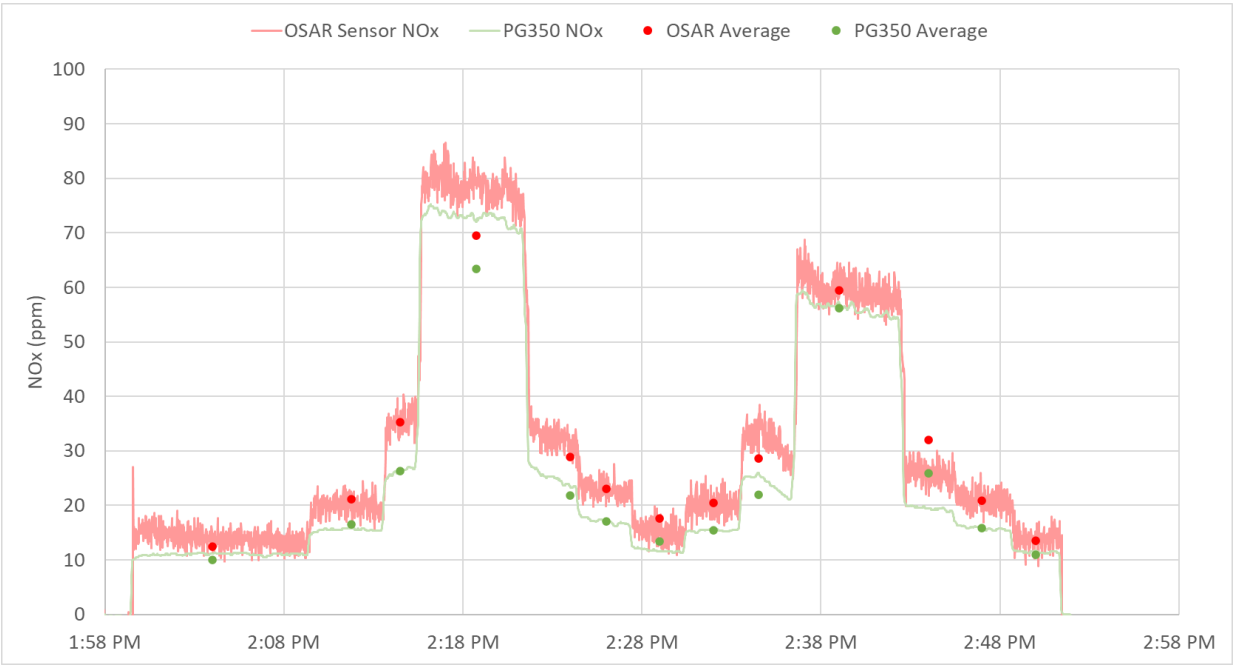

Figure 3-10. Average Real-Time Concentration Plot For the final calibration method

3.4 OSAR and HEM Field Demonstration

The OSAR systems were installed on the different vehicles at the different fleet for a period of one month per vehicle. The OSAR system components include the sensors, the ECM data logger, and

the data acquisition module. The HEM loggers used were installed on the vehicles OBD port and monitored the available activity data as well as NOx sensor data. A schematic of a general OSAR installation is provided in Figure 3-11. Pictures of an actual typical installation for a goods movement vehicle are provided in Figure 3-12. It should be noted that the installations for different vehicle, vocation, and engine types varied considerably based on the specific configurations of the vehicles and their engines. The sensors themselves are installed in a short extension piece attached to the tailpipe that includes bung fittings to secure the sensors, as shown in Figure 3-12. The associated control modules for the sensors were attached to the frame near the tailpipe extender. The data acquisition system was attached to the truck body on the rear of the truck, such that it was not in the way during typical operations.

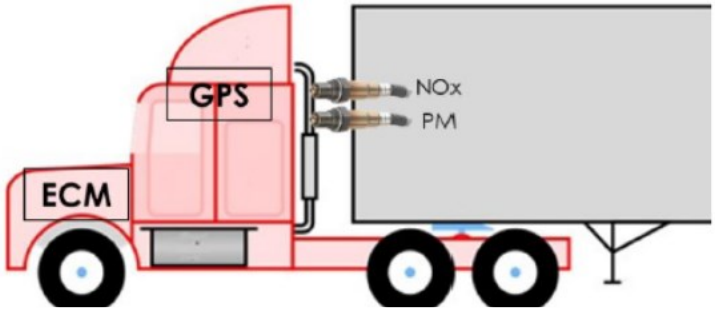

Figure 3-11 Example of the OSAR system on a truck.

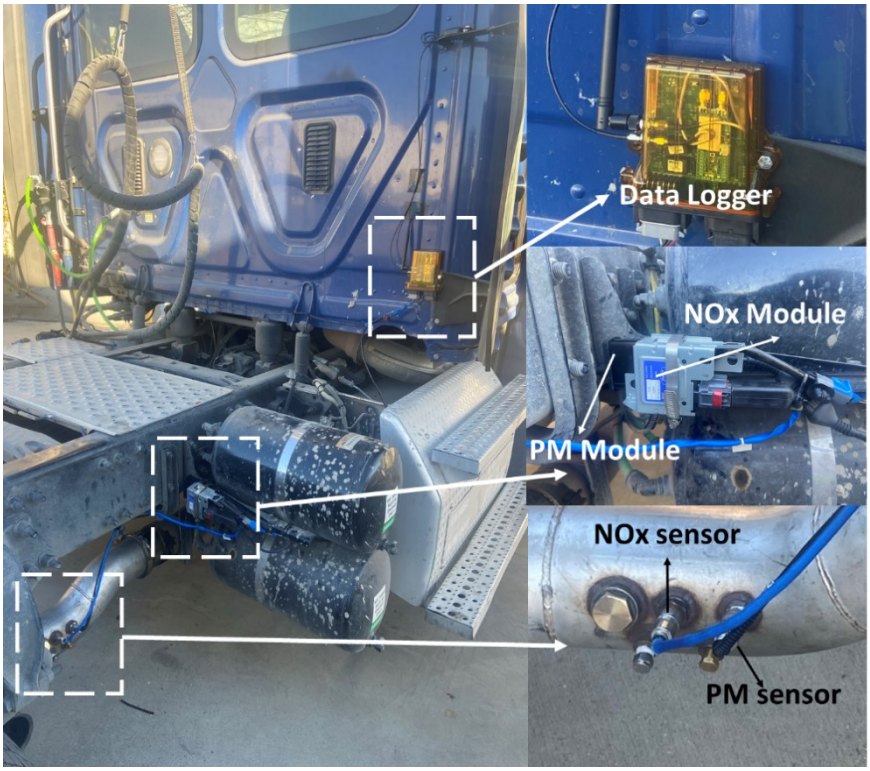

Figure 3-12 OSAR system installed on a Class-8 truck

3.5 Data Analysis

The OSAR generates files in an OSAR format. These were processed through an executable program to a CSV file, which is in turn read into an Excel where it was reviewed, QA/QC'd, and corrected as needed. QA/QC procedures consisted of first a quick visual verification that non-zero/non-blank data existed for each of the main parameters, such as RPM, GPS, and Sensor NOx. The RPM, NOx, wheel-based speed, latitude, and longitude were then plotted to verify that the ECM, GPS, and NOx sensors data represented reasonable engineering values, and that there were no significant breaks in the data or major sections of zero/blank data or sections where the data were at or above maximum values.

The real-time NOx data from the trucks NOx sensor were processed along with the engine torque and revolutions per minute (rpm) data to provide NOx emissions on a g/bhp-hr basis. For these calculations, the exhaust flow rate was obtained from the fuel flow rate from the OBD system. These data were compiled to determine the trip average NOx emissions on a g/bhp-hr basis for the full trip and the total grams of NOx per trip for each truck. Real-time NOx emissions plots were also developed for a subset of trucks. The calculations performed to determine NOx emissions rate in g/s are shown below. The algorithm used for the data calculations is provided in Appendix C. The parameters were taken from the vehicle's ECM data set and calculated per second.

3.5.1 Mass Emission Calculations

For diesel-fueled vehicles Engine Exhaust Flow Rate (PGN: 64587) is available directly from the ECM. Finally, Emission Mass Rates in g/s were calculated using the following equation, where the Emission concentration is in ppm, $\rho_{emission}$ is the density of the emission in g/L, and ρ_e is the density of exhaust in g/L.

$$Emission\ Mass\ Rate\ \left[\frac{g}{s}\right] = Emission\ [ppm] * 10^{-6} * \frac{\rho_{emission}}{\rho_e} * Exhaust\ flow\ [g/s]$$

The PM calculation can be seen below to calculate the PM emissions from pA as described by EmiSense.

$$PM\ Concentration\ \left[\frac{mg}{m^3}\right] = PM\ Signal\ [pA]\ /\ 3200\ [pA/\frac{mg}{m^3}]$$

The CO_2 has been approximated based on EPA (2005) guidelines of gallons of fuel to kilograms of CO_2. This calculation is shown below.

$$CO_2\ [kg] = Fuel\ [gal]\ * 10.1\ [kg/gal]$$

3.5.2 Daily Average Emission Rates and Data Filtering

Two approaches were considered to generate average emission factors for each of the vehicles monitored. The first was to take the average emissions over each day, and averaging this over the number of days of operation. A daily simple average was obtained using all the data collected for each day and averaging this into a single number for each vehicle. The daily averages are helpful to view the entire dataset in with individual points for each day of operation. This methodology

was used to generate box whisker plots of daily operations for the different fleets over all vehicles in that fleet, and for plots of daily average emissions vs. aftertreatment temperature for each fleet.

For the daily results, the data was filtered to only include days of data that were longer than 20 minutes and produced more than 23 bhp-hr of work. This is to only show data that is representative of operation that is at least the duration of certification cycles. The sum over sum histogram shows all of the data points. For the PM data, we also hope to filter out anything produced when the sensor was not fully warmed up to 150 ºC. Data were also filtered to remove any SAE maximum and minimum values, with Appendix C showing all of the details of the code used for the data analysis.

3.5.3 Sum over Sum Average Emission Rates

A simple average does not necessarily weight the overall data correctly for individual vehicles on a time basis for the total period of operation. For example, a short day with a high brake specific emissions of 2 g/hp-hr would be averaged with a long day of 0.2 g/hp-hr to 1.1 g/hp-hr, even though the emissions weighted on a time basis would be closer to the 0.2 g/bhp-hr value. As such, a sum over sum approach was used to generate a single value average emission factor for each vehicle. This sum over sum approach, explained below, weights days with very little activity more appropriately relative to the vehicle's full operations over the monitoring period. This method was used to generate the values in the NOx emission factors in the histogram in section 5.1.2 of the results section. This calculation is outlined and described here.

$$NOx\ Emission\ Factor\ (\frac{g}{bhp\ hr}) = \frac{\sum Total\ NOx\ in\ Grams}{\sum Total\ Work\ in\ Brake\ Horsepower\ Hours}$$

By weighting the emissions based on the total work of all operations, this method normalized based on total operation. As such, days when only minor operations are conducted are given a lower weighting relative to days where the vehicle operates for a longer period of time. When this method is used, outliers that normally would disrupt the mass emission average value, are accounted for as a valid data record, but it is not given equal weight as normal days of operation.

3.5.4 CARB REAL

The California Air Resources Board has recently implemented its Real Emissions Assessment Logging (REAL) approach as a component of the recent amendments to CARB's on-board diagnostic (OBD) regulations. The REAL methodology emphasizes on-board emissions monitoring (CARB, 2018). For the REAL binning method, instantaneous data are distributed across 16 bins, based on varying vehicle speeds and engine brake output powers, see Figure 3-13. Bin 1 represents the aggregate of the complete route test results, equivalent to the sum of values from Bins 2 to 14. Bin 2 is designated for idling periods, occurring when the engine is running but the vehicle is stationary. Bins 3 to 14 encompass a comprehensive range of vehicle activities excluding idling.

The CARB REAL binning method is represented by a sum of an array of 100 hours of the more recent active operation, a stored array of 100 hours of operation, and an array for the full lifespan of the data, see Table 3-6. The 100 hours may represent 4 to 5 long days of driving or may be up

to a month of operation. Thus, binning by the REAL method is not a daily analysis metric like the EPA binning method, but a longer sum over sum method spanning multiple days or trips. This longer duration may have some benefit of reducing the impact of variability between days in comparison to the EPA binning method. Additionally, there is not a limitation of hours in a day, so the CARB binning method includes all data that can be summed up into the different arrays.

Table 3-6 REAL Binning Method

Parameter	Active 100 Hour Array	Stored 100 Hour Array	Lifetime Array	Lifetime Engine Activity Array
NOx mass – engine out (g)	x	x	x	n/a
NOx mass – tailpipe (g)	x	x	x	n/a
Engine output energy (kWh)	x	x	x	x
Distance traveled (km)	x	x	x	x
Engine run time (hours)	x	x	x	x
Vehicle fuel consumption (liters)	x	x	x	x

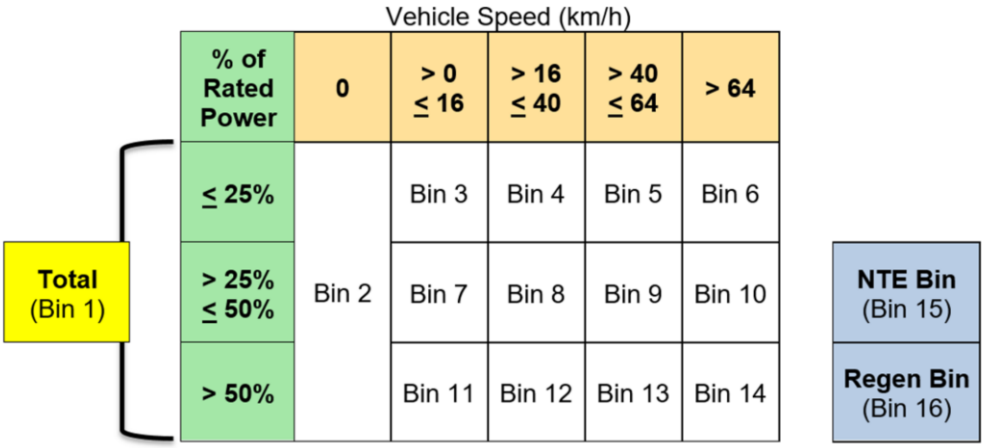

Figure 3-13 REAL Binning Method

3.5.5 EPA 2 BIN MAW

The study also included analysis using the EPA's two-bin moving average window (2B-MAW) method, which places an emphasis on off-cycle emissions and is set to be implemented with the next round of regulations by CARB and EPA (40 CFR Part 1036). This approach, established under a recent agreement between CARB, EPA, and the Engine Manufacturers Association (EMA), is to be implemented for future compression ignition (diesel) engines. The basis of this method is to calculate the normalized CO_2 emission mass for each 300-second interval over a day of operation, where the total CO_2 emission mass are ratioed to the engine family certification level (FCL) CO_2 emissions over the Federal Test Procedure (FTP) duty cycle for the maximum rated power of a given engine configuration. It primarily uses normalized CO_2 levels to allocate test data into two distinct bins: the first bin for the idle state of the engine, and the second bin encompassing all other data points, indicative of varying loading conditions. The engine's FTP FCL for CO_2

emissions and the maximum power of the engine family were determined from the engines Executive Order (EO).

The EPA 2B-MAW does have a criterion for trip sizes to be considered valid that is defined by the number of windows in each bin. A window is the 300 second interval that can be counted for each BIN each day. A valid trip is defined by EPA when Bin 1 has 2400 or more windows and Bin 2 has 10,000 or more windows. These different bin window sizes were selected to prevent over representing one bin compared to the other. These windows sizes were selected based on discussions between industry and EPA for diesel engines, which may or may not apply for NG engines. As such, for this study, UCR utilized the regulatory window size and also a shorter window size of 2400 for both Bin 1 and 2. The binning calculations and formulas utilized for the 2B-MAW analysis are shown below: The equation below is used to determine the normalized CO_2 emission mass over each 300 second test interval.

$$m_{\mathrm{CO2,norm,testinterval}} = \frac{m_{\mathrm{CO2,testinterval}}}{e_{\mathrm{CO2FTPFCL}} \cdot P_{\mathrm{max}} \cdot t_{\mathrm{testinterval}}}$$

Eq. 1036.530-2

Where $m_{CO2,testinterval}$ is the total CO_2 emission mass over the test interval. $e_{CO2FTPFCL}$ is the engine's FCL for CO_2 over the FTP duty cycle. If the engine family includes no FTP testing, the engine's FCL for CO_2 over the SET duty cycle is to be used. P_{max} is the highest value of rated power for all the configurations included in the engine family. And finally, $t_{testinterval}$ is duration of the test interval. Note that the normative $t_{testinterval}$ value is 300 seconds.

The identification of the appropriate bin for each of the 300 second test intervals is based on the normalized CO_2 emission mass. Table 3-7 describes these criteria.

Table 3-7 Binning Criteria for CE-CERT off-cycle analysis

	Normalized CO_2 emission mass over the 300 second test interval
Bin 1	$m_{CO2,\ norm,\ testinterval} \leq 6.00\%$.
Bin 2	$6.00\% < m_{CO2,\ norm,\ testinterval}$

The off-cycle emission quantity for bin 1 is the mean mass emission rate from all test intervals associated with bin 1 as calculated using the following equation with NOx as the example pollutant.

$$\bar{\dot{m}}_{\mathrm{NOx,offcycle,bin1}} = \frac{\sum_{i=1}^{N} m_{\mathrm{NOx,testinterval},i}}{\sum_{i=1}^{N} t_{\mathrm{testinterval},i}}$$

Eq. 1036.530-4

Where i is an indexing variable that represents one 300 second test interval. N is total number of 300 second test intervals in bin 1. $m_{NOxtestinterval,i}$ is the total NOx emission mass over the test interval i in bin 1. Other pollutants can be inserted here in place of NOx when necessary. $t_{testinterval,i}$ is the total time of test interval i in bin 1. Note that the normative value is 300 seconds.

The off-cycle emission quantity for Bin 2 is the value for emission mass for a given pollutant of all the 300 second test intervals in Bin 2 and converted to a brake-specific value, as calculated for each measured pollutant using the following equation.

$$e_{[\text{emissions}],\text{offcycle,bin2}} = \frac{\sum_{i=1}^{N} m_{[\text{emission}],\text{testinterval},i}}{\sum_{i=1}^{N} m_{\text{CO2,testinterval},i}} \cdot e_{\text{CO2,FTP,FCL}}$$

Where i is an indexing variable that represents one 300 second test interval. N is total number of 300 second test intervals in bin 2. $m_{[emission],testinterval,i}$ is the total emission mass for a given pollutant over the test interval i in Bin 2. $m_{CO2,testinterval,i}$ is the total CO_2 emission mass over the test interval i in bin 2. And finally, $e_{CO2FTPFCL}$ is the engine's FCL for CO_2 over the FTP duty cycle to convert the units to a brake specific value.

The parameters used for CE-CERTs use of the off cycle 2 Bin-MAW analysis included the engine's FTP FCL CO_2 emission value ($e_{CO2\ FTP\ FCL}$) which is referenced from each vehicle's Executive Order and the engine family max power, P_{max}, which is based on the vehicle's engine label.

4 Vehicle OSAR and HEM Activity Results

This section discusses the results for the activity data logging for the monitored diesel vehicles. Based on the OSAR data collection, the data were analyzed to provide hours of operation, average miles traveled per day, and average speed. The subsections below discuss the results for different vehicles in terms of daily hours of operation, average speed, distance, energy used, fuel use, and average SCR temperature. The results are shown in whisker plots based on the data from each day of operation for each vehicle within each fleet. The whisker plots show the 75th, 50th, and 25th percentiles as the higher side of the box, the middle line, and the lower side of the box, respectively. The x represents the average value of the data for all days of operation for each fleet. The error bars represent the 99th and 1st percentile of the data for the upper and lower error bars, respectively. The data values falling above the 99th percentile are shown as dots, and represent outliers. The fleets are identified as diesel goods movement fleets #1 through #6 (DGM 1, DGM 2, DGM 3, DGM 4, DGM 5, and DGM 6), the diesel transfer truck fleet #1 (DTT 1), and the diesel off road fleet #1 (DOR 1). The diesel off-road fleet data was not included for some plots, such as daily average speed or distance traveled, as these are not metrics typically used to characterize off-road activity. The diesel off-road fleet is shown also shown on the right side of the graphs, as its activity pattern is inherently different from those of the on-road fleets.

4.1 Hours of Operation per day

Figure 4-1 shows the average hours of operation per day for each fleet. The average number of hours of operation for the different on-road fleet types was 7 hours, with a range for different fleets from 6 to 8 hours. The DGM 5 fleet showed the largest range of daily hours of operation, while DGM 6 showed the tightest range daily hours of operation. The off-road fleet averaged 3 hours of daily operation.

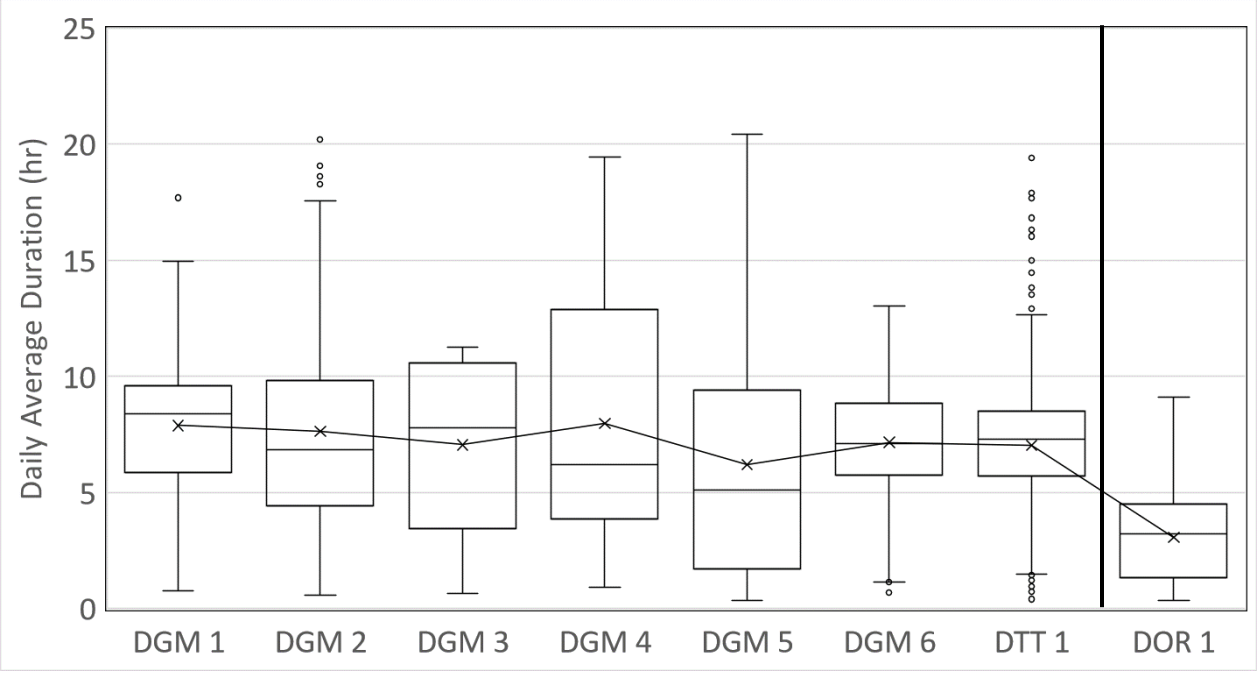

Figure 4-1 Daily Hours of Operation for each Fleet

4.2 Average Speed

Figure 4-2 shows the daily average speed for each vehicle. On average, the on-road fleets operated at around 24 mph. The average speed for the different on-road fleets ranged from 11 to 52 mph. The majority of the on-road fleets had average speeds between 15 and 25 mph. The DGM 3 fleet showed highest daily average speed, while the DGM 6 had the lowest speed. The DGM 3 fleet was used more extensively for longer haul operation on highways than the other goods movement fleets, and it showed a highest daily distance traveled also, as discussed in section 4.4.

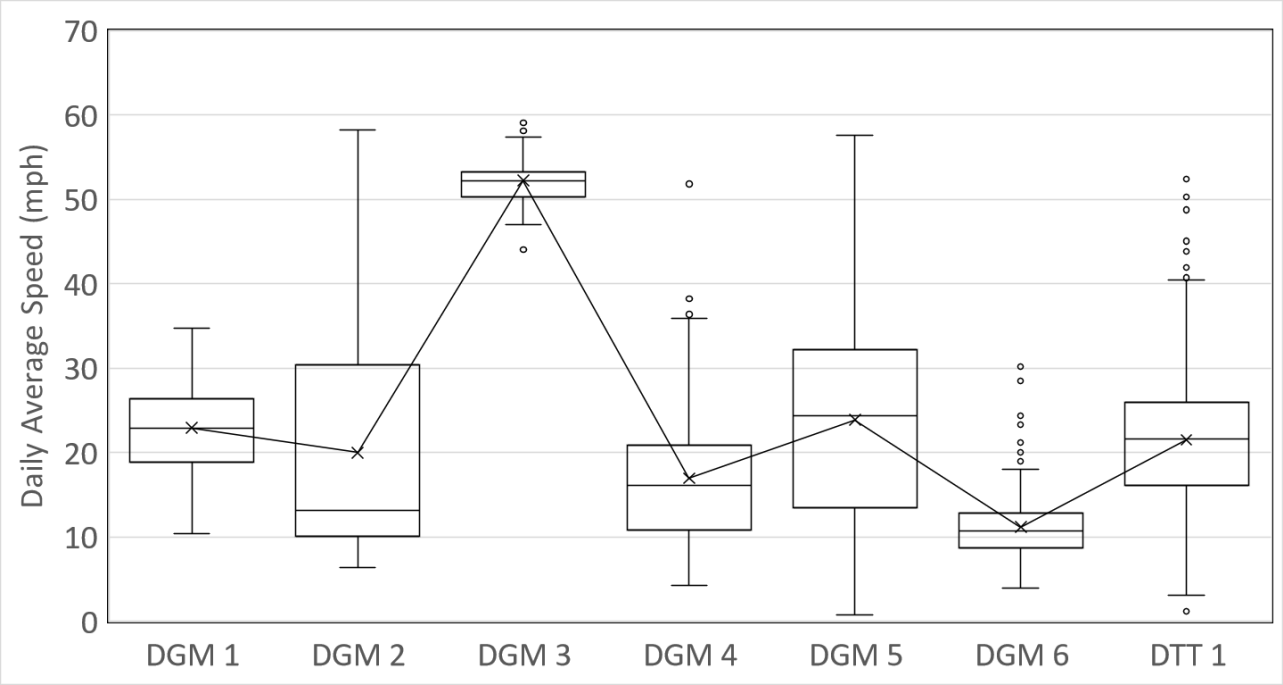

Figure 4-2 Daily Average Speed for the Fleets

4.3 Average Energy Use/bhp-hr

Figure 4-4 shows the average daily energy use/bhp-hr for each fleet. On average, the on-road fleets used 524 bhp-hr. The average daily energy use for the on-road different fleets ranged from 389 to 1061 bhp-hr/day. Most of the fleets, on average, produced a similar amount of work at 500 bhp-hr day, with the range of data being the largest for DGM 3 and the smallest for DGM 6. DGM 3 had the highest work due to its consistent operation. The off-road fleet, DOR 1, had the lowest amount of daily work at 178 bhp-hr/day.

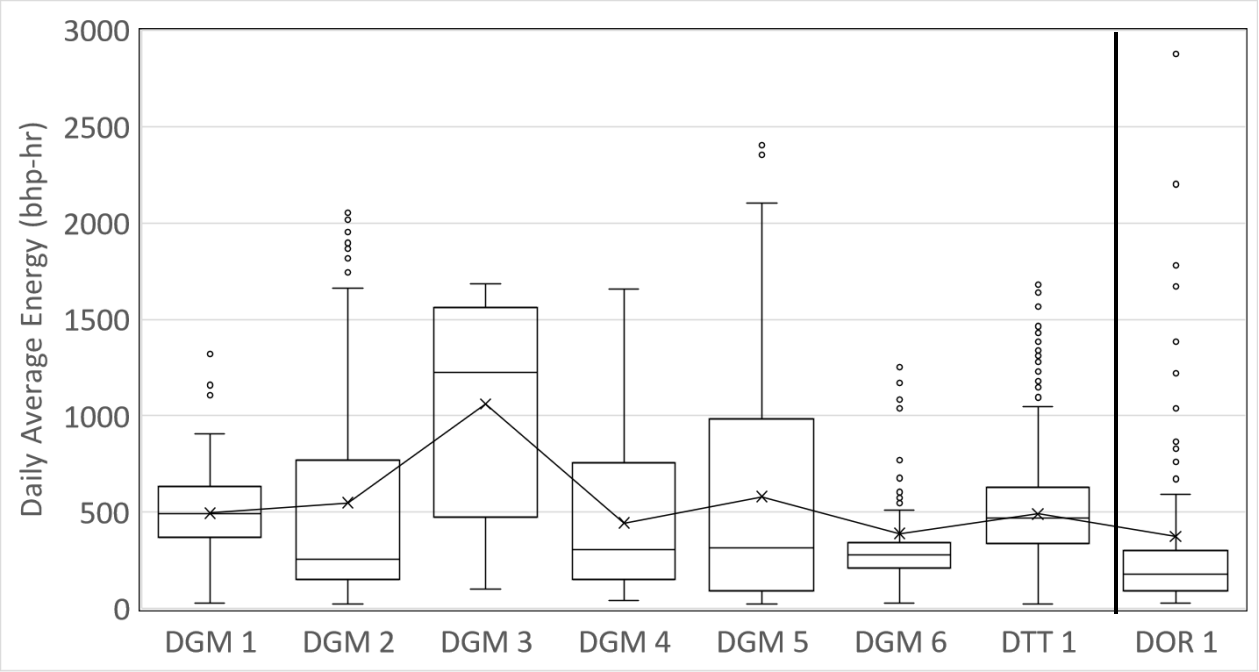

Figure 4-3 Daily Average Energy Use for the fleets

4.4 Average Distance

Figure 4-4 shows the daily average distance traveled in miles per day for each fleet. The on-road fleets on average had a distance traveled of 158 miles. The on-road fleets had a distance range of 78 to 374 miles. DGM 3 had the highest average mileage range at 374 miles. The off-road fleet, DOR 1, is not shown due to distance not being a common activity data perspective of typical operation of off-road equipment.

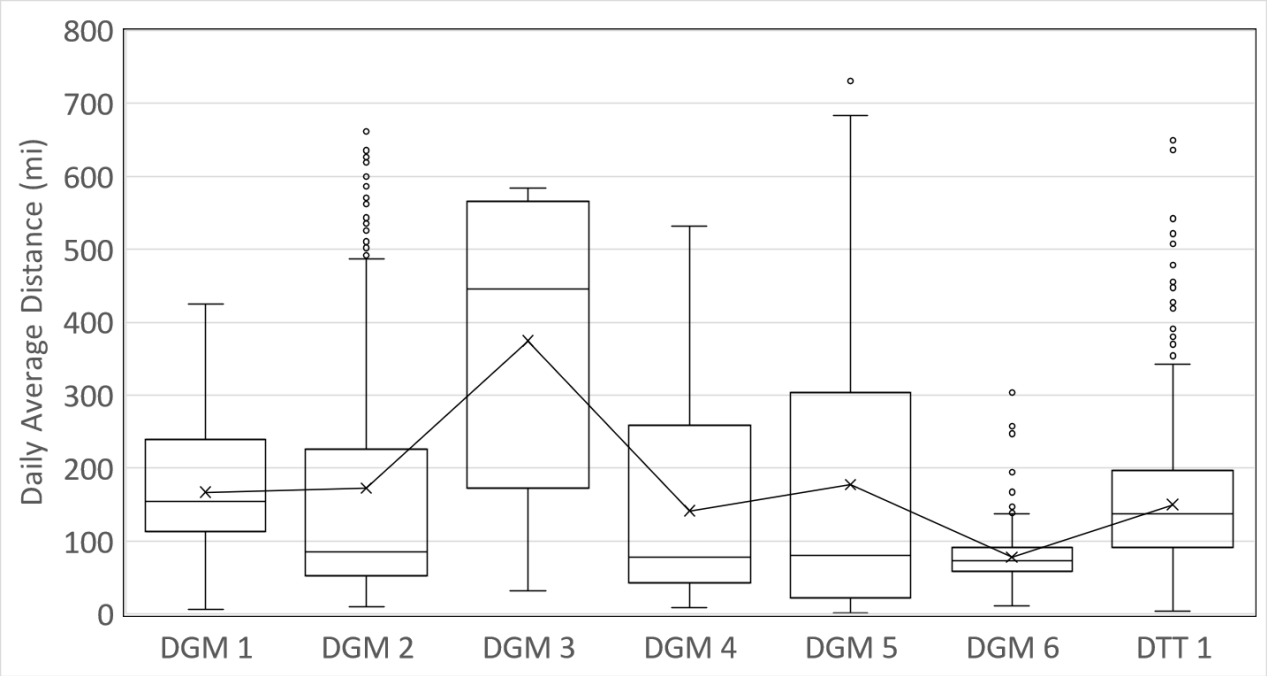

Figure 4-4 Daily Average Distance for each Fleet

4.5 Average Fuel Use per Hour

Figure 4-5 shows the average hourly fuel use for each fleet. The on-road fleets on average had a hourly fuel use of 3 gal/hour. The hourly fuel use varied from about 7 gallons to 2 gallons per hour. The highest average hourly fuel use for was for the DGM 3 fleet. DGM 6 fleets showed the lowest average hourly fuel use at 2 gallons per hour. The off-road fleet had an average hourly fuel use of 3 gal/hour

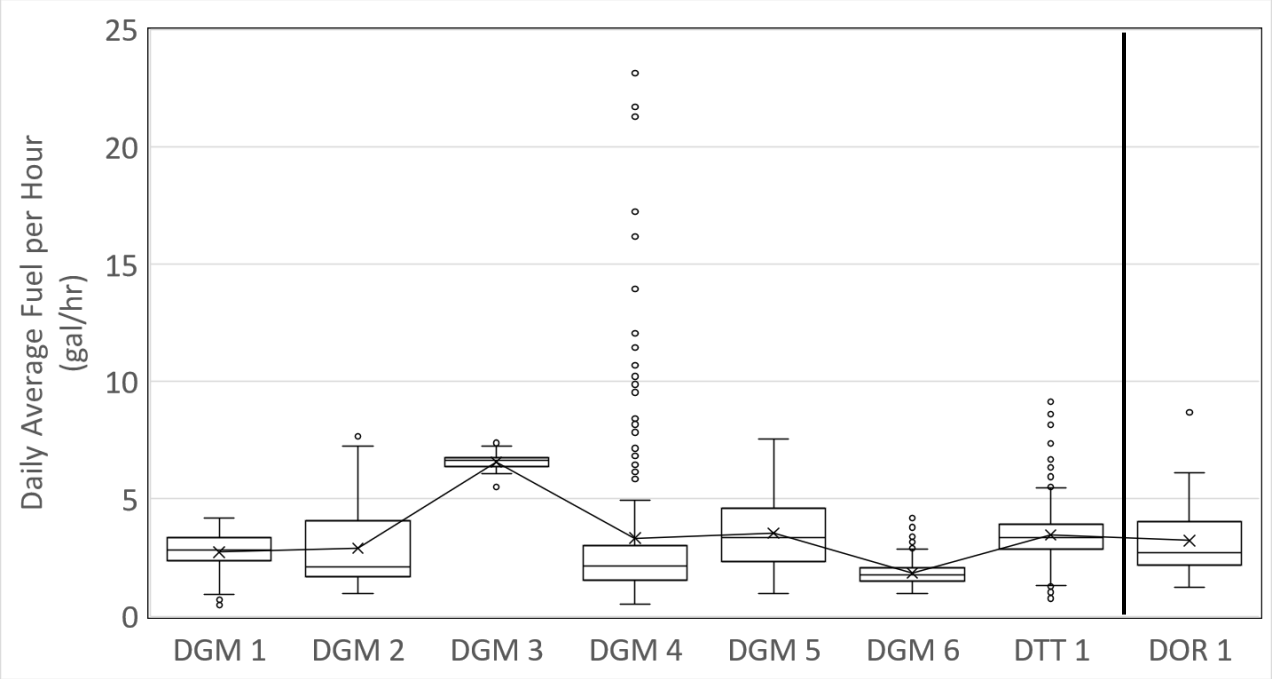

Figure 4-5 Fuel Use for the fleets

4.6 Average Daily SCR Temperature

Figure 4-6 shows the daily average SCR temperature for each fleet. The fleets showed average SCR temperatures ranging from 297 to 153 °C. DOR 1 showed the highest range of data, with the average temperature at 288 °C. DGM 3 showed a tight range of temperatures and an average of 297 °C. Three of the fleet had average SCR temperatures of 250 °C or above, which suggests the vehicle SCR systems in these fleets are probably are working a good fraction of the time in a good operating temperature range. DGM 6 shows the lowest average temperature at 153 °C, suggesting low load operation where the SCR might be operating a good fraction of the time below its optimal level.

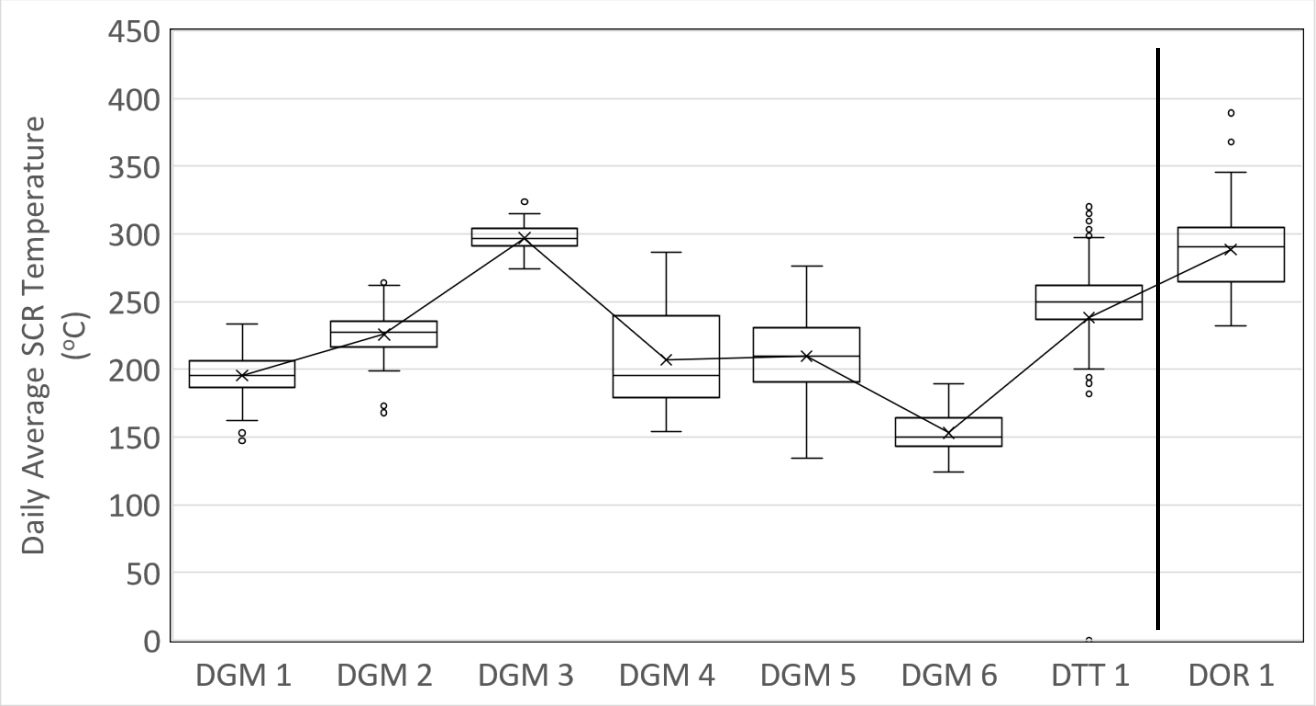

Figure 4-6 Daily Average SCR Temperature for the fleets

5 OSAR Emissions Results

This section covers the OSAR emissions results from the 8 fleets and 100 vehicles monitored as part of this project. The section includes NOx, PM, and CO_2 emission rates. Additional analyses were also conducted for the NOx emissions based on the 2 Bin EPA analysis method and the CARB REAL emission bins.

5.1 NOx Emissions

5.1.1 Simple average

Average brake-specific, distance-specific, and grams per gallon NOx emissions for the different test fleets are shown in Figure 5-1, Figure 5-2, and Figure 5-3, respectively. These averages represent the averages over all the vehicles tested in each fleet. The box's upper and lower lines represent the 75th and 25th percentiles, respectively, while the middle line represents the 50th percentile. The 'x' indicates the average for the fleet. The error bars represent the 99th (upper bar) and 1st (lower bar) percentiles. The dots are outliers that fall outside of these percentiles. The red line indicates the emission standard of 0.2 g/bhp-hr.

On a g/bhp-hr basis, average NOx emissions across the fleets ranged from less than 0.02 to about 0.82 g/bhp-hr. 36 of 56 vehicles showed average emission rates at or below 0.2 g/bhp-hr, which is comparable to the emissions standard. DGM 1, 2, 4, 5 and DTT 1 all had average emission rates of more than 0.2 g/bhp-hr, ranging from 0.22 to 0.82 g/bhp-hr. The results for individual vehicles did show some variability, indicating a wider range in emission rates for the individual vehicles. Several fleets showed outliers that were greater than 1.0 g/bhp-hr, even though the average emissions were around 0.2 g/bhp-hr. The average off road emissions were 0.11 g/bhp-hr and 2.04 g/gal.

Fleet DGM 3 had lower emissions which can be attributed to the highway speeds, and the higher aftertreatment temperatures, as shown below in Figure 5-8. In contrast, DGM 1, which had the highest emissions, showed lower aftertreatment temperatures, closer to 200 ºC, as seen in Figure 5-6. DGM 1 also included much older model year vehicles, ranging from 2013 to 2019, compared to DGM 3 which only utilized 2023 engine model year vehicles low odometer readings.

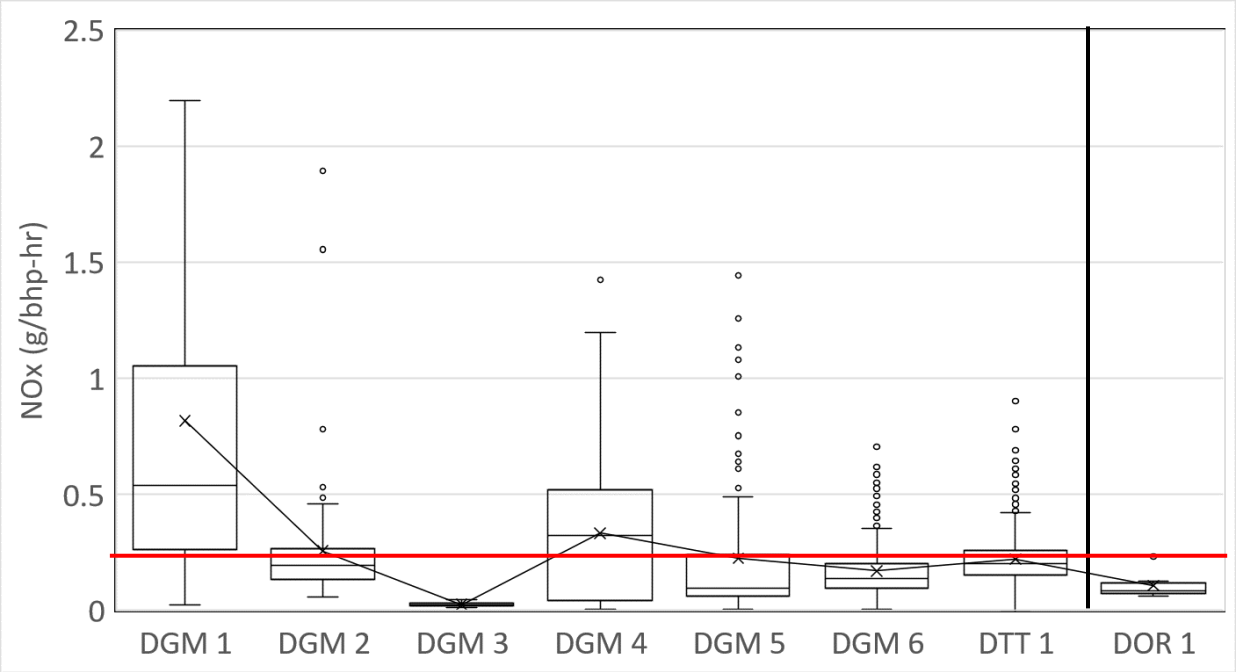

Figure 5-1 OSAR NOx Emission Rates in g/bhp-hr units

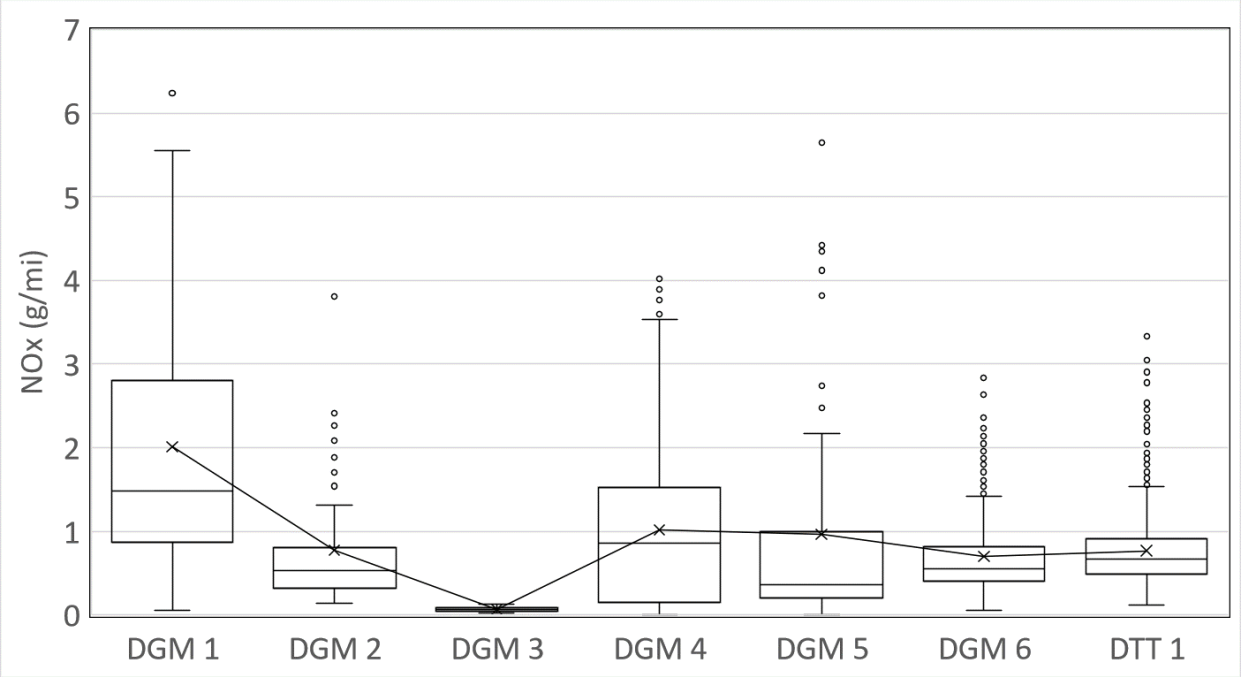

Figure 5-2 OSAR NOx Emission Rates in g/mi units

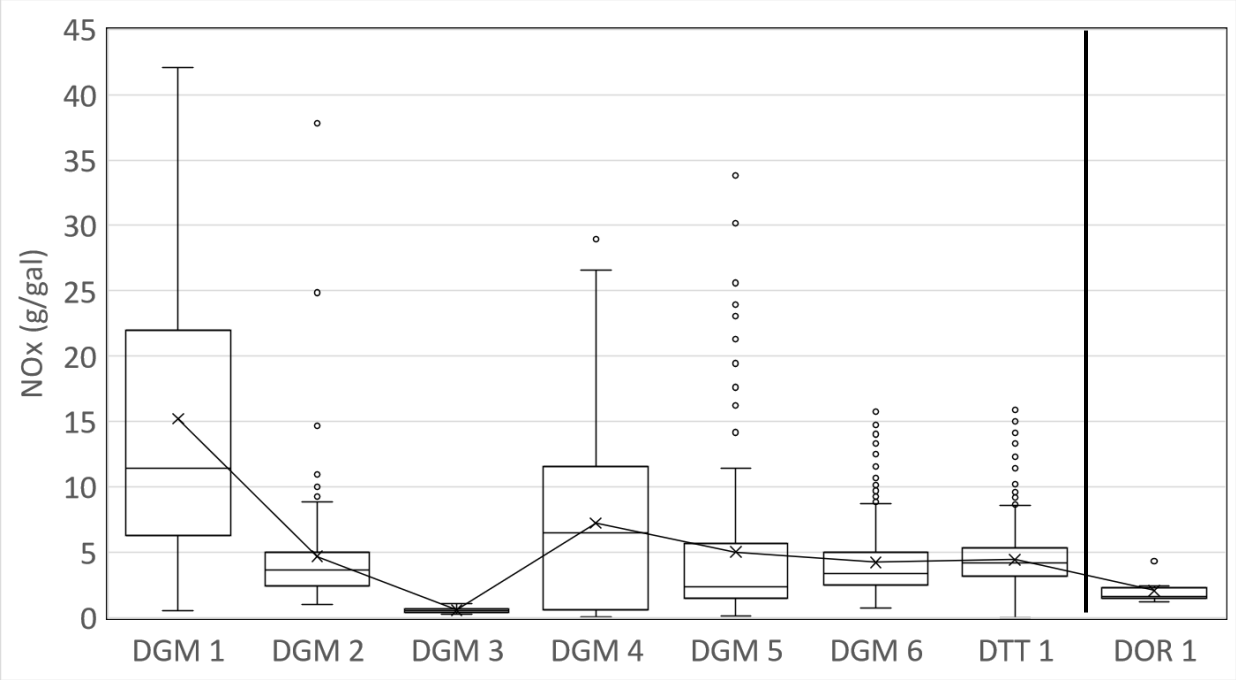

Figure 5-3 OSAR NOx Emission Rates in g/gal units

5.1.2 Sum over Sum

The histogram of the average emission rates for individual vehicles is provided in Figure 5-4. The results show that 36 of 56 vehicles showed emissions below 0.2 g/bhp-hr, with another 15 of 56 vehicles showing emissions below 0.4 g/bhp-hr. A total of 5 vehicles showed emissions >0.4 g/bhp-hr, with 2 of those having emissions >1.0 g/bhp-hr.

Table 5-1 provides additional information on the four vehicles with a sum-over sum emissions factors above 0.5 g/bhp-hr. These vehicles ranged in model year from 2013 to 2022, and included three vehicles from the same fleet. The two highest emitters included on older 2013 vehicle, and 2019 vehicle, and were both from the same fleet. The other two vehicles, with emission rates of 0.66 and 0.67 g/bhp-hr, included on older 2015 vehicle and one newer 2022 vehicle.

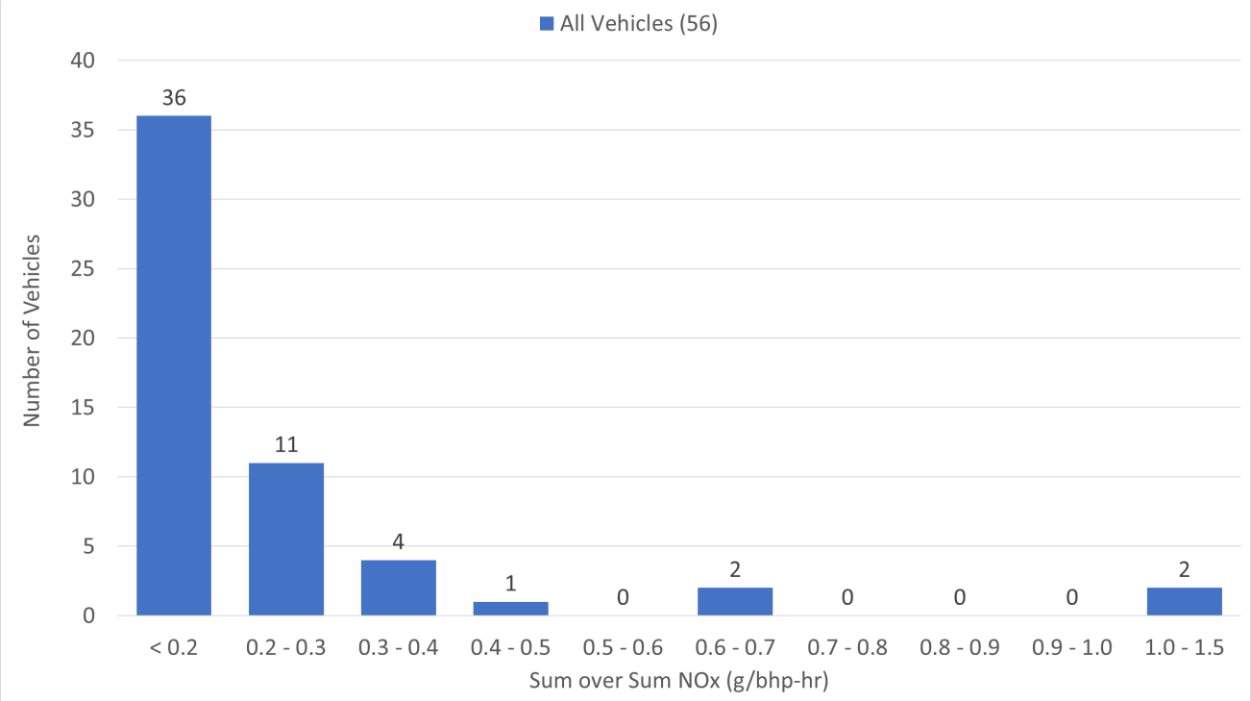

Figure 5-4 OSAR NOx Sum over Sum Emissions Factor Histogram

Table 5-1 Summary of high emitters

Install ID	Model Year	Fleet	Total Hours	Average Daily Hours	Average Daily Distance (mi)	Sum over Sum NOx (g/bhp-hr)
22001	2013	DGM 1	160	4.0	78	1.492
22004	2019	DGM 1	161	8.4	196	1.155
H25014	2022	DTT 1	114	9.9	34	0.671
22002	2015	DGM 1	144	2.5	150	0.661
25020	2023	DGM 4	373	2.6	231	0.445

Figure 5-5 shows the emissions factors with breakdowns by model year. The results show that the majority of vehicles across all model years were operating within twice the emissions standard, with a majority operating near or below the emission standard. The limited number of higher emitters were found for model years ranging from new to old, suggesting that the reasons for the higher emissions were more vehicle-specific, as opposed to a strong trend of increasing emissions with vehicle age.

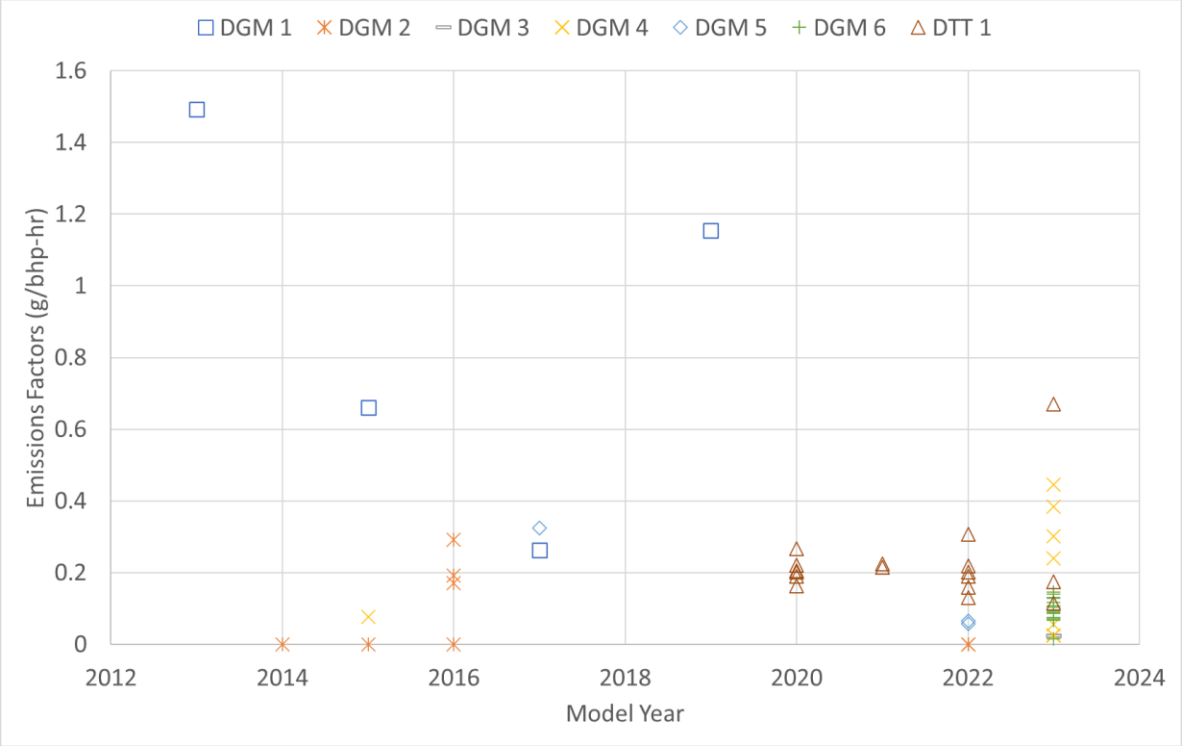

Figure 5-5 OSAR NOx Sum over Sum Emissions Factor Scatter Plot with Model Years

The results for the individual days of operation were also evaluated for the different fleets. Figure 5-6 through Figure 5-12 show the NOx emissions for individual vehicle days in a scatter plot as a function of the aftertreatment temperature for different fleets. Note that the individual days in these graphs only include days of operation where the vehicle was operated for at least 20 minutes and worked had a work of at least 23 bhp-hr. Overall, these plots show a relationship between higher emissions and lower aftertreatment temperatures, but that other factors are also contributing to the emissions differences between different days as well. The DGM 3 fleet showed the lowest emissions, with all of the daily emissions well below 0.2 g/bhp-hr, with can be attributed to the aftertreatment temperature being above 250 °C for the all of the days of operation. The DGM 2, DGM 6, and DTT 1 fleets had the majority of days below 0.4 g/bhp-hr, with DGM 6 also showing a patch of days from 0.4 to 0.7 g/bhp-hr. For fleet DGM 2, only a limited number of days with higher emissions were observed, which correspond to days where the aftertreatment temperature was below 200 °C and the operation load was low, with the total work for all days being less than 150 bhp-hr. For DTT 1, some of the higher emission days had aftertreatment temperatures around 200 °C, but there was also a number of days with emissions above 0.4 g/bhp-hr where the aftertreatment temperature was between 200 °C and 260 °C. Interestingly, for DGM 6, aftertreatment temperature did not seem to have a strong impact on the NOx emissions, even though the aftertreatment temperature for the individual days was below 200 °C for a majority of the days. The DGM 1, DGM 4, and DGM 5 fleets showed a wider range of emission rates for the individual days. For these fleets, the higher emission days appear to be correlated with average aftertreatment temperatures in the range of 200 °C or less. DGM 1, for example, showed a majority of the operating days at temperatures near or below 200 °C. Similarly, for DGM 4 and DGM 5, the vast majority of the days with higher emissions had aftertreatment temperatures near or below 200 °C.

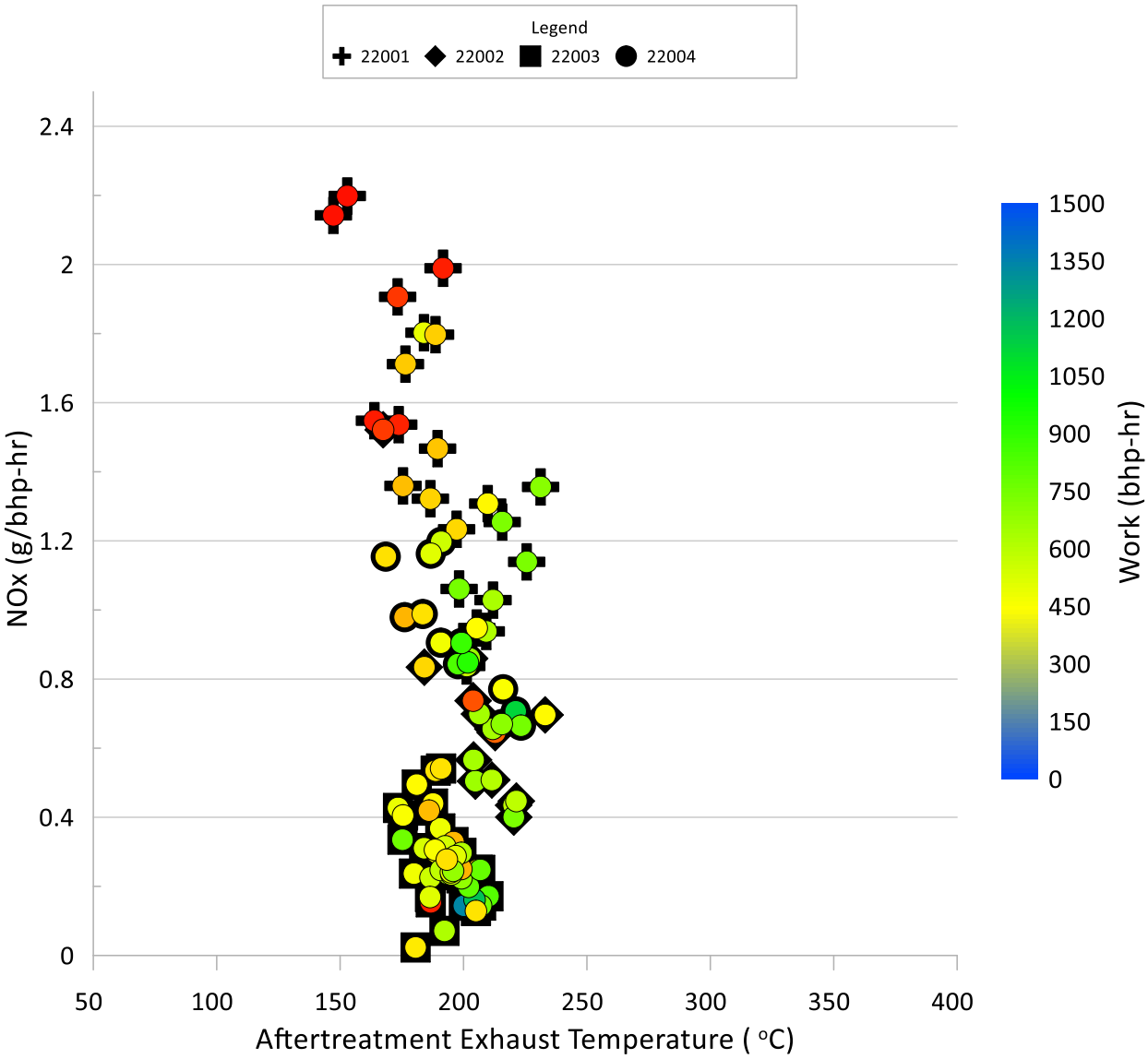

Figure 5-6 OSAR NOx Emission Rates in g/bhp-hr units for individual days of operation for vehicles in DGM 1

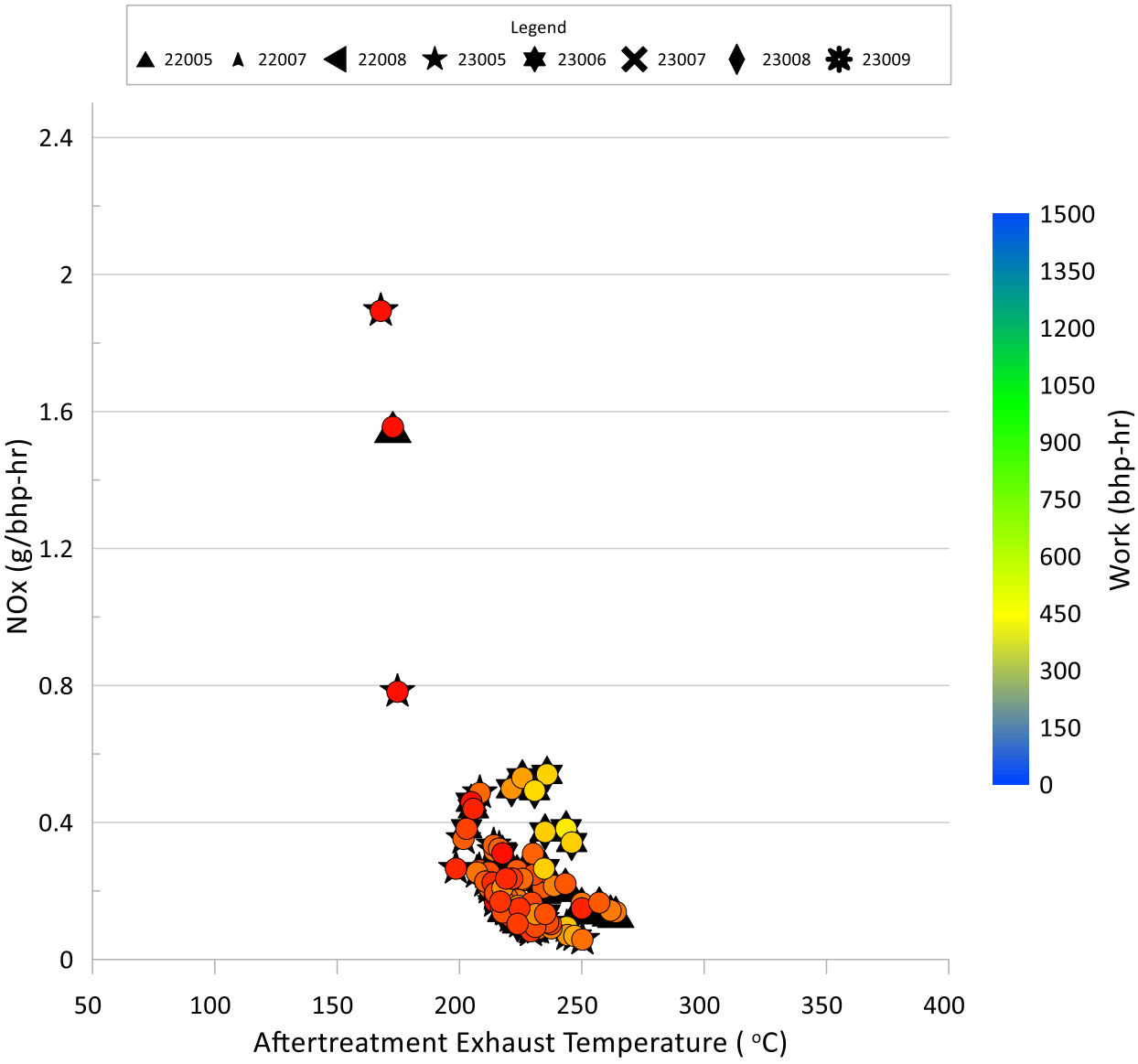

Figure 5-7 OSAR NOx Emission Rates in g/bhp-hr units for DGM 2

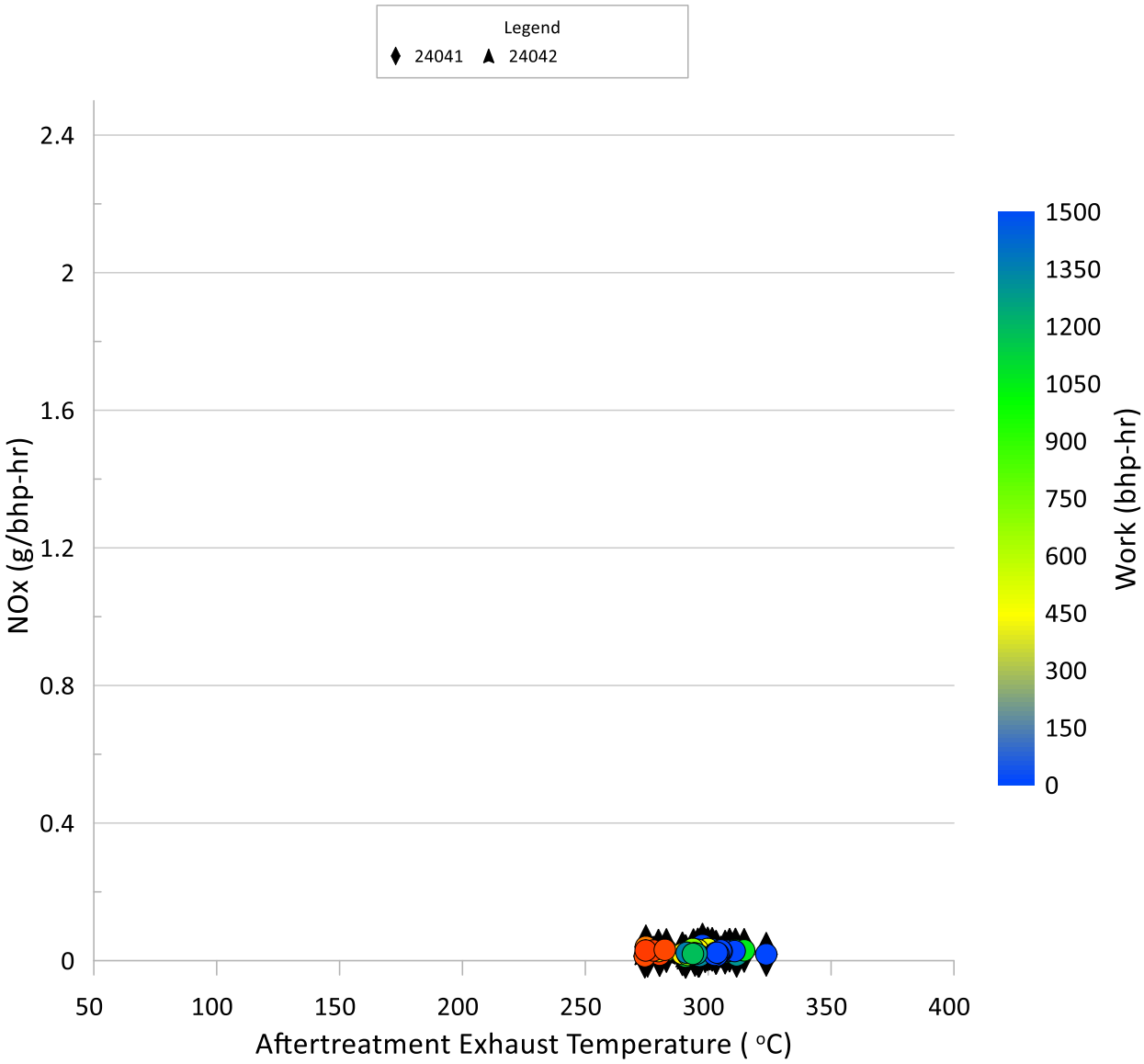

Figure 5-8 OSAR NOx Emission Rates in g/bhp-hr units for DGM 3

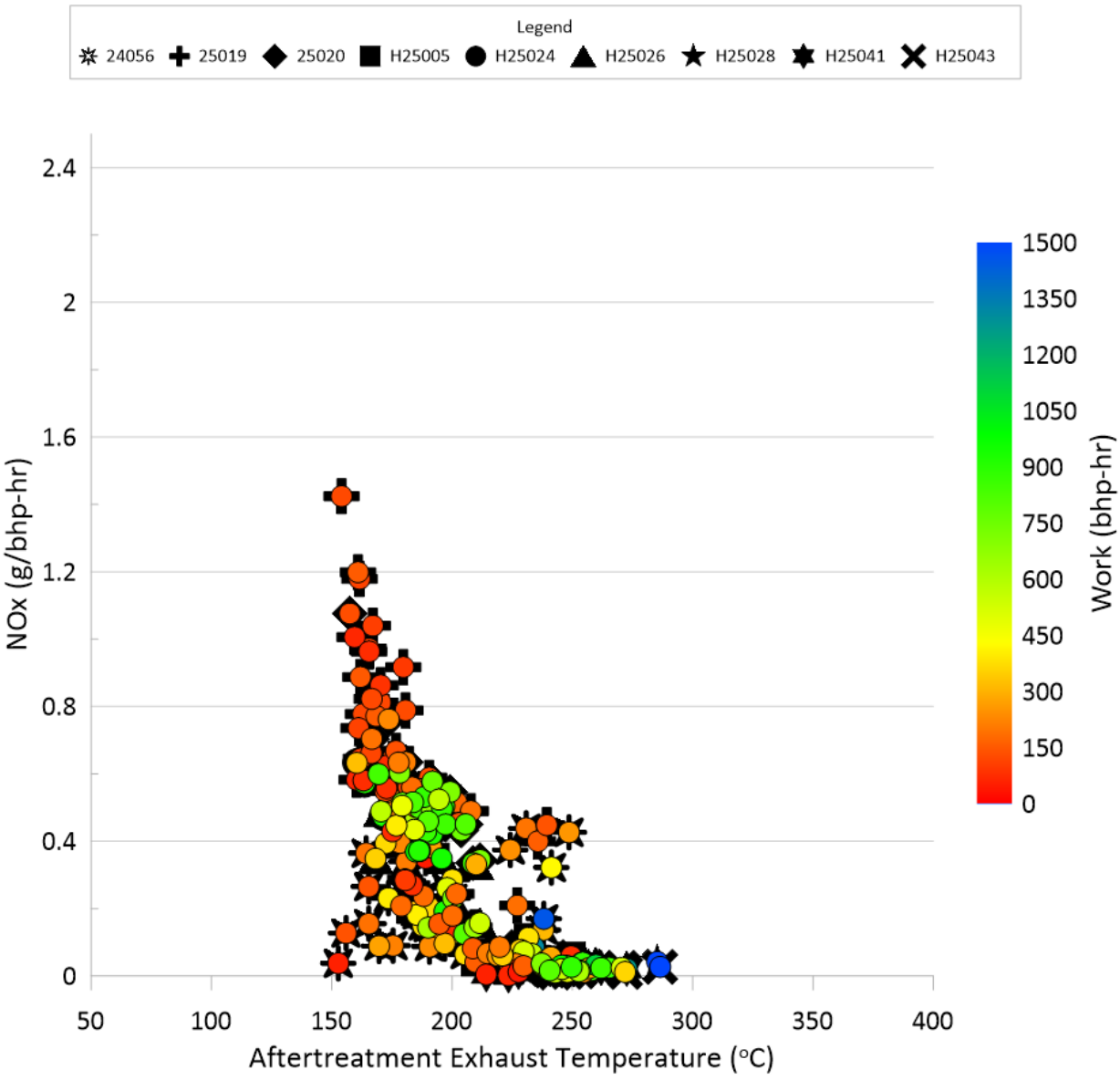

Figure 5-9 OSAR NOx Emission Rates in g/bhp-hr units for DGM 4

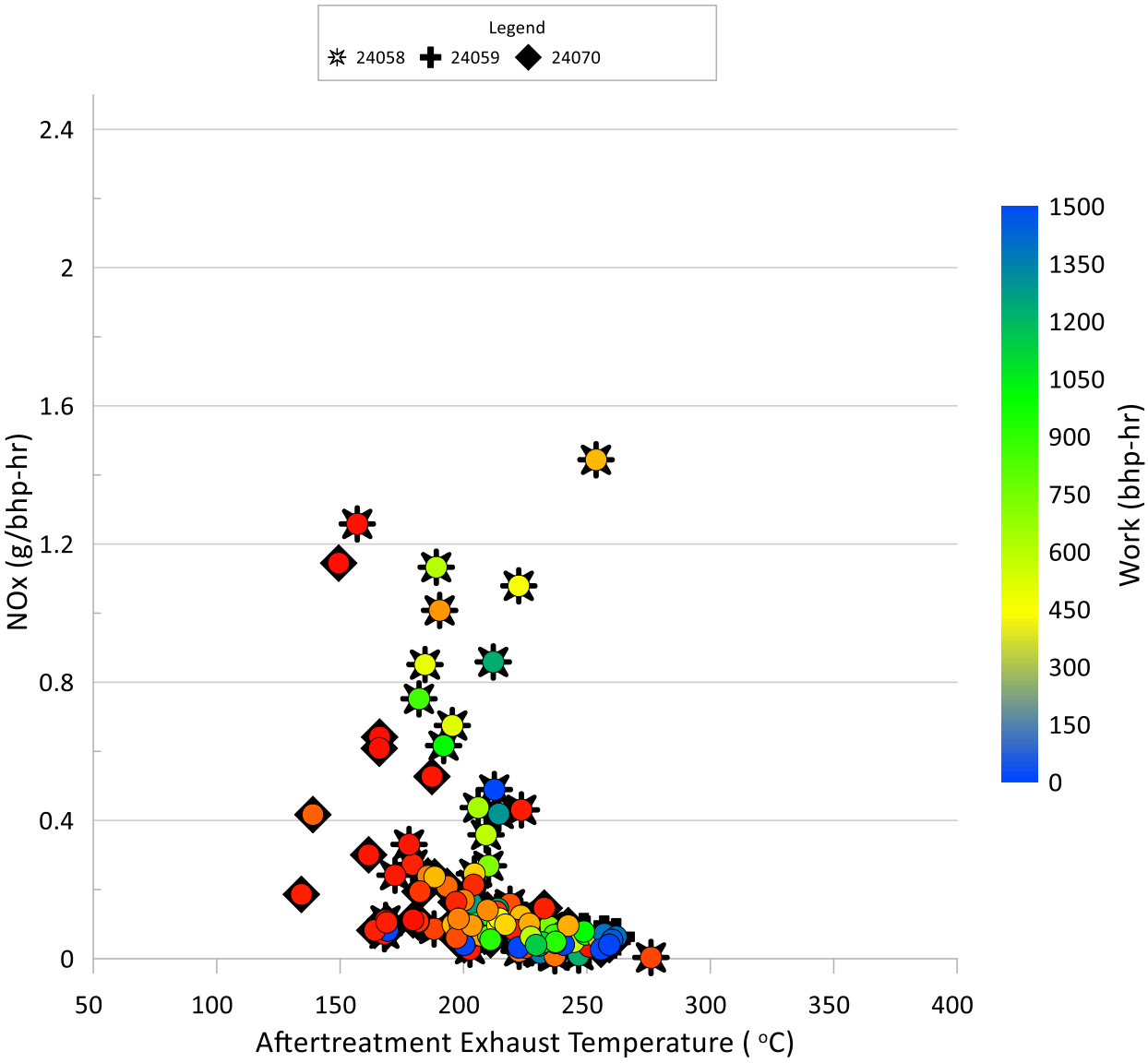

Figure 5-10 OSAR NOx Emission Rates in g/bhp-hr units for DGM 5

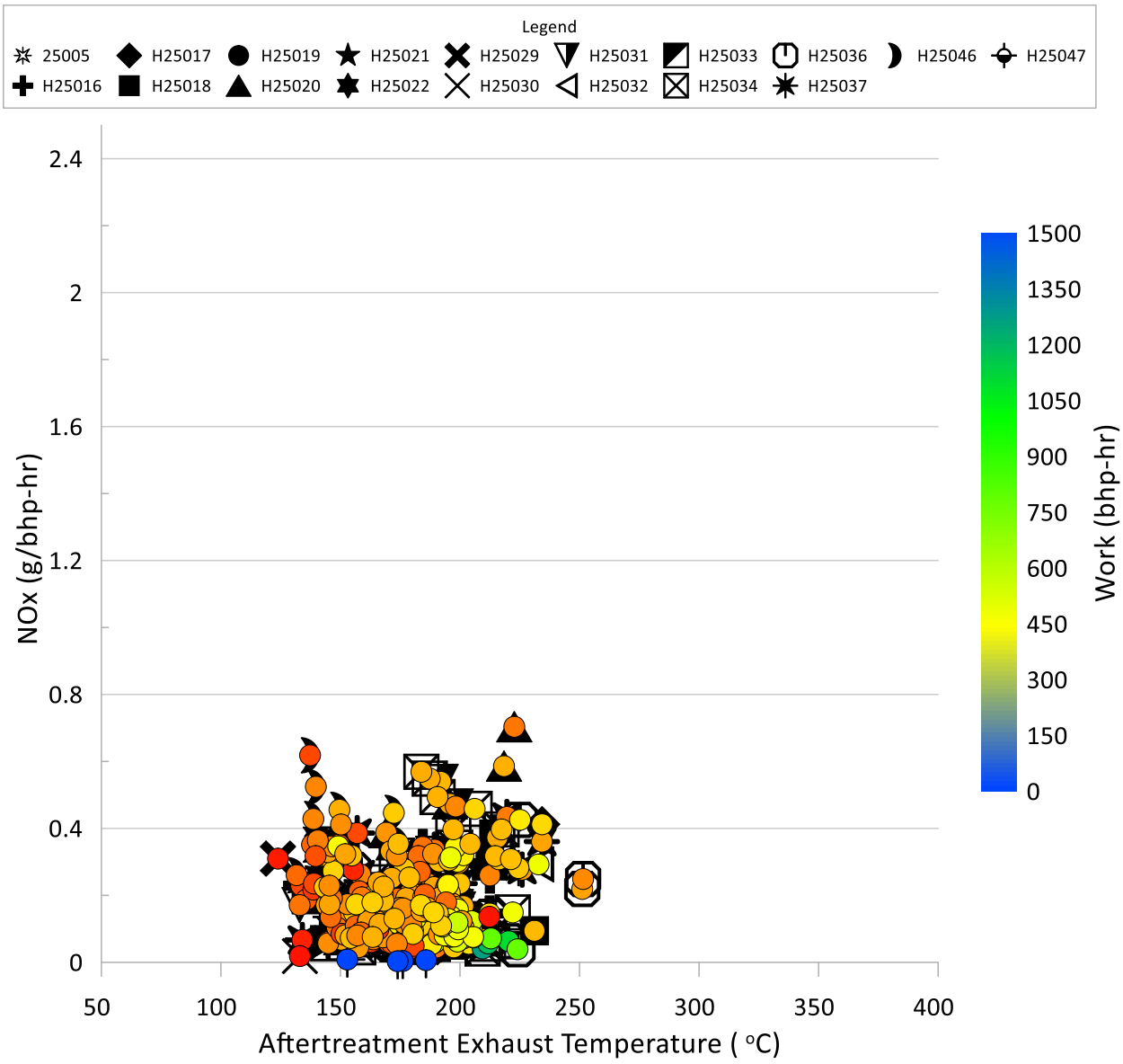

Figure 5-11 OSAR NOx Emission Rates in g/bhp-hr units for DGM 6

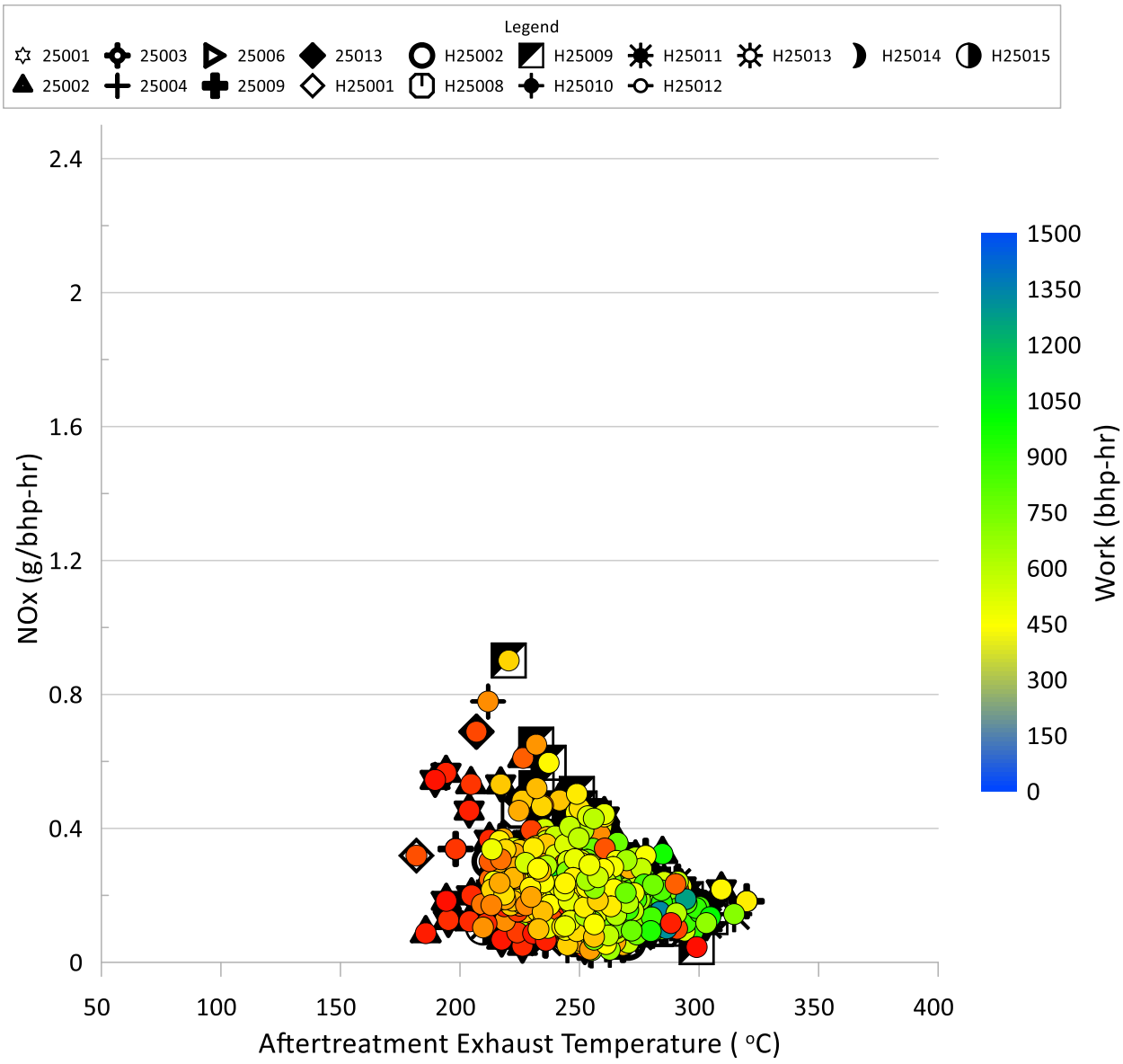

Figure 5-12 OSAR NOx Emission Rates in g/bhp-hr units for DTT 1

5.1.3 Real-time

Real-time emissions data were analyzed to better understand the trends for the different vehicles. Real-time emissions for higher emitting vehicles in the DGM 1 and DTT 1 fleets are shown in Figure 5-13 and Figure 5-14, respectively. The higher emitter for the DGM 1 fleet was a 2014 model year vehicle, while the higher emitter for the DTT 1 fleet was a 2022 model year vehicle. These graphs show accumulated NOx in grams per second, engine speed, and SCR outlet temperature. For comparison, real-time NOx emissions for two lower emitting vehicles from the same fleets can be seen in Figure 5-15 and Figure 5-16. These figures show that the emission levels for the higher emitting vehicles have a much higher magnitude than the lower emitting vehicles throughout the course of the vehicle's operation. This includes periods where the SCR outlet temperatures are at or above the 200 ºC - 250 ºC, which is the temperature range where the SCR

would be expected to effectively reduce NOx emissions. Between the high and normal emitters, OSAR measured and HEM logger measured data sets are shown for comparison.

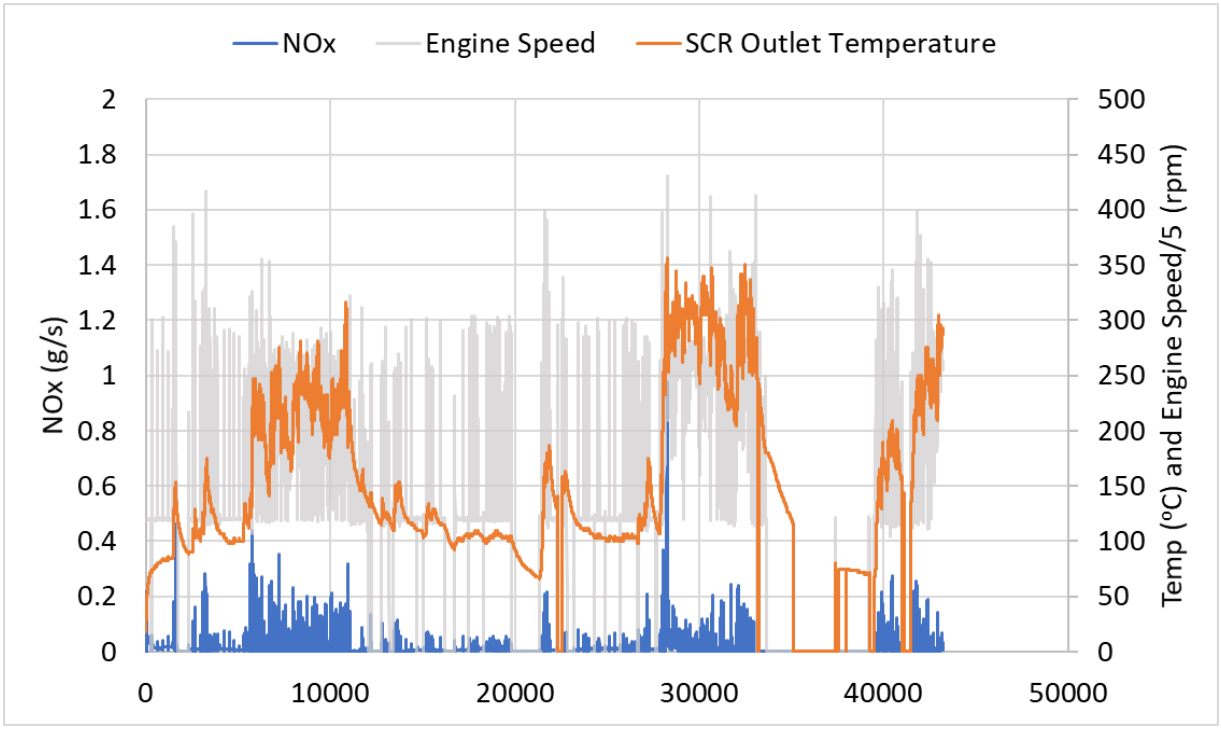

Figure 5-13 NOx real-time emission as function of vehicle speed and temperature for DGM 1 – High Emitter 1 – OSAR Measurement

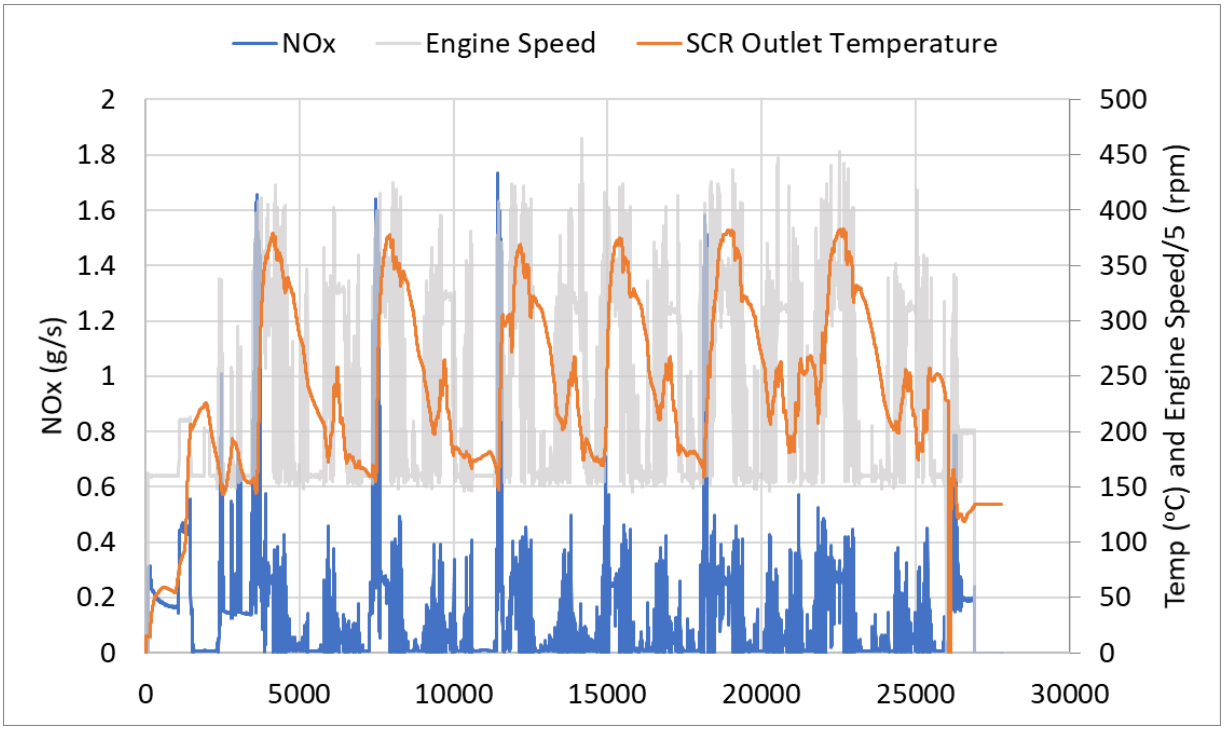

Figure 5-14 NOx real-time emission as function of vehicle speed and temperature for DTT 1 – High Emitter 2 – HEM Measurement

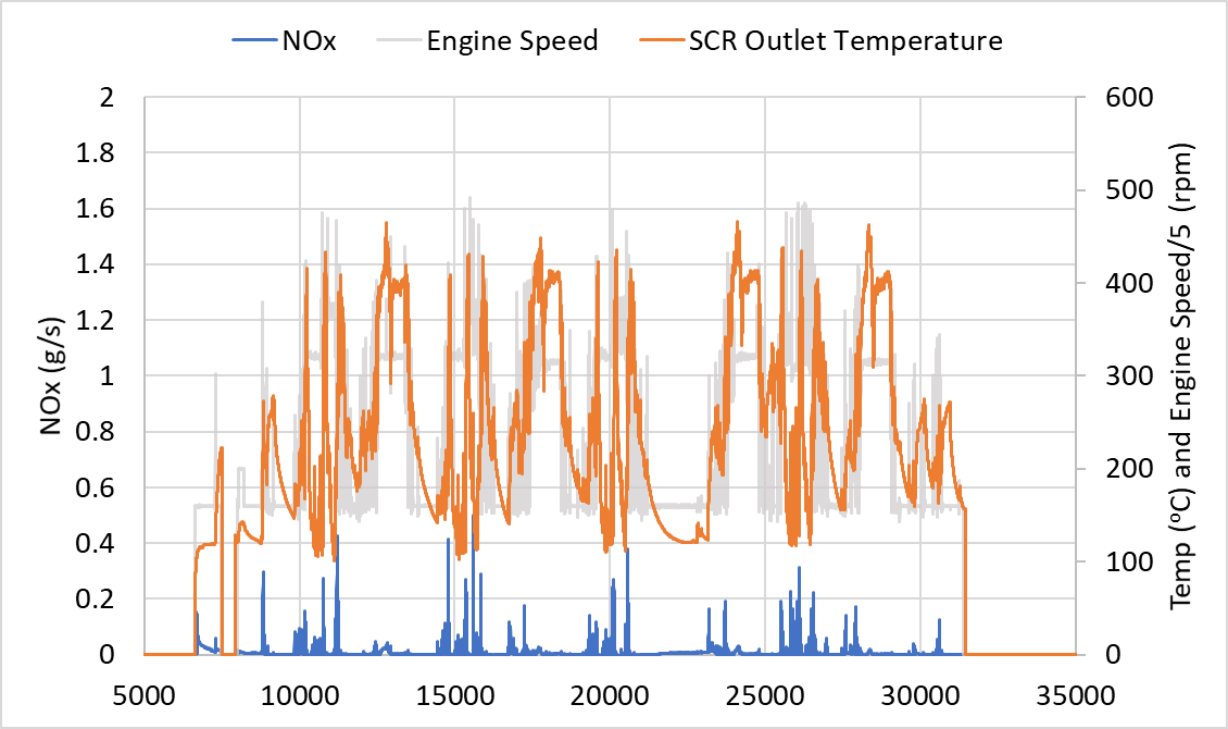

Figure 5-15 NOx real-time emission accumulation as of vehicle speed and temperature for DTT 1 – Lower Emitter 1 – OSAR Measurement

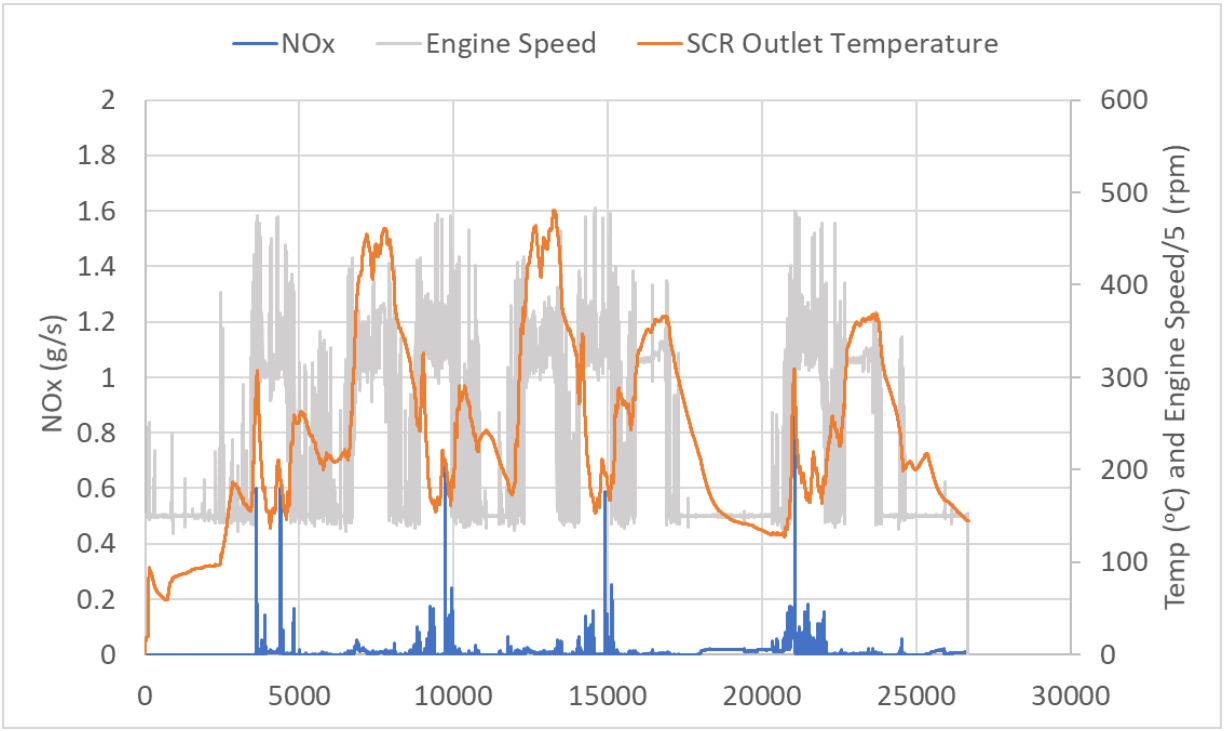

Figure 5-16 NOx real-time emission as function of vehicle speed and temperature for DTT 1 – Lower Emitter 2 – HEM Measurement

5.1.4 EPA 2Bin

EPA 2 bin analysis results for NOx for the average of the different test vehicles with the different fleets are presented in Table 5-2 based on the regulatory BIN window requirements. For Bin 1, the two tables show that the idling NOx emissions were on average less than 20 g/hr for all but the DGM 1 and DTT 1 fleets. For Bin 2, two fleets were found to already meet the future 0.035 g/bhp-hr in-use off-cycle requirement (DMG 3 and DMG 4). Three other fleets showed Bin 2 emissions near the current emissions standard (DGM 2 and DGM 6) or closer to twice the standard (DGM 5). Two other fleets (DGM 1 and DTT 1) showed higher emissions. The higher emissions for DGM 1 is consistent with the higher emissions seen in Figure 5-1, and the generally lower aftertreatment temperatures, as shown in Figure 5-6.

Table 5-2 Summary of Average and Standard Deviation for NOx emissions for the EPA 2Bin MAW (2400 windows for bin 1 and bin 2)

	Average and Standard Deviation NOx emissions							
Bin	**DGM 1**	**DGM 2**	**DGM 3**	**DGM 4**	**DGM 5**	**DGM 6**	**DTT 1**	**Total Average**
Bin 1 (g/hr)	32.4 ± 12.4	11.0 ± 14.4	9.54 ± 16.3	-	7.47 ± 13.9	4.98 ± 4.69	21.4 ± 27.7	14.46 ± 14.89
Bin 2 (g/bhp-hr)	0.801 ± 0.600	0.277 ± 0.535	0.011	0.032	0.443 ± 0.698	0.223	1.81 ± 1.22	0.514 ±0.763

5.1.5 CARB Real

CARB REAL bin analysis results for the different test vehicles with the different fleets are presented in Figure 5-17, Figure 5-18, Table 5-3 and Table 5-4. Figure 5-17 shows the histogram of total hours for Bin 1, which represents the total number of hours in the data set. Figure 5-18 shows a bar chart with the average NOx emissions over all the tested vehicles and all of the monitoring time for the different bins. Table 5-3 shows the total hours for all the Bins, with the table entries shaded in blue for higher number of hours to red for lower number of hours. Table 5-4 shows the sum over sum NOx emissions for each of the bins. Note that Bins 15 and 16 are not included in the Figures and Tables, as there are no regenerations or NTE events recorded.

The total hours in Bin 1, as shown in Figure 5-17, ranged from 80 hours to 220 hours on average per fleet. This indicates that the data sets for individual vehicles in most cases were either comparable to or greater than the 100 hours that is used for the regulatory basis for REAL.

The REAL binning analysis shows that most of the NOx emissions were generated when the fleet vehicles are under low load (i.e., < 25%), low speed, and idle conditions. Table 5-3 shows that about 1/3rd of the monitoring time was spent under idle conditions, with another 1/3rd of the time spent at loads ≤ 25%. The emission rates under idle conditions ranged from 0.552 to 17.34 g/hr, with g/hr emissions rates all being below 20 g/hr. Under low load conditions, the emissions for most fleets and bins were within twice the emissions standard or less, with a range from 0.081 to 1.487 g/bhp-hr across the different fleets. Once higher speeds and loads are reached, NOx

emissions greatly decrease, with the average emission rates for most bins with loads above 25% being comparable to or below 0.2 g/bhp-hr.

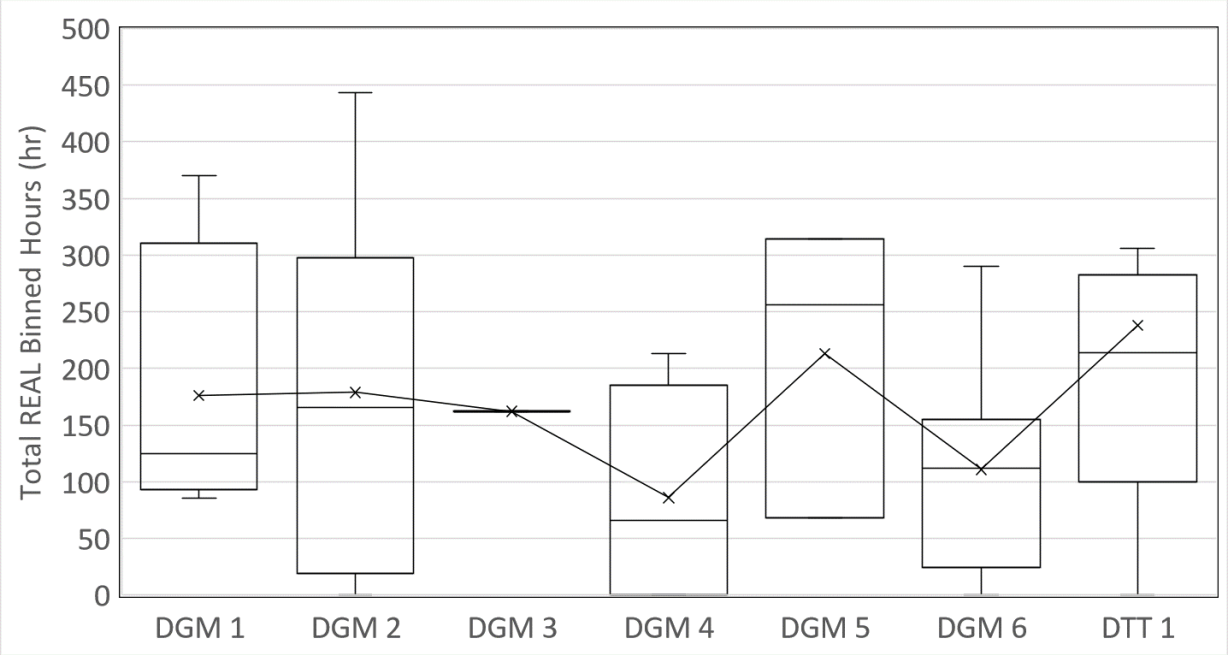

Figure 5-17 Total hours per fleet for REAL Bin 1

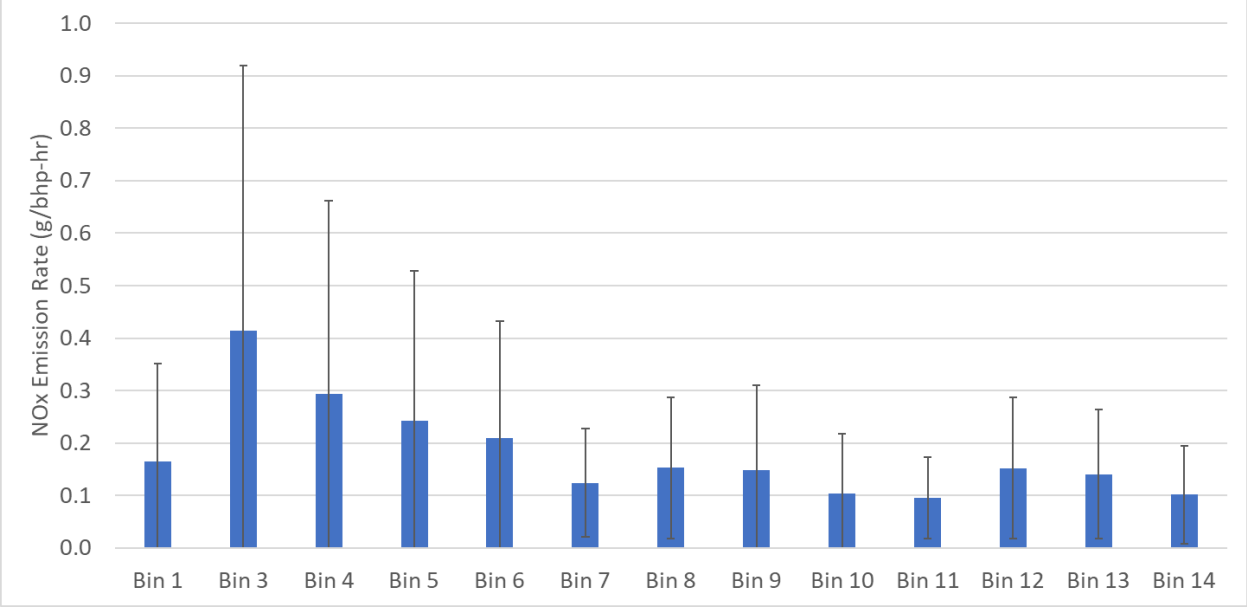

Figure 5-18 Average Emissions Across the REAL Bins

Table 5-3 Total Hours per REAL Bin

REAL			Total Hours Per Bin							
Bin	**Speed (mph)**	**Load**	**DGM 1**	**DGM 2**	**DGM 3**	**DGM 4**	**DGM 5**	**DGM 6**	**DTT 1**	**Total Average**
1	Total		704	1431	324	775	639	1995	4285	1450
2	Idle (g/hr)		193	556	14	165	168	480	1339	416
3	0-16	⩽ 25%	115	169	8	215	83	844	880	331
4	16-40	⩽ 25%	85	87	4	89	46	226	282	117
5	40-64	⩽ 25%	49	73	23	55	26	129	151	72
6	64 <	⩽ 25%	93	129	65	94	83	90	441	142
7	0-16	25%-50%	4	10	1	9	4	12	40	11
8	16-40	25%-50%	14	25	1	16	13	46	62	25
9	40-64	25%-50%	16	33	8	18	12	43	78	30
10	64 <	25%-50%	81	156	133	61	90	57	391	138
11	0-16	50% ⩽	1	2	0	2	1	2	24	5
12	16-40	50% ⩽	5	22	3	10	8	17	90	22
13	40-64	50% ⩽	10	34	7	10	11	22	120	31
14	64 <	50% ⩽	39	135	58	30	94	28	386	110

Table 5-4 Summary of Sum over Sum NOx emissions for REAL Bins in g/bhp-hr

Bin	Speed (mph)	Load	DGM 1	DGM 2	DGM 3	DGM 4	DGM 5	DGM 6	DTT 1	Total Average
1	Total		0.559	0.037	0.024	0.062	0.152	0.107	0.215	0.165
2	Idle (g/hr)		5.092	17.344	3.317	1.180	0.552	3.064	0.867	4.488
3	0-16	⩽ 25%	1.487	0.201	0.081	0.054	0.544	0.131	0.398	0.414
4	16-40	⩽ 25%	1.084	0.073	0.011	0.090	0.305	0.159	0.337	0.294
5	40-64	⩽ 25%	0.823	0.038	0.017	0.063	0.360	0.127	0.272	0.243
6	64 <	⩽ 25%	0.535	0.001	0.010	0.065	0.374	0.070	0.410	0.209
7	0-16	25%-50%	0.311	0.169	0.026	0.026	0.092	0.063	0.181	0.124
8	16-40	25%-50%	0.426	0.091	0.020	0.069	0.132	0.116	0.217	0.153
9	40-64	25%-50%	0.494	0.044	0.021	0.063	0.151	0.103	0.163	0.148
10	64 <	25%-50%	0.339	0.001	0.022	0.048	0.114	0.062	0.140	0.104
11	0-16	50% ⩽	0.234	0.103	0.027	0.026	0.065	0.052	0.162	0.096
12	16-40	50% ⩽	0.421	0.066	0.039	0.072	0.135	0.096	0.234	0.152
13	40-64	50% ⩽	0.388	0.021	0.035	0.103	0.135	0.115	0.186	0.140
14	64 <	50% ⩽	0.279	0.001	0.026	0.065	0.096	0.081	0.161	0.101

5.2 PM Emissions

Figure 5-19 shows the daily average PM emissions in mg/bhp-hr for the seven different fleets. Average PM emissions across the fleets ranged from 0.5 to 46 mg/bhp-hr. DGM 4 showed the highest PM rate at 46 mg/bhp-hr. While DGM 2 and DTT 1 showed the lowest emission rates, of 8.1 and 6.5 mg/bhp-hr, respectively. Compared to emission standards of 5 mg/bhp-hr, only two fleets had emission rates below the certification standards.

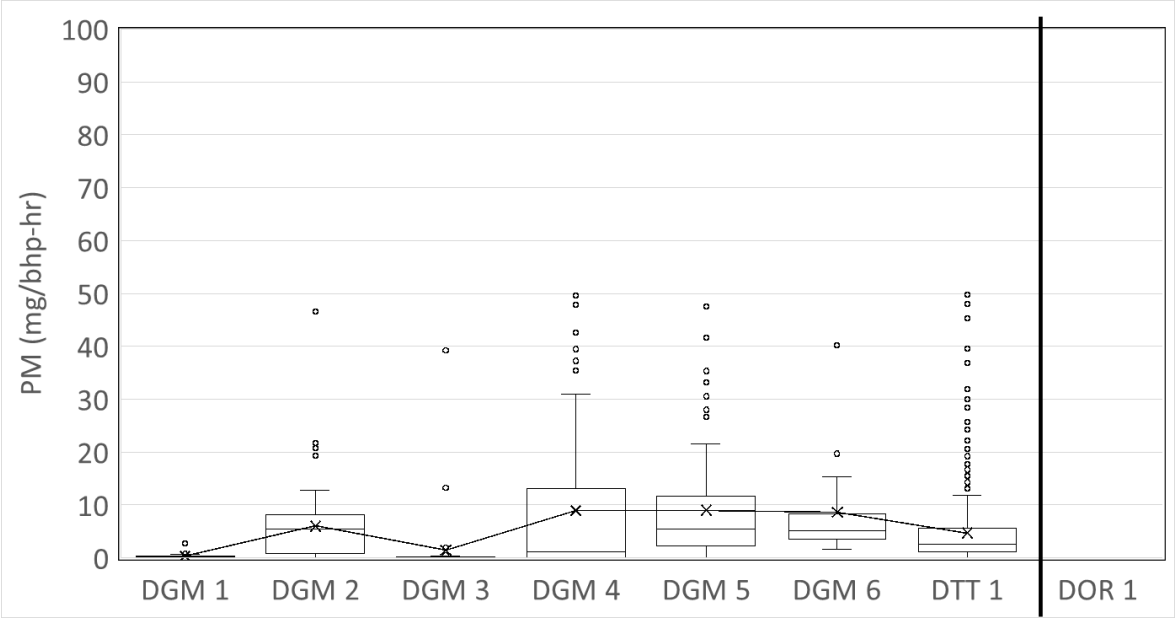

Figure 5-19 Daily Average PM for Fleet in mg/bhp-hr

5.3 CO_2 Emissions

As shown in Figure 5-20, the daily average CO_2 emissions for each fleet type ranged from 441 to 516 g/bhp-hr. On average, the fleets emitted 473 g/bhp-hr, with DOR 1 and DTT 1 showing slightly higher CO_2 values. This is comparable to the certification values for the engines. The average CO_2 emissions on a g/mi basis was 1645 g/mi for the on-road fleets, with a range from 1271 to 2066 g/mi, and 761 g/mi for the off-road fleet. DGM 3 had the lowest g/mi CO_2 emissions, while DGM 4 had the highest g/mi CO_2 emissions. The lower CO_2 emissions for DGM 3 can be attributed to its higher average speed driving patterns. By contrast, DGM 4 included a much lower milage, on average, with similar load levels, so the g/mi emissions ended up higher on average.

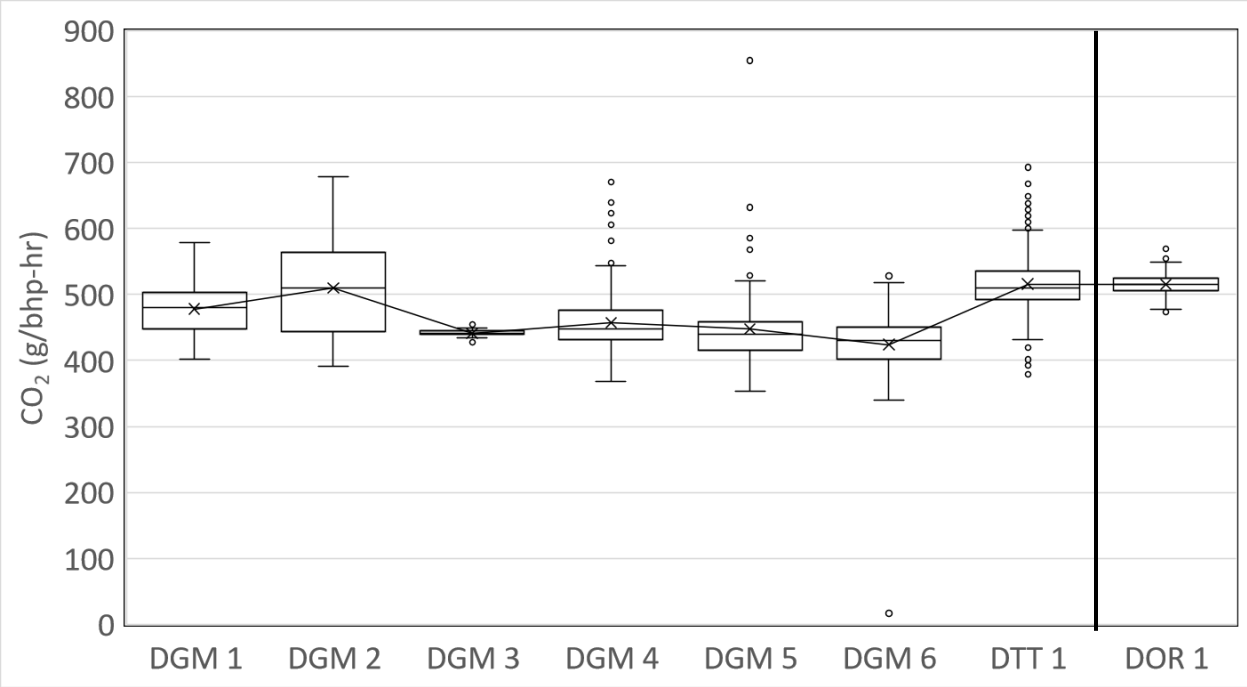

Figure 5-20 Measured Daily Average CO_2 for Fleet in g/bhp-hr

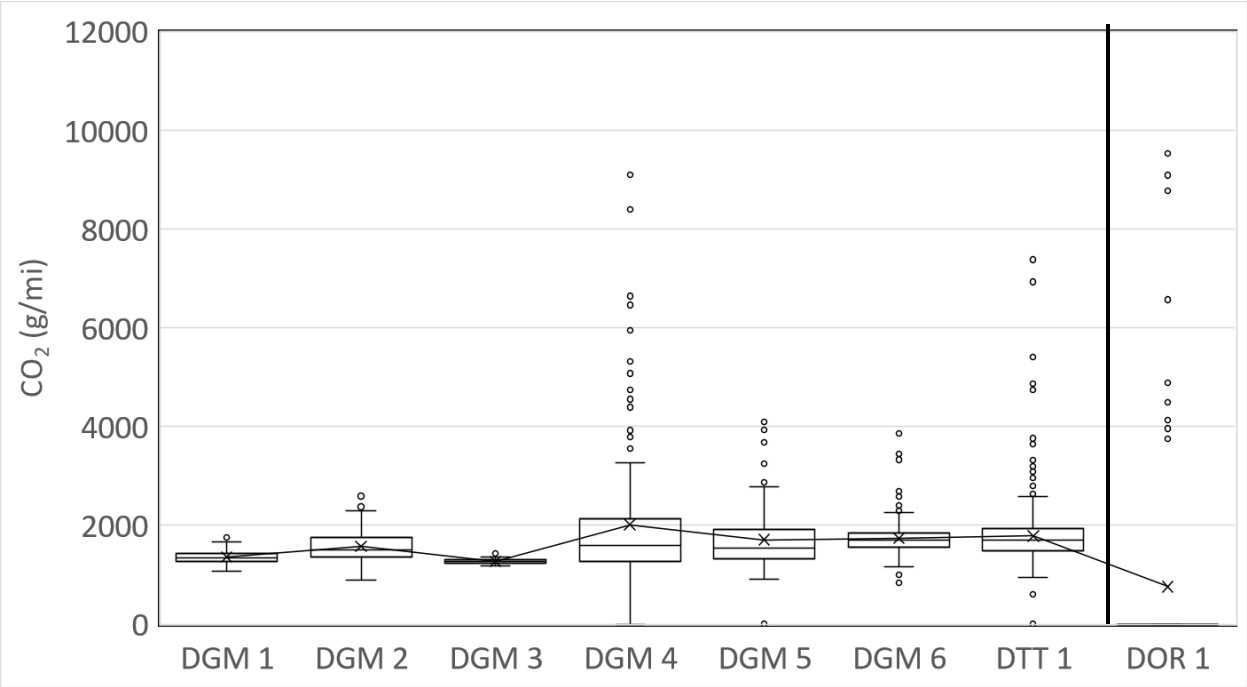

Figure 5-21 Measured Daily Average CO_2 for Fleet in g/mi

6 Summary and Conclusions

Reducing emissions from mobile sources remains one of the most important environmental challenges in the near term, and extending out over the next few decades. The California Air Resources Board (CARB) has been a leader in developing and implementing regulations to deal with both air pollutants, such as nitrogen oxides (NOx), and carbon dioxide (CO_2) emissions, as the primary greenhouse gas (GHG) of concern. This is being carried out through a range of different regulatory programs that include both increasing tighter emissions standards, as well as the monitoring of heavy-duty diesel vehicle (HDDV) performance and emissions using sensors and the vehicles on-board diagnostic (OBD) system. The objective of this research is to evaluate the potential of state-of-the-art and innovative sensor technologies in meeting the monitoring needs for recently implemented and future regulatory programs. The research included the monitoring of NOx, particulate matter (PM), and CO_2 emissions from on-road HDDVs and large off-road diesel engines (ORDEs) using sensors.

The intercept ranged from 0.9 to 10.0 for the initial calibrations and -0.8 to 17.3 for the final calibrations. The R^2 ranged from 0.751 to 1.000 for the initial and final calibrations. Percent differences ranged from 0.6% to 25% for the R2, 1% to -5027% for the slope, and -1693% to 1318% for the intercept.

On a g/bhp-hr basis, average NOx emissions across the fleets ranged from less than 0.02 to about 0.82 g/bhp-hr. The results for individual vehicles did show some variability, indicating a wider range in emission rates for the individual vehicles. Several fleets showed outliers that were greater than 1.0 g/bhp-hr, even though the average emissions were around 0.2 g/bhp-hr. The results from the histogram show that the majority of the vehicles (36 of 56) showed emissions below 0.2 g/bhp-hr, with another 15 of 56 vehicles showing emissions below 0.4 g/bhp-hr. A total of 5 vehicles showed emissions >0.6 g/bhp-hr, with 2 of those having emissions >1.0 g/bhp-hr. The higher emitting vehicles ranged in model year from 2013 to 2022, and included three vehicles from the same fleet. The two highest emitters included one older 2013 vehicle and a 2019 vehicle, and were both from the same fleet. The other two vehicles, with emission rates of 0.66 and 0.67 g/bhp-hr, included on older 2015 vehicle and one newer 2022 vehicle.

The daily results show a broader distribution of emission rates with a number of days showing emissions above 1 g/bhp-hr. DGM 6 and DTT 1 showed a bulk of the days of operation with emissions from 0.2 to 0.4 g/bhp-hr, which is still within twice the standard. The DGM 3 fleet showed the lowest emissions, with all of the daily emissions well below 0.2 g/bhp-hr. The DGM 3 fleet had the lowest emissions, which can be attributed to the highway speeds, and the higher aftertreatment temperatures. In contrast, DGM 1, which had the highest emissions, showed lower aftertreatment temperatures, closer to 200 ºC. DGM 1 also included much older model year vehicles, ranging from 2013 to 2019, compared to DGM 3, which only utilized 2023 model year vehicles with low odometer readings.

For EPA Bin 1, the two tables show that the idling NOx emissions were on average less than 20 g/hr for all but the DTT 1 and DGM 1 fleets. For EPA Bin 2 all but DGM 3 and 4 were on average above the 0.035 g/hp-hr in-use off-cycle requirement.

The REAL binning analysis shows that most of the NOx emissions were generated when the fleet vehicles are under low load (i.e., < 25%), low speed, and idle conditions. Table 5-3 shows that about 1/3rd of the monitoring time was spent under idle conditions, with another 1/3rd of the time spent at loads ⩽ 25%. The emission rates under idle conditions ranged from 0.552 to 17.34 g/bhp-hr and under low load conditions ranged 0.081 to 1.487 g/bhp-hr of NOx across the different fleets. Once higher speeds and loads are reached, NOx emissions greatly decrease, with the average emission rates for most bins with loads above 25% being comparable to or below 0.2 g/bhp-hr.

The real-time emission results show that the spikes for the higher emitting vehicles have a much higher magnitude than the normal emitting vehicles. The SCR outlet temperatures for these days appear to be consistently around 250 ºC so this seems to indicate that the aftertreatment systems for these vehicles are likely working appropriately. Between the high and normal emitters, OSAR measured and HEM logger measured data sets are shown for comparison. Between the different methods, there appears to be more noise in the OSAR measurements, while the HEM data is smoother overall. While this may be the case, both the OSAR system and the HEM system are able to identify the higher emitting vehicles and the OSAR system has the benefit of collecting the cold start data which the HEM logger is unable to collect.

Average PM emissions across the fleets ranged from 0.5 to 46 mg/bhp-hr. DGM 4 showed the highest PM rate at 46 mg/bhp-hr. While DGM 2 and DTT 1 showed the lowest emission rates, of 8.1 and 6.5 mg/bhp-hr, respectively. The daily average CO_2 emissions for each fleet type ranged from 441 to 516 g/bhp-hr. On average, the fleets emitted 473 g/bhp-hr, with DOR 1 and DTT 1 showing slightly higher CO_2 values. The average CO_2 emissions on a g/mi basis was 1645 g/mi for the on-road fleets, with a range from 1271 to 2066 g/mi.

References

Achhammer, R., Ante, J., Bierl, R., Heinrich, S., Herrmann, M., Lauerer, W., Ott, A., Weigl, M., and Wildgen, A. (2014). SOOT SENSOR. USOO8653.838B2 (10).

Aliramezani, M., Koch, C.R., and Patrick, R. (2018). Phenomenological model of a solid electrolyte NOx and O_2 sensor using temperature perturbation for on-board diagnostics. *Solid State Ion* 321 (x):62–68. doi:10.1016/j.ssi.2018.04.004.

Andersson, M., Khajavizadeh, L., and Lloyd Spetz, A. (2020). Development of an FET-based NH_3/NOx sensor unit for SCR-control. (x):425–426. doi:10.5162/imcs2018/fe.2.

Baier, T., Dupeux, G., Herbert, S., Hardt, S., and Quere, D. (2012). Propulsion Mechanisms for Leidenfrost Solids on Ratchets. 1 (12):0–4. doi:10.1103/PhysRevE.87.021001.

Besch, M.C., Thiruvengadam, A., Kappanna, H.K., Cozzolini, A., Carder, D.K., Gautam, M., and Tikkanen, J. (2011). Assessment of Novel In-Line Particulate Matter Sensor With Respect to OBD and Emissions Control Applications*., in ASME 2011 Internal Combustion Engine Division Fall Technical Conference,* ASMEDC, pp. 689–701.

Bilby, D., Kubinski, D.J., Maricq, M.M. (2016) Current amplification in an electrostatic trap by soot dendrite growth and fragmentation: Application to soot sensors, J. Aerosol Sci., 98, 41–58.

Bleicker, D. and Noack, F. (2016). Neues Sensorprinzip zur NOx-Messung. *ATZ worldwide* 9 (3):36–39. doi:10.1007/s35746-016-0023-y.

Bleicker, D., Noack, F., Costa, L., and Ruhl, S. (2020). NOx Sensor for commercial vehicle and mobile machines. *ATZ worldwide* 38–41.

CALSTART 2020 Volvo Lights Total Cost of Ownership Fleet Evaluation, Final Report to AQMD January 2020.

CARB. (2020c). EMFAC Model. Retrieved from https://arb.ca.gov/emfac/

Cheng, Y., He, L., He, W., Zhao, P., Wang, P., Zhao, J., Zhang, K., and Zhang, S. (2019). Evaluating on-board sensing-based nitrogen oxides (NOX) emissions from a heavy-duty diesel truck in China. *Atmos Environ* 216 (X):116908. doi:10.1016/j.atmosenv.2019.116908.

Chou, C.C., Chiang, C.J., Su, Y.H., and Ku, Y.Y. (2014). Identification of cross-sensitivity of smart nox sensors to ammonia in urea-selective catalyst reduction systems via fast fourier transform*., in Sensors and Materials,* pp. 313–318.

Chowdhury, M.F., Hopper, R., Ali, S.Z., Gardner, J.W., and Udrea, F. (2016). MEMS Infrared Emitter and Detector for Capnography Applications. *Procedia Eng* 168:1204–1207. doi:10.1016/j.proeng.2016.11.415.

Dixit, P., Miller, J.W., Cocker, D.R., Oshinuga, A., Jiang, Y., Durbin, T.D., and Johnson, K.C. (2017). Differences between emissions measured in urban driving and certification testing of heavy-duty diesel engines. *Atmos Environ* 166:276–285. doi:10.1016/j.atmosenv.2017.06.037.

Dmitrzak, M., Jasinski, P., and Jasinski, G. (2020). Limited selectivity of amperometric gas sensors operating in multicomponent gas mixtures and methods of selectivity improvement. *Bulletin of the Polish Academy of Sciences Technical Sciences* 68 (No. 6):1275–1282.

Elumalai, P., Plashnitsa, V. V., Fujio, Y., and Miura, N. (2008). Stabilized zirconia-based sensor attached with NiOAu sensing electrode aiming for highly selective detection of ammonia in automobile exhausts. *Electrochemical and Solid-State Letters* 11 (11):J79. doi:10.1149/1.2971171.

Energy, U.S.D.o., U.S. Life Cycle Inventory Database Roadmap. 2009., (n.d.).

Figueroa, O.L., Lee, C., Akbar, S.A., Szabo, N.F., Trimboli, J.A., Dutta, P.K., Sawaki, N., Soliman, A.A., and Verweij, H. (2005). Temperature-controlled CO, CO_2 and NOx sensing in a diesel engine exhaust stream. Sens Actuators B Chem 107 (2):839–848. doi:10.1016/j.snb.2004.12.025.

Galindo, J., Serrano, J.R., Guardiola, C., Blanco-Rodriguez, D., and Cuadrado, I.G. (2011). An on-engine method for dynamic characterisation of NOx concentration sensors. *Exp Therm Fluid Sci* 35 (3):470–476. doi:10.1016/j.expthermflusci.2010.11.010.

Gautam, M., Riddle, W.C., Thompson, G.J., Carder, D.K., Clark, N.N., and Lyons, D.W. (2002). Measurement of brake-specific NOX emissions using zirconia sensors for in-use, on-board heavy-duty vehicle applications*., in SAE Technical Papers, .*

Gieshoff, J., Schäfer-Sindlinger, A., Spurk, P.C., Van Den Tillaart, J.A.A., and Garr, G. (2000). Improved SCR Systems for Heavy Duty Applications*., in SAE Technical Papers, .*

Gouma, P.I. and Kalyanasundaram, K. (2008). A selective nanosensing probe for nitric oxide. *Appl Phys Lett* 93 (24):18–21. doi:10.1063/1.3050524.

Guardiola, C., Martín, J., Pla, B., and Bares, P. (2017). Cycle by cycle NOx model for diesel engine control. *Appl Therm Eng* 110:1011–1020. doi:10.1016/j.applthermaleng.2016.08.170.

Hagen, G., Rieß, G., Schubert, M., Feulner, M., Müller, A., Brüggemann, D., and Moos, R. (2015). Capacitive Soot Sensor. *Procedia Eng* 120:241–244. doi:10.1016/j.proeng.2015.08.590.

Heepen, F. (2019). Introduction to SEMS Guidelines*., in 9th UCR PEMS Conference and Workshop,* pp. 1–6.

Hofmann, L., Rusch, K., Fischer, S., and Lemire, B. (2004). Onboard emissions monitoring on a HD truck with an SCR system using Nox sensors*., in SAE Technical Papers, .*

Ioannou, M., Papalambrou, G., Kyrtatos, N.P., Dumele, H., and Diessner, M. (2013). Evaluation of emission sensors for four-stroke marine diesel engines. *Journal of Marine Engineering and Technology* 12 (3):20–29. doi:10.1080/20464177.2013.11020284.

ISO, I.O.f.S., Environmental management - Life Cycle Assessment - Requirements and guidelines. 2010., (n.d.).

Jeong, J.W., Cha, J., Chon, M.S., and Lee, K. (2022). A Study on the Suitability of Sems Equipment for Monitoring Rde Tests. *SSRN Electronic Journal*. doi:10.2139/ssrn.4088435.

Johansson, P. (2008). Oil-related Particle Emissions from Diesel Engines, Licentiate Thesis. KTH University.

Johnson, K.C., Durbin, T., and Yang, J. (2018). Evaluation of NTK Compact Emission Meter PEMS : Assess Real World Emissions.

Kadijk, G., Heijne, V.A.M., Ligterink, N.E., and ... (2017). Variations of Real-world NOx Emissions of Diesel Light Commercial Vehicles. *TAP Zurich conference …* (November).

Kannan, S., Steinebach, H., Rieth, L., and Solzbacher, F. (2010). Selectivity, stability and repeatability of In2O3 thin films towards NOx at high temperatures (≥500 °C). *Sens Actuators B Chem* 148 (1):126–134. doi:10.1016/j.snb.2010.04.026.

Kawamoto, Y., Todo, Y., Shimokawa, H., Aoki, K., Kawai, M., and Ide, K. (2019). Development of High Accuracy NOx Sensor*., in SAE Technical Papers,* pp. 1–7.

Khalek, I. (2019). State of Spark-Plug Sized Exhaust Sensors for Real World Emissions Monitoring*., in 23rd ETH Nanoparticle Conference on Combustion Generated Particles, .*

Khalek, I., Premnath, V., and Sharp, C. (2021). Laboratory Investigation of Exhaust NO X / NH 3 Sensors for Onboard Emissions Monitoring. (X).

Kittelson, D.B. (1998). Engines and nanoparticles: A review. *J Aerosol Sci* 29 (5–6):575–588. doi:10.1016/S0021-8502(97)10037-4.

Kondo, A., Yokoi, S., Sakurai, T., Nishikawa, S., Egami, T., Tokuda, M., and Sakuma, T. (2011). New particulate matter sensor for on board diagnosis*., in 15th ETH Conference on Combustion Generated Nanoparticles, .*

Konstandopoulos, A.G., Skaperdas, E., and Masoudi, M. (2002). Microstructural Properties of Soot Deposits in Diesel Particulate Traps., *in SAE Technical Papers,* .

Kontses, D. (2019). Development of algorithms for estimation of particle emissions using soot sensor for on-board diagnostic systems. Aristotle Univeristy of Thessaloniki.

Kotz, A.J., Kittelson, D.B., and Northrop, W.F. (2016). Lagrangian Hotspots of In-Use NO x Emissions from Transit Buses. *Environ Sci Technol* 50 (11):5750–5756. doi:10.1021/acs.est.6b00550.

Lee. A., O'Cain, J., Avila. J., Lemieux, S., Karim, Sahay, K., Berdahi. S., Sahay, K., Na, K., Chang, O., and Macias, K., 2018. Findings from carb's heavy-duty in-use compliance testing program. Presentation at 28th CRC Real World Emissions Workshop, Garden Grove, CA, March.

Liati, A., Schreiber, D., Dimopoulos Eggenschwiler, P., and Arroyo Rojas Dasilva, Y. (2013a). Metal particle emissions in the exhaust stream of diesel engines: An electron microscope study. *Environ Sci Technol* 47 (24):14495–14501. doi:10.1021/es403121y.

Liati, A., Schreiber, D., Dimopoulos Eggenschwiler, P., and Arroyo Rojas Dasilva, Y. (2013b). Metal particle emissions in the exhaust stream of diesel engines: An electron microscope study. *Environ Sci Technol* 47 (24):14495–14501. doi:10.1021/es403121y.

Maeda, E. and Kimata, T. (2012). PARTICULATE MATTER DETECTION Publication Classification SENSOR. US 2012/008514.6 A1.

Maricq, M.M., Bilby, D. (2016) The impact of voltage and flow on the electrostatic soot sensor and the implications for its use as a diesel particulate filter monitor, J. Aerosol Sci., 124, 41–53.

Masoudi, M. (2002). Hydrodynamics of Diesel Particulate Filters., *in SAE Technical Papers,* .

McCaffery, C., Zhu, H., Tang, T., Li, C., Karavalakis, G., Cao, S., Oshinuga, A., Burnette, A., Johnson, K.C., and Durbin, T.D. (2021). Real-world NOx emissions from heavy-duty diesel, natural gas, and diesel hybrid electric vehicles of different vocations on California roadways. *Science of The Total Environment* 784:147224. doi:10.1016/J.SCITOTENV.2021.147224.

Ménil, F., Coillard, V., and Lucat, C. (2000). Critical review of nitrogen monoxide sensors for exhaust gases of lean burn engines. *Sens Actuators B Chem* 67 (1):1–23. doi:10.1016/S0925-4005(00)00401-9.

Meyer, C., Baumann, R., Günther, A., Vashook, V., Schmiel, T., Guth, U., and Fasoulas, S. (2013). Development of a solid state sensor for nitrogen oxides with a nitrate electrolyte. *Sens Actuators B Chem* 181:77–84. doi:10.1016/j.snb.2013.01.023.

Misra, C., Ruehl, C., Collins, J., Chernich, D., Herner, J. In-use NOx emissions from diesel and liquefied natural gas refuse trucks equipped with SCR and TWC, respectively. Environ, Sci. Technol. 2017, 51, 6981-6989.

Misra, C., Collins, J.F., Herner, J.D., Sax, T., Krishnamurthy, M., Sobieralski, W., Burntizki, M., and Chernich, D. (2013). In-Use NO $_x$ Emissions from Model Year 2010 and 2011 Heavy-Duty Diesel Engines Equipped with Aftertreatment Devices. *Environ Sci Technol* 47 (14):7892–7898. doi:10.1021/es4006288.

Miura, N., Koga, T., Nakatou, M., Elumalai, P., and Hasei, M. (2006). Electrochemical NOx sensors based on stabilized zirconia: Comparison of sensing performances of mixed-potential-type and impedancemetric NOx sensors., *in Journal of Electroceramics,* pp. 979–986.

Montes, T. (2018). Diesel OBD Programs ECARD Division presentation., *in SAE OBD Symposium Indianapolis,* .

Nishiyama, H., Kakimoto, S., Inoue, R., Yokoi, H., Ishida, N., Oshima, T., Sugaya, S., Imaeda, K., Hattori, T., and Satsuma, A. (2003). Ammonia sensor. US7341694B2.

Ntziachristos, L., Fragkiadoulakis, P., Samaras, Z., Janka, K., and Tikkanen, J. (2011). Exhaust Particle Sensor for OBD Application., *in SAE International,* .

Ochs, T., Schittenhelm, H., Genssle, A., and Kamp, B. (2010). Particulate Matter Sensor for On Board Diagnostics (OBD) of Diesel Particulate Filters (DPF). *SAE Int J Fuels Lubr* 3 (1):2010-01–0307. doi:10.4271/2010-01-0307.

Ono, T., Hasei, M., Kunimoto, A., Yamamoto, T., and Noda, A. (2001). Performance of the NO sensor based on mixed potential for automobiles in exhaust gases. 22:4–10.

Orban, J.E., Naber, S.J., Sharp, C.A., Khair, M.K., and McGill, R.N. (2005). Long-term aging of NOx sensors in heavy-duty engine exhaust. *SAE Technical Papers* (724). doi:10.4271/2005-01-3793.

Pohle, R., Magori, E., Tawil, A., Davydovskaya, P., and Fleischer, M. (2017). Detection of NOx in Combustion Engine Exhaust Gas by Applying the Pulsed Polarization Technique on YSZ Based Sensors*., in Proceedings of Eurosensors 2017, Paris, France, 3–6 September 2017,* MDPI, Basel Switzerland, p. 490.

Prasad, A.K., Gouma, P.I., Kubinski, D.J., Visser, J.H., Soltis, R.E., and Schmitz, P.J. (2003). Reactively sputtered MoO3 films for ammonia sensing. *Thin Solid Films* 436 (1):46–51. doi:10.1016/S0040-6090(03)00524-8.

Premnath, V., Khalek, I., Thompson, P., and Woo, L. (2020). Evaluation of an On-Board, Real-Time Electronic Particulate Matter Sensor Using Heavy-Duty On-Highway Diesel Engine Platform*,* SAE Technical Paper 2020-01-0385, doi:10.4271/2020-01-0385.

Qiu, T., Li, X., Lei, Y., Liu, X., Zhang, C., Feng, X., and Xu, H. (2015). The prediction of fuel injection quality using a NOx sensor for the on-board diagnosis of heavy-duty diesel engines with SCR systems. *Fuel* 141:192–199. doi:10.1016/j.fuel.2014.10.015.

Querel, C., Bonfils, A., Grondin, O., and Creff, Y. (2013). Control of a SCR system using a virtual NOx sensor*., in IFAC Proceedings Volumes (IFAC-PapersOnline),* pp. 9–14.

Quiros, D.C., Thiruvengadam, A., Pradhan, S., Besch, M., Thiruvengadam, P., Demirgok, B., Carder, D., Oshinuga, A., Huai, T., and Hu, S. (2016). Real-World Emissions from Modern Heavy-Duty Diesel, Natural Gas, and Hybrid Diesel Trucks Operating Along Major California Freight Corridors. *Emission Control Science and Technology* 2 (3):156–172. doi:10.1007/s40825-016-0044-0.

Quiros, D.C., Ham, W.A., Ianni, R., Smith, J.D., Sobieralski, W., Chernich, D.J., Hu, S., Huai, T., 2017. Assessing Emission Control System Durability using ARB's Pilot Heavy-Duty Truck and Bus Surveillance Program. Presentation at the 27th CRC Real World Emissions Workshop, Long Beach, CA, March.

Raju A., Hao, P., Life Cycle Assessment (LAC) for the Volvo Lights Project, Final Report February 2022.

Rheaume, J.M. (2010). UC Berkeley UC Berkeley Electronic Theses and Dissertations *Solid State Electrochemical Sensors for Nitrogen Oxide (NOx) Detection in Lean Exhaust Gases*.

Romanovskaya, V., Ivanovskaya, M., and Bogdanov, P. (1999). A study of sensing properties of Pt- and Au-loaded In2O3 ceramics. *Sens Actuators B Chem* 56 (1–2):31–36. doi:10.1016/S0925-4005(99)00018-0.

Rostedt, A., Ntziachristos, L.D., Simonen, P., Rönkkö, T., Samaras, Z.C., Hillamo, R., Janka, K., and Keskinen, J. (2017). A New Miniaturized Sensor for Ultra-Fast On-Board Soot Concentration Measurements. *SAE Int J Engines* 10 (4):1859–1865. doi:10.4271/2017-01-1008.

Samaras, Z.C., Andersson, J., Bergmann, A., Hausberger, S., Toumasatos, Z., Keskinen, J., Haisch, C., Kontses, A., Ntziachristos, L.D., Landl, L., Mamakos, A., and Bainschab, M. (2020). Measuring Automotive Exhaust Particles Down to 10 nm. doi:10.4271/2020-01-2209.

Sappok, A. and Bromberg, L. (2014). Radio Frequency Diesel Particulate Filter Soot and Ash Level Sensors: Enabling Adaptive Controls for Heavy-Duty Diesel Applications. *SAE Int J Commer Veh* 7 (2):2014-01–2349. doi:10.4271/2014-01-2349.

Sappok, A., Bromberg, L., Parks, J.E., and Prikhodko, V. (2010). Loading and Regeneration Analysis of a Diesel Particulate Filter with a Radio Frequency-Based Sensor*., in SAE Technical Papers, .*

Sappok, A.G. and Wong, V.W. (2007). Detailed chemical and physical characterization of ash species in diesel exhaust entering aftertreatment systems*., in SAE Technical Papers,* pp. 776–790.

Sasaki, H., Scholl, D., Parsons, M., Inagaki, H., Shiotani, K., Visser, J., Zawacki, G., Kawai, T., Teramoto, S., and Kubinski, D. (2010). Development of an Al_2O_3/ZrO_2-composite high-accuracy NOx sensor*., in SAE Technical Papers, .*

Sato, S., Abe, S., Himeno, R., Nagasawa, T., Kosaka, H., Tanaka, K., and Tange, T. (2020). Real-World Emission Analysis Methods Using Sensor-Based Emission Measurement System*., in SAE Technical Papers, .*

Schenk, C., McDonald, J., and Olson, B. (2001). High-efficiency NOx and PM exhaust emission control for heavy-duty on-highway diesel engines*., in SAE Technical Papers, .*

Schwelberger, M., Mamakos, A., Fierz, M., and Giechaskiel, B. (2019). Experimental Assessment of an Electrofilter and a Tandem Positive-Negative Corona Charger for the Measurement of Charged Nanoparticles formed in Selective Catalytic Reduction Systems. *Applied Sciences* 9 (6):1051. doi:10.3390/app9061051.

Sekhar, P.K., Brosha, E.L., Mukundan, R., Li, W., Nelson, M.A., Palanisamy, P., and Garzon, F.H. (2010). Application of commercial automotive sensor manufacturing methods for NOx/NH_3 mixed potential sensors for on-board emissions control. *Sens Actuators B Chem* 144 (1):112–119. doi:10.1016/j.snb.2009.10.045.

Siegberg, D. and Killinc, M. (2014). Thermal and Chemical Robustness of the Smart NOx Sensor*., in CTI Conference Exhaust Systems, .*

Söderena, P., Laurikko, J., Weber, C., Tilli, A., Kuikka, K., Kousa, A., Väkevä, O., Venho, A., Haaparanta, S., and Nuottimäki, J. (2020). Monitoring Euro 6 diesel passenger cars NOx emissions for one year in various ambient conditions with PEMS and NOx sensors. *Science of The Total Environment* 746 (x):140971. doi:10.1016/j.scitotenv.2020.140971.

Soufian, M., Irshaidat, M., Babaie, M., Elliott, G., Mahood, D., Pendlebury, L., Hughes, B., Darbyshire, N., Williams, J., Lupu, M.B., Jenkins, J.W., Jones, D., Havery, N., Abadaki, G., and Raynes, T. (2019). Real-time emission monitoring and display to reduce vehicle pollution using wireless network*., in Proceedings - International Conference on Developments in ESystems Engineering, DeSE,* pp. 960–963.

Spetz, A.L. and Bjorklund, R. (2012). Silicon carbide based sensor system for minimized emissions in flue gases.

Steppan, J., Henderson, B., Johnson, K., Yusuf Khan, M., Diller, T., Hall, M., Lourdhusamy, A., Allmendinger, K., and Matthews, R.D. (2011). Comparison of an On-Board, Real-Time Electronic PM Sensor with Laboratory Instruments Using a 2009 Heavy-Duty Diesel Vehicle*., in SAE 2011 World Congress & Exhibition, .*

Sur, R., Peng, W.Y., and Kempema, N. (2022). Laser-Based In-Exhaust Gas Sensor for On-Road Vehicles*., in SAE Technical Papers,* pp. 1–6.

Sur, R., Peng, W.Y., Strand, C., Mitchell Spearrin, R., Jeffries, J.B., Hanson, R.K., Bekal, A., Halder, P., Poonacha, S.P., Vartak, S., and Sridharan, A.K. (2017). Mid-infrared laser absorption spectroscopy of NO_2 at elevated temperatures. *J Quant Spectrosc Radiat Transf* 187 (2):364–374. doi:10.1016/j.jqsrt.2016.10.016.

Suresh, A., Khan, A., and Johnson, J.H. (2000). An Experimental and Modeling Study of Cordierite Traps - Pressure Drop and Permeability of Clean and Particulate Loaded Traps. *SAE Technical Paper Series* 1 (724). doi:10.4271/2000-01-0476.

Tan, P., Li, Y., and Shen, H. (2017). Effect of lubricant sulfur on the morphology and elemental composition of diesel exhaust particles. *J Environ Sci (China)* 55 (2003):354–362. doi:10.1016/j.jes.2017.01.014.

Tan, Y., Collins, J., Yoon, S., Herner, J., Henderick, P., Montes, T., Ham, W., Howard, C., Hu, S., Johnson, K., Scora, G., Sandez, D., Durin, T., 2018. NOx Emission Estimates from the Activity Data of On-Road Heavy-Duty Diesel Vehicles. Presentation at 28th CRC Real World Emissions Workshop, Garden Grove, CA, March.

Tan, Y., Henderick, P., Yoon, S., Herner, J., Montes, T., Boriboonsomsin, K., Johnson, K., Scora, G., Sandez, D., and Durbin, T.D. (2019). On-Board Sensor-Based NOx Emissions from Heavy-Duty Diesel Vehicles. *Environ Sci Technol* 53 (9):5504–5511. doi:10.1021/acs.est.8b07048.

Tang, W., Cai, Y., and Wang, J. (2015). Experimental studies on the diesel engine urea-SCR system using a double NOx sensor system. *Environmental Engineering Research* 20 (4):397–402. doi:10.4491/eer.2015.097.

Thermal Infrared emitters | IST AG (n.d.). Available at https://www.ist-ag.com/en/thermal-infrared-emitters (Accessed 11 October 2022).

Toorisaka, H., Minamikawa, J., Narita, H., Muramatsu, T., Kominami, T., and Sone, T. (2004). DPR Developed for Extremely Low PM Emissions in Production Commercial Vehicles*., in SAE Technical Papers,* pp. 447–456.

Toumasatos, Z., Raptopoulos-Chatzistefanou, A., Kolokotronis, D., Pistikopoulos, P., Samaras, Z., and Ntziachristos, L. (2022). The role of the driving dynamics beyond RDE limits and DPF regeneration events on pollutant emissions of a Euro 6d-temp passenger vehicle. *J Aerosol Sci* 161:105947. doi:10.1016/J.JAEROSCI.2021.105947.

Tsui, L., Benavidez, A.D., Palanisamy, P., Evans, L., and Garzon, F.H. (2016). A Three Electrode Mixed Potential Sensor for Gas Detection and Discrimination. *ECS Meeting Abstracts* MA2016-02 (50):3734–3734. doi:10.1149/ma2016-02/50/3734.

Tsui, L. kun, Benavidez, A., Evans, L., and Garzon, F.H. (2019). Additively manufactured mixed potential electrochemical sensors for NOx, C_3H_8, and NH_3 detection. *Progress in Additive Manufacturing* 4 (1):13–21. doi:10.1007/s40964-018-0054-2.

Tsui, L. kun, Benavidez, A., Palanisamy, P., Evans, L., and Garzon, F. (2018). Automatic signal decoding and sensor stability of a 3-electrode mixed-potential sensor for NOx/NH_3 quantification. *Electrochim Acta* 283 (x):141–148. doi:10.1016/j.electacta.2018.06.133.

Viricelle, J.-P., Vernoux, P., Gao, J., Romanytsia, I., Breuil, P., and Pijolat, C. (2016). NO 2 -Selective Electrochemical Sensors for Diesel Exhausts. *Procedia Eng* 168 (2):7–10. doi:10.1016/j.proeng.2016.11.112.

Vouitsis, E., Ntziachristos, L., Samaras, Z., Chrysikou, L., Samara, C., and Miltsios, G. (2011). Effect of Lube Oil on the Physicochemical Characteristics of Particulate Matter Emitted from a Euro 4 Light Duty Diesel Vehicle. *SAE Technical Paper Series* 1 (x). doi:10.4271/2007-24-0110.

Wang, D.Y., Yao, S., Shost, M., Yoo, J.H., Cabush, D., Racine, D., Cloudt, R., and Willems, F. (2008). Ammonia sensor for closed-loop SCR control. *SAE Technical Papers* 1 (1). doi:10.4271/2008-01-0919.

Wang, Y.Y., Zhang, H., and Wang, J. (2016). NOx Sensor Reading Correction in Diesel Engine Selective Catalytic Reduction System Applications. *IEEE/ASME Transactions on Mechatronics* 21 (1):460–471. doi:10.1109/TMECH.2015.2434846.

Willems, F., Cloudt, R., van den Eijnden, E., van Genderen, M., Verbeek, R., de Jager, B., Boomsma, W., and van den Heuvel, I. (2007). Is Closed-Loop SCR Control Required to Meet Future Emission Targets?*, in SAE Technical Papers,* .

Xu, C.N., Miura, N., Ishida, Y., Matsuda, K., and Yamazoe, N. (2000). Selective detection of NH_3 over NO in combustion exhausts by using Au and MoO3 doubly promoted WO3 element. *Sens Actuators B Chem* 65 (1–3):163–165. doi:10.1016/S0925-4005(99)00413-X.

Yang, J., Durbin, T.D., Jiang, Y., Tange, T., Karavalakis, G., Cocker, D.R., and Johnson, K.C. (2018). A comparison of a mini-PEMS and a 1065 compliant PEMS for on-road gaseous and particulate emissions from a light duty diesel truck. *Science of the Total Environment* 640–641:364–376. doi:10.1016/j.scitotenv.2018.04.383.

Yang, K., Fox, J.T., and Hunsicker, R. (2016). Characterizing Diesel Particulate Filter Failure During Commercial Fleet Use due to Pinholes, Melting, Cracking, and Fouling. *Emission Control Science and Technology* 2 (3):145–155. doi:10.1007/s40825-016-0036-0.

Yang, L., Zhang, Shaojun, Wu, Y., Chen, Q., Niu, T., Huang, X., Zhang, Shida, Zhang, L., Zhou, Y., and Hao, J. (2016). Evaluating real-world CO_2 and NOx emissions for public transit buses using a remote wireless on-board diagnostic (OBD) approach. *Environmental Pollution* 218 (X):453–462. doi:10.1016/j.envpol.2016.07.025.

Yoon, S., Collins, J.F., Misra, C., Herner, J.D., Carter, M.W., and Sax, T.P. (2017). In-Use Emissions from 2010-Technology Heavy-Duty Trucks: Impact on Air Quality Planning in California. *Transportation Research Record: Journal of the Transportation Research Board* 2627 (1):1–8. doi:10.3141/2627-01.

Zhang, S., Zhao, P., He, L., Yang, Y., Liu, B., He, W., Cheng, Y., Liu, Y., Liu, S., Hu, Q., Huang, C., and Wu, Y. (2020). On-board monitoring (OBM) for heavy-duty vehicle emissions in China: Regulations, early-stage evaluation and policy recommendations. *Science of the Total Environment* 731. doi:10.1016/j.scitotenv.2020.139045.

Appendix A – List of ECM Parameters Requested

SAE Name	PGN/PID	SPN
Accelerator Pedal Position 1	61443	91
Actual Engine-Percent Torque	61444	513
Actual Maximum Available Engine - Percent Torque	61443	3357
Actual Retarder - Percent Torque	61440	520
Aftertreatment 1 Exhaust Gas Mass-Flow-Rate	65247	3236
Aftertreatment 1 Outlet NOx	61455	3226
Aftertreatment 1 Selective Catalytic Reduction Intake Nox	61454	3216
Aftertreatment 1 Three Way Catalyst Intake Temperature	64838	4289
Aftertreatment 1 Three Way Catalyst Outlet Temperature	64838	4290
Ambient Air Temperature	65266	171
ASR Brake Control Active	61441	562
Brake Pedal Position	61441	521
Brake Switch	65265	597
EBS Brake Switch	61441	1121
Engine Coolant Temperature	65262	110
Engine Exhaust Flow Rate	64587	6895
Engine Exhaust O2 Sensor 1 Air/Fuel Equivalence Ratio	64060	22139
Engine Exhaust O2 Sensor 2 Air/Fuel Equivalence Ratio	64060	22141
Engine Exhaust Temperature	65270	173
Engine Fuel Rate	65266	183
Engine Fuel Temperature 1	65262	174
Engine Intake Air Mass Flow Rate	61450	132
Engine Intake Air Pressure	65270	106
Engine Intake Manifold #1 Absolute Pressure	64976	3563
Engine Intake Manifold #1 Pressure	65270	102
Engine Intake Manifold #2 Pressure	64976	3562
Engine Intake Manifold 1 Temperature	65270	105
Engine Oil Temperature 1	65262	175
Engine Percent Load At Current Speed	61443	92
Engine Reference Torque	65251	544
Engine Speed	61444	190
Nominal Friction-Percent Torque	65247	514
Specific Humidity	64992	4490
Total Power Takeoff Hours	65255	248
Total Vehicle Distance	65248	245
Total Vehicle Hours	65254	246

Appendix B – Specifications for Individual Vehicles/Pieces of Equipment

Install ID	Anonymous Fleet Name	Category	OEM	Model Year	Engine Model	Displacement (L)
22001	DGM 1	On-Road	Detroit Diesel	2013	DD13	12.8
22002	DGM 1	On-Road	Detroit Diesel	2015	DD13	12.8
22003	DGM 1	On-Road	Detroit Diesel	2017	DD13	13.8
22004	DGM 1	On-Road	Detroit Diesel	2019	DD13	14.8
22005	DGM 2	On-Road	Cummins	2016	ISB6.7 260	6.7
22006	DGM 2	On-Road	Volvo	2014	D13J425	12.8
22007	DGM 2	On-Road	Volvo	2015	D13J425	12.8
22008	DGM 2	On-Road	Volvo	2016	D13J425	12.8
23005	DGM 2	On-Road	PACCAR	2016	ISB6.7 260	6.7
23006	DGM 2	On-Road	PACCAR	2016	ISB6.7 260	6.7
23008	DGM 2	On-Road	Volvo	2022	D13N-425	12.8
23009	DGM 2	On-Road	Volvo	2022	D13N-425	12.8
24041	DGM 3	On-Road	Detroit Diesel	2023	DD15 Gen 5 IDP (455 HP)	14.8
24042	DGM 3	On-Road	Detroit Diesel	2023	DD15 Gen 5 IDP (455 HP)	14.8
24060	DGM 3	On-Road	Detroit Diesel	2023	DD15 Gen 5 IDP (455 HP)	14.8
24061	DGM 3	On-Road	Detroit Diesel	2023	DD15 Gen 5 IDP (455 HP)	14.8
24056	DGM 4	On-Road	Detroit Diesel	2015	1700 455	NaN
25019	DGM 4	On-Road	Detroit Diesel	2023	NaN	NaN
25020	DGM 4	On-Road	Detroit Diesel	2023	NaN	NaN
H25005	DGM 4	On-Road	Detroit Diesel	2023	A14B 23	NaN
H25024	DGM 4	On-Road	Cummins	2023	X15 450	NaN
H25026	DGM 4	On-Road	Detroit Diesel	2023	NaN	NaN
H25028	DGM 4	On-Road	Detroit Diesel	2023	DD13	12.8
H25041	DGM 4	On-Road	Detroit Diesel	2023	DD13	12.8
H25043	DGM 4	On-Road	Detroit Diesel	2023	DD13	12.8

Install ID	Anonymous Fleet Name	Category	OEM	Model Year	Engine Model	Displacement (L)
24058	DGM 5	On-Road	Detroit Diesel	2017	NaN	NaN
24059	DGM 5	On-Road	Detroit Diesel	2022	DD13TCO	12.8
24070	DGM 5	On-Road	Detroit Diesel	2022	DD15TCD	14.2
25005	DGM 6	On-Road	PACCAR	2023	MX-13	12.9
H25016	DGM 6	On-Road	PACCAR	2023	MX-13	12.9
H25017	DGM 6	On-Road	PACCAR	2023	MX-13	12.9
H25018	DGM 6	On-Road	PACCAR	2023	MX-13	12.9
H25019	DGM 6	On-Road	PACCAR	2023	MX-13	12.9
H25020	DGM 6	On-Road	PACCAR	2023	MX-13	12.9
H25021	DGM 6	On-Road	PACCAR	2023	MX-13	12.9
H25022	DGM 6	On-Road	Cummins	2023	X15 500V	NaN
H25029	DGM 6	On-Road	Cummins	2023	MX-13	12.9
H25030	DGM 6	On-Road	Cummins	2023	MX-13	12.9
H25031	DGM 6	On-Road	Cummins	2023	MX-13	12.9
H25032	DGM 6	On-Road	Cummins	2023	MX-13	12.9
H25033	DGM 6	On-Road	Cummins	2023	MX-13	12.9
H25034	DGM 6	On-Road	Cummins	2023	MX-13	12.9
H25036	DGM 6	On-Road	Cummins	2023	MX-13	12.9
H25037	DGM 6	On-Road	Cummins	2023	MX-13	12.9
H25046	DGM 6	On-Road	Cummins	2023	ISX/ISX15/X15	14.9
H25047	DGM 6	On-Road	Cummins	2023	NaN	NaN
23020	DOR 1	Off-Road	Cummins	NaN	NaN	NaN
23021	DOR 1	Off-Road	Cummins	NaN	NaN	NaN
23022	DOR 1	Off-Road	Cummins	NaN	NaN	NaN
23023	DOR 1	Off-Road	Cummins	NaN	NaN	NaN
25001	DTT 1	On-Road	Cummins	2020	2017 ISL	8.9
25002	DTT 1	On-Road	Cummins	2021	PX9	8.9
25003	DTT 1	On-Road	Cummins	2020	L9 370	8.9
25004	DTT 1	On-Road	Cummins	2023	L9 370	8.9
25006	DTT 1	On-Road	Cummins	2021	L9 370	8.9
25009	DTT 1	On-Road	Cummins	2023	I9-370	8.9
25013	DTT 1	On-Road	Cummins	2020	L9 370	8.9
H25001	DTT 1	On-Road	Cummins	2022	L9 370	8.9
H25002	DTT 1	On-Road	Cummins	2020	L9 370	8.9
H25008	DTT 1	On-Road	Cummins	2020	L9 370	8.9

Install ID	Anonymous Fleet Name	Category	OEM	Model Year	Engine Model	Displacement (L)
H25009	DTT 1	On-Road	Cummins	2020	L9 370	8.9
H25010	DTT 1	On-Road	Cummins	2023	L9 370	8.9
H25011	DTT 1	On-Road	Cummins	2022	L9 370	8.9
H25012	DTT 1	On-Road	Cummins	2022	L9 370	8.9
H25013	DTT 1	On-Road	Cummins	2022	L9 370	8.9
H25014	DTT 1	On-Road	Cummins	2022	L9 370	8.9
H25015	DTT 1	On-Road	Cummins	2022	L9 370	8.9
H25027	DTT 1	On-Road	Cummins	2023	L9 370	8.9

Appendix C – Code used for Calculation of the OSAR Emission Results

OSAR Calculations

```
%
% This function is called from convertServerFile:runFileCorrection
% Use this function to add calculated variables to data table during
% OSAR conversion
%
% fuelType{'Diesel','CNG'}
%
function [data,units] = osarCalculations(data,units,installInfo)

    %% Conversions
    per_to_ppm = 10000;

    %% Initialize new parameters
    fuelType = installInfo.fuelType;
    if strcmp(fuelType,'Defaulting to NG')
        fuelType = 'NG';
    end

    %% Calculate torque and power using valid torque and valid RPM values
    [data,units] = addPower(data,units,installInfo);

    %% Exhaust flow
    [data,units] = addExhaustFlow(data,units,installInfo);

    %% Rename NOx Variables
    data.OBD_NOx_outlet_ppm                                                    =
cleanNOxPPM(getFromTable(data,{'Aftertreatment1OutletNOx','Aftertreatment1OutletNOx1pp
m'}));
    data.OBD_NOx_inlet_ppm                                                     =
cleanNOxPPM(getFromTable(data,{'Aftertreatment1SelectiveCatalyticReductionIntakeNox',
'Aftertreatment1IntakeNOx', 'Aftertreatment1SCRIntakeNOx1ppm', 'EngineExhaustNOxppm'}));
    data.OBD_NOx_outlet_cor_ppm                                                =
cleanNOxPPM(getFromTable(data,{'NOxSensorCorrectedConcentrationBank1Sensor2',
'Aftertreatment1OutletCorrectedNOxppm'}));
    data.OBD_NOx_inlet_cor_ppm                                                 =
cleanNOxPPM(getFromTable(data,{'NOxSensorCorrectedConcentrationBank1Sensor1'}));
    data.OSAR_NOx_outlet_ppm = cleanNOxPPM(getFromTable(data,{'NOx'}));

    %% OSAR NOx signal correction
    data.OSAR_NOx_outlet_ppm = removeSignalDrop(data.OSAR_NOx_outlet_ppm,50);

    %% NH3 and NOx Correction for N2
    data.OSAR_NOx_used_ppm = data.OSAR_NOx_outlet_ppm;
```

```
    data.OSAR_NH3_used_ppm = getFromTable(data,{'NH3'});

    if strcmp(fuelType,'NG')
        o2Neg = find(data.O2_Sensor <= 0);
        data.NOxCalc_ppm(o2Neg) = 0;
        data.NH3Calc_ppm(o2Neg) = data.OSAR_NOx_used_ppm(o2Neg);

        o2Pos = find(data.O2_Sensor > 0);
        data.NOxCalc_ppm(o2Pos) = data.OSAR_NOx_used_ppm(o2Pos);
        data.NH3Calc_ppm(o2Pos) = 0;

        data.OSAR_NOx_used_ppm = data.NOxCalc_ppm;
        data.OSAR_NH3_used_ppm = data.NH3Calc_ppm;
    end

    %% PM correction for low temp
    if any(ismember(data.Properties.VariableNames,'Aftertreatment1ExhaustTemperature1'))
        data.PMCurrent(data.Aftertreatment1ExhaustTemperature1 < 100) = nan;
    end

    %% Calculate emissions using exhaust flow
    fc = getFuelConstants(fuelType);

    %% NOx mass emissions
    data.OBD_NOx_outlet_gs = data.OBD_NOx_outlet_ppm .* fc.uGas_NOx .*
data.exhaustFlow_kgps;
    data.OBD_NOx_inlet_gs = data.OBD_NOx_inlet_ppm .* fc.uGas_NOx .*
data.exhaustFlow_kgps;
    data.OBD_NOx_outlet_cor_gs = data.OBD_NOx_outlet_cor_ppm .* fc.uGas_NOx .*
data.exhaustFlow_kgps;
    data.OBD_NOx_inlet_cor_gs = data.OBD_NOx_inlet_cor_ppm .* fc.uGas_NOx .*
data.exhaustFlow_kgps;
    data.OSAR_NOx_outlet_gs = data.OSAR_NOx_used_ppm .* fc.uGas_NOx .*
data.exhaustFlow_kgps;

    %% Other mass emissions
    data.NH3_gs = data.OSAR_NH3_used_ppm .* fc.uGas_NH3 .* data.exhaustFlow_kgps; %
OSAR only

    data.PM_mgm3 = getFromTable(data,{'PMCurrent'})/3200;
    data.PM_mgs = data.exhaustFlow_kgps .* data.PM_mgm3 ./ fc.pE_kgm3;

    COW = getFromTable(data,{'COW'});
    data.CO_gs = COW .* per_to_ppm .* fc.uGas_CO .* data.exhaustFlow_kgps;

    %% Add unit values (Not really used for anything)
```

```
    units.OBD_NOx_outlet_ppm = "ppm";
    units.OBD_NOx_inlet_ppm = "ppm";
    units.OBD_NOx_outlet_cor_ppm = "ppm";
    units.OBD_NOx_inlet_cor_ppm = "ppm";
    units.OSAR_NOx_outlet_ppm = "ppm";
    units.OSAR_NOx_used_ppm = "ppm";
    units.OSAR_NH3_used_ppm = "ppm";
    units.NOxCalc_ppm = "ppm";
    units.NH3Calc_ppm = "ppm";

    units.OBD_NOx_outlet_gs = "g/s";
    units.OBD_NOx_inlet_gs = "g/s";
    units.OBD_NOx_outlet_cor_gs = "g/s";
    units.OBD_NOx_inlet_cor_gs = "g/s";
    units.OSAR_NOx_outlet_gs = "g/s";

    units.NH3_gs = "g/s";
    units.PM_mgm3 = "mg/m3";
    units.PM_mgs = "mg/s";
    units.CO_gs = "g/s";

end

function nox_ppm = cleanNOxPPM(nox_ppm)
    if isnumeric(nox_ppm)
        max_nox_ppm = 2500;  % Limit from ParameterFilteringLimits.csv from EFR
        min_nox_ppm = -50;
        nox_ppm(nox_ppm < min_nox_ppm | nox_ppm > max_nox_ppm) = nan;
    end
end

function Notes

    % OBD
    %     OBD NOx outlet          <====  "Aftertreatment 1 Outlet NOx",
    %                                    "Aftertreatment 1 Outlet NOx 1 (ppm)"
    %
    %     OBD NOx inlet             <====  "Aftertreatment 1 Selective Catalytic Reduction Intake
Nox",
    %                                    "Aftertreatment 1 Intake NOx",
    %                                    "Aftertreatment 1 SCR Intake NOx 1 (ppm)",
    %                                    "Engine Exhaust NOx (ppm)"
    %
    %     OBD NOx outlet-cor     <==== "NOx Sensor Corrected Concentration Bank 1 Sensor 2",
    %                                   "Aftertreatment 1 Outlet Corrected NOx (ppm)"
    %
```

```
    %    OBD NOx inlet-cor      <==== "NOx Sensor Corrected Concentration Bank 1 Sensor 1"
    %
    % OSAR
    %    OSAR NOx outlet        <====  "NOx"
    %    OSAR NOx outlet-cor    <====  ?
    %    OSAR NOx flag          <====  "NOx-Flags'
    %    OSAR O2                <====  "NOx-O2"

End
```

Power addition

```
function [data,units] = addPower(data,units,installInfo)

    nm_to_ftlb = 0.73776;

    data.Torque_ftlb(:) = nan;
    data.Power_hp(:) = nan;
    units.Torque_ftlb = "ft-lb";
    units.Power_hp = "hp";

    % Calculate torque and power using valid torque and valid RPM values
    vr = data.EngineSpeed < 8000;
    vt = data.ActualEnginePercentTorque >= data.NominalFrictionPercentTorque;
    vrt = vr & vt;

    if ismember('EngineReferenceTorque',data.Properties.VariableNames)
        engineReferenceTorque_nm                                                    =
mode(data.EngineReferenceTorque(data.EngineReferenceTorque~=0));

    elseif ismember('EngineReferenceTorqueNm',data.Properties.VariableNames)
        engineReferenceTorque_nm                                                    =
mode(data.EngineReferenceTorqueNm(data.EngineReferenceTorqueNm~=0));

          else
        units.EngineReferenceTorque = "nm";
        engineReferenceTorque_nm = nan;
    end

    if isnan(engineReferenceTorque_nm)
        engineReferenceTorque_nm = get_reference_torque(installInfo.EngineModel);
    end

    data.Torque_ftlb(vrt)              =              (engineReferenceTorque_nm              *
nm_to_ftlb).*(data.ActualEnginePercentTorque(vrt)                                          -
data.NominalFrictionPercentTorque(vrt))/100;
    data.Power_hp(vrt) = data.Torque_ftlb(vrt) .* data.EngineSpeed(vrt) / 5252;
```

```
end
```

Remove signal drop out

```
%
% Simple one second signal drop
% If signal drops more than threshold value in one second to zero, interpolate
%
function x = removeSignalDrop(x,dropThreshold)

   try
      if ~exist('x','var')
         testSignalDrop
         return
      end

      % Default threshold is 20% of max value
      if ~exist('dropThreshold','var')
         dropThreshold = .2 * max(x);
      end

      if isrow(x)
         x = x';
      end

      d = [0;diff(x)];

      di = find(d<-dropThreshold & x ==0);
      if isempty(di)
         return;
      end

      for i = 1:length(di)
         if di(i) == 1 || di(i)+1 > length(x)
            continue;
         end

         if x(di(i)+1)~=0
            x(di(i)) = mean(x([di(i)-1,di(i)+1]));
         end
      end

   catch me
      getReport(me)
      keyboard
   end
```

```
end

function testSignalDrop

   a =10*sin(.1:.1:3);
   a(10) = 0;
   a(25) = 0;
   a(30) = 0;

   figure('color','w')
   plot(a,'--r','Linewidth',1,'MarkerFaceColor','r');
   hold on
   plot(removeSignalDrop(a,4),'-b','Linewidth',1)
   plot(removeSignalDrop(a),'ok','MarkerFaceColor','k','MarkerSize',3)
   legend({'Original','Corrected (Threshold: 4)','Corrected (Threshold: default(20% of max))'})

end
```

Speed signal

```
function speed_kph = selectSpeed(speed_wheel_kph,speed_gps_kph)
   % All values in kph

   km_to_mi = 0.621371;

   speed_wheel_kph(speed_wheel_kph > 100/km_to_mi) = nan;
   speed_gps_kph(speed_gps_kph > 100/km_to_mi) = nan;

   max_gap = 45;
   speed_wheel_kph = fillmissing(speed_wheel_kph,"linear","MaxGap",max_gap);
   speed_gps_kph = fillmissing(speed_gps_kph,"linear","MaxGap",max_gap);

   if sum(speed_wheel_kph > 0) > sum(speed_gps_kph > 0)
      speed_kph = speed_wheel_kph;
   else
      speed_kph = speed_gps_kph;
   end

end
```

Exhaust flow

```
function [data,units] = addExhaustFlow(data,units,installInfo)

   % fuelDensityList_kgm3 = {'Diesel',840;'NG',790};
   %                                                pFuel_kgm3                                                =
fuelDensityList_kgm3{strcmp(fuelDensityList_kgm3(:,1),installInfo.fuelType),2};
   data.exhaustFlow_kgphr(:) = nan;
```

```
    data.exhaustFlow_kgps(:) = nan;
    units.exhaustFlow_kgphr = "kg/hr";
    units.exhaustFlow_kgps = "kg/s";
    validAirFlow = false;
    validFuelRate = false;

    fc = getFuelConstants(installInfo.fuelType);

          massAirFlow_kghr = nan;
    if isValidTableParameter(data,'EngineInletAirMassFlowRate')
       massAirFlow_kghr = data.EngineInletAirMassFlowRate;
       validAirFlow = true;
    end
    if isValidTableParameter(data,'EngineIntakeAirMassFlowRatekgh')
       massAirFlow_kghr = data.EngineIntakeAirMassFlowRatekgh;
       validAirFlow = true;
    end

          engineFuelRate_lph = nan;
    if isValidTableParameter(data,'EngineFuelRate')
       engineFuelRate_lph = data.EngineFuelRate;
       validFuelRate = true;
    end
    if isValidTableParameter(data,'EngineFuelRatelh')
       engineFuelRate_lph = data.EngineFuelRatelh;
       validFuelRate = true;
    end

    if validAirFlow && validFuelRate
       data.exhaustFlow_kgphr = engineFuelRate_lph * fc.pFuel_kgm3/1000 +
massAirFlow_kghr;

    else  % Tries to model if switch case is true
       switch installInfo.Displacement_L_
          case 8.9
             data.exhaustFlow_kgphr = data.Power_hp * 2.52 + 33.20;
          case {11.9, 11.99}
             data.exhaustFlow_kgphr = data.Power_hp * 2.52 + 46.22;
                          otherwise
                                data.exhaustFlow_kgphr = nan;
       end
    end
          data.exhaustFlow_kgps = data.exhaustFlow_kgphr / 3600;

end
```